A STUDY OF ^{17}O AND ^{17}F THROUGH CHARGED PARTICLE REACTIONS

By

Ivan Dwight Proctor

A THESIS

Submitted to

Michigan State University

in partial fulfillment of the requirements

for the degree of

DOCTOR OF PHILOSOPHY

Department of Physics

1972

ABSTRACT

A STUDY OF ^{17}O AND ^{17}F THROUGH CHARGED PARTICLE REACTIONS

By

Ivan Dwight Proctor

Six transfer reactions leading to states in ^{17}O and ^{17}F have been studied. Spectra and angular distributions are presented for the following reactions and beam energies: $^{16}O(d,p)^{17}O$ at 20.93 MeV, $^{16}O(h,d)^{17}F$ at 34.64 MeV, $^{16}O(\alpha,h)^{17}O$ and $^{16}O(\alpha,t)^{17}F$ at 46.16 MeV, and $^{19}F(p,h)^{17}O$ and $^{19}F(p,t)^{17}F$ at 39.82 MeV. The triton and helion spectra from the alpha and proton induced reactions were recorded simultaneously to facilitate an accurate comparison of the yield from these two sets of mirror reactions.

Distorted wave approximation calculations were performed for these reactions using the code DWUCK. Spectroscopic factors S were extracted for the single nucleon stripping reactions. The two nucleon (p,h) and (p,t) reactions were analyzed with a microscopic description of the two nucleon transfer process. Enhancement factors $\mathcal{E}$ are extracted for these reactions.

The spectroscopic factors S^{+} for the 1d5/2 and 2s1/2 single particle states obtained from the (h,d), (α,h) and (α,t) analyses were compared to those obtained from the (d,p) analysis. This comparison serves as a test of the distorted wave approximation description for the stripping process induced by particles more complex than the

deuteron. Values for S^+ extracted from the analysis of the (h,d) reaction were found to agree with values obtained from the analysis of the (d,p) reaction. Values for S^+ obtained from the analysis of the (α,h) and (α,t) reactions were found to depend strongly on the optical model description of the entrance and exit channels. Reliable values for absolute spectroscopic factors from the (α,h) and (α,t) reactions could not be obtained. The relative values $S^+(\alpha,t)/(\alpha,h)$ were also found to be sensitive to details of the distorted wave approximation calculation.

The enhancement factors $\mathcal{E}^+$, extracted from the microscopic (p,h) and (p,t) analysis to the ground and first excited states in ^{17}O and ^{17}F respectively, were compared for different wavefunctions describing ^{19}F. A shell model wavefunction for ^{19}F was necessary to describe adequately the two nucleon stripping process. The addition of a spin-orbit force to the description of the two nucleon stripping process was not necessary to account for the different (p,t) and (p,h) stripping processes.

TABLE OF CONTENTS

I. INTRODUCTION

Transfer reactions are a powerful method for determining many important aspects of nuclear structure. Using the distorted wave approximation, it is now possible to analyze accurately transfer reactions involving protons, deuterons and neutrons. These reactions may be classified as "simple" reactions because the projectiles involved can be considered as either elementary particles without structure, or as a simple, weakly bound combination of elementary particles. The reaction mechanism in this case is well understood and the nuclear structure information extracted from experiment is reliable.

The problem with the simple one nucleon transfer reaction arises experimentally when neutrons are involved. The (n,d) reaction is almost impossible to study because neutron beams having sufficient quality to allow study of direct transfer reactions are difficult to produce. The (d,n) reaction has been studied on some nuclei, but the difficulty of detecting neutrons with sufficient efficiency and energy resolution makes this reaction unfeasible in many cases. To avoid the experimental difficulties associated with neutrons, one can go to complex reactions involving projectiles of mass three and four. For example, the extremely difficult (n,d) experiment can be replaced by a $(d,{}^3He)$ experiment and the (d,n) experiment can be replaced by a $({}^3He,d)$ or a (α,t) experiment.

The trouble with these complex reactions for studying nuclear structure is in the theoretical treatment of the reaction mechanism. The complex projectiles are strongly absorbed at the nuclear surface which should give, in principal, some reduction in sensitivity to

optical model parameters (Au 70). That this reduction in optical model sensitivity is not found for transfer reactions involving alphas, helions, or tritons, is attributed to the transition between a tightly bound projectile and a loosely bound, easily deformable one (Au 70). The optical model parameters are in turn less well known for the complex projectiles than for the simple ones. Second order effects, such as two step processes, may also be more important in the complex transfer reactions, since the cross sections are generally weaker for the complex projectiles.

Accurate studies of mirror nuclei by mirror pairs of reactions are greatly hindered by the neutron problem. In this case one is forced to use complex reactions for an accurate determination of the mirror state nuclear structure information. One can then check the reliability of the results by comparison to the simple reaction not involving the neutron problem.

These considerations led to an investigation of six single and double nucleon transfer reactions, all of which populated one of two mirror final states, and an attempt to analyze these reactions in the framework of the distorted wave approximation (DWA). The mirror pair ^{17}O and ^{17}F were chosen for study because they are formed by adding a neutron or proton to the nominally closed ^{16}O core. The ^{16}O and ^{16}O-plus-nucleon systems have received a thorough theoretical treatment. The $^{16}O(d,p)$ reaction has been studied extensively at deuteron energies below 15 MeV, but only one study has been reported at a higher energy (Aj 71). Similarly the $^{16}O(h,d)^{17}F$ reaction has not been studied at the higher energies (Aj 71, Ec 66, Me 70). No previous studies including an analysis in the DWA framework have been reported for the $^{16}O(\alpha,t)^{17}F$

$^{16}O(\alpha, ^{3}He)^{17}O$, $^{19}F(p,t)^{17}F$ and $^{19}F(p, ^{3}He)^{17}O$ reactions.

The DWA analysis of these reactions is, in principle, quite straightforward. If the reaction mechanism is adequately described, then the single nucleon stripping reactions yield spectroscopic information related to the shell model single particle wavefunctions of the target and residual nucleus. In the same simple picture, the two nucleon pick-up reactions describe a coherent two particle component of the shell model wavefunction. This analysis will attempt to investigate the adequacy of the straightforward DWA description for both the complex and simple transfer processes and the resulting extracted spectroscopic information.

II.1.a The Distorted Wave Method

The Distorted Wave Method (DWM) for analysis of direct reaction processes has been extensively developed by Satchler (Sa 64a, Sa 66) and many other authors and has been reviewed by Austern (Au 70) and Preedom (Pr 71). A brief outline of the method applied to transfer reactions as presented by the above authors is given in the following sections. The abbreviations DW and DWA will be used for distorted wave and distorted wave approximation, respectively.

The reaction is written as A(a,b)B, where A is the target nucleus, a is the incident particle, B is the residual nucleus, and b is the outgoing (detected) particle. For a transfer reaction $a = b \pm x$, where x is the transferred nucleon(s). The reaction is classified as direct if it proceeds in a time interval comparable to the time necessary for the incident particle to traverse the nucleus. The residual nucleus is further assumed to be similar to the target nucleus in that minimal nucleon rearrangement has occured during the formation process.

The differential cross section in the DWA for an unpolarized projectile on an unpolarized target is given by (Sa 64a)

$$\sigma(\theta)_{DW} = \frac{\mu_a \mu_b}{(2\pi\hbar^2)^2} \frac{k_b}{k_a} \frac{\sum_{M_A m_a M_B m_b} |T|^2}{(2J_A+1)(2S_a+1)} , \qquad \text{(II.1.a)}$$

where μ is a reduced mass, k is a relative momentum, J and S are total and spin angular momenta, and the sum on the absolute square of the transition amplitude T is over all allowed projections of the angular

momenta. The transition amplitude in the DWA is given by

$$T = J \int d\vec{r}_a \int d\vec{r}_b \, \chi_b^{(-)*}(\vec{k}_b,\vec{r}_b) \langle B,b|V|A,a\rangle \, \chi_a^{(+)}(\vec{k}_a,\vec{r}_a) \ , \quad \text{(II.1.b)}$$

where J is the Jacobian of the transformation to the coordinates $\vec{r}_a,\vec{r}_b$. These are the coordinates for the separation of the centers of mass of A,a and B,b. The matrix element $\langle B,b|V|A,a\rangle$ acts to produce the transition between the initial and final elastic scattering states χ_a and χ_b, respectively, which are taken to be optical model wave functions (Ho 63). All of the nuclear structure is contained in this matrix element.

The matrix element $\langle B,b|V|A,a\rangle$ may be expanded into terms corresponding to the transfer of a definite angular momentum j and isospin t to the nucleus. The transferred isospin and angular momentum are defined by

$$\vec{t} = \vec{T}_B - \vec{T}_A = \vec{t}_a - \vec{t}_b \qquad \text{(II.1.c)}$$

and

$$\vec{j} = \vec{J}_B - \vec{J}_A, \quad \vec{s} = \vec{S}_a - \vec{S}_b, \quad \vec{\ell} = \vec{j} - \vec{s}.$$

In this expansion the matrix element is

$$\begin{aligned} J\langle B,b|V|A,a\rangle = \sum_{\ell sj} i^{-\ell}(-)^{S_b-m_b} \, & G_{\ell sjm}(\vec{r}_b,\vec{r}_a) \\ & \times \langle T_A,t,M_{TA},m_t|T_B,M_{TB}\rangle \langle t_b,t,m_{tb},m_t|t,m_{ta}\rangle \\ & \times \langle S_a,S_b,m_a,-m_b|S,m_a-m_b\rangle \langle J_A,j,M_A,M_B-M_A|J_B,M_B\rangle \\ & \times \langle \ell,s,m,m_a-m_b|j,M_B-M_A\rangle \ , \end{aligned} \qquad \text{(II.1.d)}$$

where $m = M_B - M_A + m_b - m_a$. All of the radial dependence is contained

in $G_{\ell sjm}$. Substitution of the expansion II.1.d into equation II.1.b defines the reduced transition amplitude $\beta_{sj}^{\ell m m_b m_a}(\vec{k}_b,\vec{k}_a)$

$$T = \sum_{\ell sj} C_T \, (2j+1)^{\frac{1}{2}} \langle J_A,J,M_A,M_B-M_A | J_B,M_B\rangle \, \beta_{sj}^{\ell m m_b m_a}(\vec{k}_b,\vec{k}_a) \quad . \qquad \text{(II.1.e)}$$

The six dimensional integral over $d\vec{r}_a$ and $d\vec{r}_b$ now appears in β and the isospin recoupling coefficient C_T is explicitly retained. The DW cross section in terms of β is

$$\sigma(\theta)_{DW} = \frac{\mu_a\mu_b}{(2\pi\hbar^2)^2} \frac{k_b}{k_a} \frac{(2J_B+1)}{(2J_A+1)(2S_a+1)} C_T^{\,2} \times \sum_{jmm_b m_a} \Big| \sum_{\ell s} \beta_{\ell s}^{\ell m m_b m_a} \Big|^2 \quad , \qquad \text{(II.1.f)}$$

where $C_T^{\,2}$ is the isospin recoupling coefficient

$$C_T^{\,2} = \langle T_A,t,M_{TA},m_t | T_B,M_{TB}\rangle^2 \langle t_b,t,m_{tb},m_t | t_a,m_{ta}\rangle^2 \quad . \qquad \text{(II.1.g)}$$

The reduced transition amplitude β is given by

$$\beta_{sj}^{\ell m m_b m_a}(\vec{k}_b,\vec{k}_a) = \frac{i^{-\ell}}{(2j+1)^{\frac{1}{2}}} \sum_{m'_a m'_b m} \langle \ell,s,m',m'_a-m'_b | j,m-m_b+m_a\rangle \times \langle S_a,S_b,m'_a,-m'_b | s,m'_a-m'_b\rangle \, (-)^{S_b-m'_b} \times \int d\vec{r}_a \int d\vec{r}_b \, \chi_{m'_b m_b}^{(-)*}(\vec{k}_b,\vec{r}_b) \, G_{\ell sjm'}(\vec{r}_b,\vec{r}_a) \, \chi_{m'_a m_a}^{(+)}(\vec{k}_a,\vec{r}_a) \quad .$$

The zero-range approximation is usually made to simplify the six dimensional integral appearing in $\beta_{sj}^{\ell m m_b m_a}$. The ZR approximation assumes that particle b is emitted at the point at which particle a is absorbed. Then $\vec{r}_b$ can be replaced by $(A/B)\vec{r}_a$, where A and B are the masses of the target and residual nucleus. This reduces the six dimensional integral to a three dimensional integral with a delta function at $\vec{r}_b - (A/B)\vec{r}_a$.

The reduced transition amplitude for a stripping reaction is formed by assuming that the interaction causing the reaction is just the potential binding the stripped nucleon(s) to the emitted particle. Then V in equation II.1.b is interpreted as V_{bx} for a stripping reaction. The DW cross section for a given L,S transfer is then calculated from equation II.1.f. The cross section for a pickup reaction is formed by evaluating the inverse stripping case, then using time reversal invariance to obtain the pickup cross section. The DW computer code DWUCK (Ku 69) was used for all of the analysis presented in this thesis. DWUCK was compared with the code JULIE (BA 62) for a few test cases. The agreement was very good at the forward maxima, deteriorating somewhat in the vicinity of sharp minima and at back angles in some cases. The relationship between the DW cross section as calculated by DWUCK and the experimental cross section is given in section II.2.a.

II.1.b Non-Locality Corrections

The non-local Schrodinger equation may be written as

$$\left(\frac{h^2}{2m} \Delta^2 + E \right) \psi(\vec{r}) = \int dr' K(\vec{r},\vec{r}') \psi(\vec{r},\vec{r}') \quad . \qquad \text{(II.2.a)}$$

Optical model potentials used in the calculation are known to be non-local in character, so at least an approximation to the effect should be included in the calculation. In the local energy approximation (Pe 64, Bu 64), the result of a non-local potential is a damping term applied to the radial form factor. The damping term calculated by DWUCK (Ku 69) is of the form

$$W^i_{NL}(r) = C \left[1 - \frac{\beta^2 m_i}{2h^2} V_i(r) \right]^{-\frac{1}{2}} , \qquad \text{(II.2.b)}$$

where C is a normalization constant and β is the range of the non-locality. The mass and potential of the incoming, outgoing or bound state particle is given by m_i and $V_i(r)$ respectively. The constant C is unity for scattering in the entrance and exit channels and is determined from a normalization requirement of the wavefunction for a bound state. The values of β used in the calculations are those given in reference (Ku 69).

II.1.c Finite-Range Corrections

A zero-range approximation is normally used in the DW codes for evaluation of the reduced transition amplitude. This approximation tends to over estimate the contribution from the nuclear interior (Sa 66). In the local energy approximation (Pe 64, Bu 64) the finite-range effect is approximated by a damping term applied to the radial form factor. The DW code DWUCK (Ku 69) uses a finite range correction of this form.

For a general one-nucleon stripping reaction A(a,b)B, the radial form factor appearing in the reduced transition amplitude is multiplied by a damping term

$$W_{FR}(r) = \left[1 + \frac{2}{\hbar^2} \frac{m_b m_x}{m_a} R^2 \left(V_s(r) - V_b(rA/B) - V_x(r) - SE_{bx}\right) \right]^{-1} \qquad \text{(II.3.a)}$$

R is the range in the LEA, V_i is the central part of the potential for particle i and $SE_{bx} = E_a - E_b - E_x$ is the separation energy of particle x from particle a. The values of the finite-range parameter used in the single nucleon transfer calculations are those given in reference (Ku 69).

Two nucleon transfer reactions have been treated in the zero-range approximation where the transfer process takes place at the c.m. of the transferred pair. This approach ignores the finite size of the two-nucleon wave function as well as the finite range of the interaction responsible for the transfer process. Bayman and Kallio (Ba 66) have shown how to get the relative s state part of the wave function for two particles moving in a finite single-particle potential. Several authors (Be 66, Ch 70, Ro 71) have recently developed methods of approximating the finite-range effect for the two nucleon transfer process.

The DW code DWUCK (Ku 69) was used to calculate the two-nucleon transfer cross sections. The separation energy was taken as one half the two-nucleon separation energy. A finite two-nucleon wave function (Ba 66) and the finite-range correction (Ro 71) were incorporated in DWUCK by Kunz. Parameter values for the two-nucleon transfer corrections are discussed in the experimental analysis.

II.2.a Extraction of Spectroscopic Factors from Experiment

The DW cross section (II.1.f) for a single nucleon transfer reaction is related to the experimental cross section by (Ku 69)

$$\sigma(\theta)^{\ell sj} = C_T^2 \frac{2J_B+1}{2J_A+1} \frac{|B_{\ell sj}|^2}{1.0\times10^4} \frac{\sigma(\theta)^{\ell sj}_{DW}}{(2j+1)} \quad . \qquad \text{(II.4.a)}$$

In the zero-range (ZR) approximation

$$|B_{\ell sj}|^2 = S_{\ell sj} \, |D_o|^2 \quad , \qquad \text{(II.4.b)}$$

where $S_{\ell sj}$ is the spectroscopic factor and D_o is the product of the

bound particle wavefunction times the unbound potential, $\phi_a V_{bx}$ for stripping. Various interactions and projectile wavefunctions have been used to evaluate $|D_o|^2$ for single-nucleon stripping (Sa 64b, Ku 69, Au 70). The values used here are those given in reference (Ku 69).

The spectroscopic amplitude for the two-nucleon pickup reaction is not well defined (Ba 64, Gl 65, To 69). If the nucleons picked up come from different orbitals, then a coherent sum over the orbitals involved is required to calculate the DW cross sections. The ZR approximation necessary to evaluate $|D_o|^2$ for two-nucleon pickup is also somewhat questionable since a complete treatment with finite-range has not been performed (To 69, Ba 71).

The single-nucleon transfer reaction spectroscopic factors for $L \neq 0$ were obtained by matching the DW cross section to the experimental cross section at forward angles. For $L = 0$ the DW cross section was matched to the first observed maximum at approximately 30^o. This far back in angle the reaction may not be entirely direct, thus the $L = 0$ amplitudes should be cautiously interpreted.

II.2.b Wavefunctions for Unbound States

The usual DW calculation for a stripping or pickup reaction prescribes that the transferred particle is bound in a Woods-Saxon well whose depth is adjusted to give the correct binding energy of the transferred particle. If a final state is slightly unbound to particle emission, in which case the usual DW prescription no longer applies, we may consider the particle to be quasi-bound by the Coulomb and centrifugal barriers. This method was applied to the unbound states in ^{17}F ($E_x \geq 0.6$ Mev) and ^{17}O ($E_x \geq 4.1$ Mev).

The program EIGENFUNK (Yo 70b, Ko 71) was used to calculate the wave functions for particles unbound in a Woods-Saxon well. The program varies the well depth to minimize the ratio of the exterior to interior amplitude of the wave function for a particle of J^{π} and binding energy $-E_B$. The normalization of these unbound wave functions is discussed in reference (Yo 70b).

II.3. Comparison of $(\alpha, {}^3He)$ and (α,t) Reactions

The "complex" single-nucleon stripping reactions $(\alpha, {}^3He)$ and (α,t) have several interesting features (Bl 64) and have recently received considerable study (Yo 70a, Ro 70, He 70, Ga 69). As in all mirror reactions, these serve as a test of the charge independence of nuclear forces. In contrast to the "simple" deuteron stripping reactions to mirror nuclei, both of the outgoing particles are charged, which simplifies detection and consequently improves resolution and detection efficiency. Also, the use of a single telescope to detect both outgoing particles during one bombardment eliminates some systematic errors which might be present in a measurement of the ratio of (d,p) to (d,n). For N = Z target nuclei these reactions populate isobaric mirror ground state nuclei and, unlike deuteron stripping, preferentially select high momentum transfers because of the large momentum mismatch in the incident and exit channels. However, the DW analysis of these complex stripping reactions is somewhat less precise than the deuteron simple stripping analysis (Yo 70a).

The usual optical model description of the entrance and exit channels is somewhat questionable for low L-transfer, α-particle stripping. Elastic scattering in these channels is primarily a surface

phenomena and the small L transfers appear to have a large contribution from the nuclear interior (Yo 70a). The determination of a zero range normalization constant $|D_o|^2$ (equation II.4.b) is also difficult (Yo 70a, He 70). This determination requires an explicit treatment of the interaction and relative motion between the outgoing three nucleon system and the stripped nucleon.

A comparison of the $(\alpha,{}^3He)$ reaction to the (α,t) reaction on ^{16}O can serve as a test of some properties of the DW analysis of these complex stripping reactions. The ratio of the DW cross sections for (α,t) to $(\alpha,{}^3He)$ using equation (II.4.a) is

$$\frac{d\sigma(\alpha,t)_{\ell sj}}{d\sigma(\alpha,{}^3He)_{\ell sj}} = \frac{k_t}{k_{^3He}} \frac{C_t^2}{C_{^3He}^2} \frac{|B_{\ell sj}^{^{17}F}|^2}{|B_{\ell sj}^{^{17}O}|^2} \frac{\sum|\beta(\alpha,t)|^2}{\sum|\beta(\alpha,{}^3He)|^2} \quad , \qquad \text{(II.5.a)}$$

where the sum $\sum$ implies summation and averaging over all necessary variables and the momentum, isospin and spectroscopic amplitudes are explicitly retained. All of the DW approximations are included in the reduced amplitudes β.

The lowest order approximation to this ratio is to consider the single particle structure of ^{17}F and ^{17}O identical and to assume an identical mechanism for the two reactions. The ratio (II.5.a) then reduces to (using equation II.1.g)

$$\frac{d\sigma(\alpha,t)}{d\sigma(\alpha,{}^3He)} = \frac{k_t}{k_{^3He}} \frac{\langle 0,\tfrac{1}{2},0,-\tfrac{1}{2}|\tfrac{1}{2},-\tfrac{1}{2}\rangle^2 \langle \tfrac{1}{2},\tfrac{1}{2},\tfrac{1}{2},-\tfrac{1}{2}|0,0\rangle^2}{\langle 0,\tfrac{1}{2},0,\tfrac{1}{2}\ \tfrac{1}{2},\tfrac{1}{2}\rangle^2 \langle \tfrac{1}{2},\tfrac{1}{2},-\tfrac{1}{2},\tfrac{1}{2}\ 0,0\rangle^2}$$

$$= \frac{k_t}{k_{^3He}} \qquad \text{(II.5.b)}$$

This simple approximation includes only the kinematic effect of the Coulomb force and the n-p mass difference. The effect on the reaction mechanism of the Coulomb force and the n-p mass difference may be investigated by modifying the bound state of the stripped nucleon.

II.4. Comparison of (p, ^{3}He) and (p,t) Reactions

The basic theory of direct two-nucleon transfer reactions has been developed by a number of authors (Gl 63, Bl 64, Ba 64, Gl 65). Towner and Hardy (To 69) have presented shell model expressions for the spectroscopic amplitudes and formulas for evaluating the two-particle coefficients of fractional parentage (cfp). Fleming, Cerny and Glendenning (Fl 68) have shown that the basic two-nucleon pickup theory does not explain the relative population of (p,t) and (p, ^{3}He) transitions to mirror nuclei. They suggest that a strong spin dependence in the nucleon-nucleon interaction or interference terms arising from either spin-orbit coupling in the optical potentials or core excitation may resolve the difference between the calculated and experimental ratios.

The DW formalism of Towner and Hardy (To 69) for (p,t) and (p, ^{3}He) with the interaction taken as a two-body potential which includes exchange of spin and isospin gives

$$\sigma(\theta) = \frac{\mu_a \mu_b}{(2\pi\hbar^2)^2} \frac{k_b}{k_a} \frac{2S_b+1}{2S_a+1} \sum_{M\sigma_a\sigma_b}^{J} \left| \sum^{[1][2]LST} C_{ST} G_{MLSJT} \beta^{LJ}_{M\sigma_a\sigma_b} \right|^2 \qquad \text{(II.6.a)}$$

where the square bracket [i] represents the single-particle orbitals $[n_i l_i j_i]$, The term $\beta^{LJ}_{M\sigma_a\sigma_a}$ contains the details of the reaction mechanism and may be evaluated by a DW code. The term G_{MLSJT} contains the nuclear structure information and is defined by

$$G_{MLSJT} = \mathcal{L}^{\frac{1}{2}}_{AB}([1][2];JT) \begin{vmatrix} \ell_1 & \ell_2 & L \\ \frac{1}{2} & \frac{1}{2} & S \\ j_1 & j_2 & J \end{vmatrix} , \qquad \text{(II.6.b)}$$

where $\mathcal{L}^{\frac{1}{2}}_{AB}$ is a spectroscopic amplitude and the bracketed term is a LS-jj transformation (To 69). The term C_{ST} is defined by

$$C_{ST} = b_{ST} \langle T_B, t, M_{TB}, m_t | T_A M_{TA} \rangle D(S,T) , \qquad \text{(II.6.c)}$$

where the Clebsch-Gordon coefficient couples the isospin of the final state T_B to the initial state T_A through the isospin transfer t. The factor b_{ST} is a spectroscopic factor for the light particles. It has the values $-\delta_{S0}\delta_{T0}$ for (p,t) and $-\frac{1}{\sqrt{2}}(\delta_{S0}\delta_{T1}-\delta_{S1}\delta_{T0})$ for (p,^{3}He). D(S,T) is a measure of the spin-isospin exchange in the interaction (To 69). It has a value of unity for (p,t) (S=0, T=1 only) and a value less than unity for (p,^{3}He). Experimental values for the magnitude of the spin triplet to singlet exchange defined by $R = |D(1,0)/D(0,1)|^2$ are given in reference (Ha 67, Fl 71) as R = 0.38, 0.28 respectively.

The coherent sums in the cross section (equation (II.6.a)) are over the single particle configurations [nℓj], and if spin-orbit coupling is included in the optical potentials, the sums over L,S,J and T. Assuming that the optical model spin-orbit coupling can be neglected, the cross section is proportional to the incoherent sum over (L,S,J,T)

$$\sigma(\theta) \propto \sum_{MLSJT} \left| \sum^{[1][2]} G_{MLSJT} \beta^{LJ}_{M} \right|^2 . \qquad \text{(II.6.d)}$$

The sums over the single particle configurations [nlj] appearing in G_{MLSJT} are still coherent and can have large effects on the calculated cross sections when contributions from different orbitals are considered

(Gl 65). This coherence of the configuration sum gives a sensitive test of a shell-model wavefunction, since both the sign and magnitude of the configuration contribute to the result.

Taking the case where no spin-orbit coupling is included, the relation between experimental and DWA cross sections as calculated by DWUCK is given by (Ku 72, Ba 72)

$$\sigma(\theta)_{exp} = N \, \mathcal{E} \sum_{LSJT} (2S+1) \, C_{ST}^{\,2} \, \frac{\sigma(\theta)^{LSJT}}{2J+1} \quad . \qquad \text{(II.6.e)}$$

In this equation, N is an overall normalization factor, $\mathcal{E}$ is an enhancement factor which will be unity if the reaction is described correctly, and $\sigma(\theta)$ is the DWUCK cross section calculated by the prescription of equation II.6.d with an incoherent sum over the allowed values of LSJT transferred in the reaction. Using equation II.6.e, the predicted DWA cross section ratio $X = \sigma(p,t)/\sigma(p,{}^3He)$ is given by

$$X = \frac{C_{01}^{\,2} \, \sigma(\theta)^{L0J1}}{C_{01}^{\,2} \, \sigma(\theta)^{L0J1} + 3 \, C_{10}^{\,2} \, \sigma(\theta)^{L1J0}} \quad , \qquad \text{(II.6.f)}$$

where the normalization and enhancement factors are taken to be the same for the (p,t) and (p,^{3}He) reactions and a summation over the allowed L and J values is implied.

III. THE EXPERIMENT

III.1. Beam and Beam Transport

The proton, deuteron, helion(^{3}He) and alpha(^{4}He) beams used for these experiments were produced by the Michigan State University sector-focused cyclotron (Be 66). Figure III.1.a shows a schematic diagram of the transport system and experimental area. The momentum analysis system includes the elements up to Box 5 (Ma67, Be 68). It is basically an object slit, two 45° dispersion magnets and momentum defining slit at Box 5. Beam energy was determined by measuring the magnetic fields of M_3 and M_4 with N.M.R. probes (Sn 67, Tr 70). After analysis the beam was bent through 22.5° by M_5 and centered on Box 10. A small steering magnet placed immediately behind Box 10 was used to place the beam over the center of the scattering chamber. A remote television monitor was used to view the beam on quartz scintillators at Boxes 3 and 5 and in the scattering chamber. The quadrupoles were adjusted to give a beam spot on target approximately 0.050 inches wide by 0.075 inches high.

III.2. Scattering Chamber

The zero angle and beam position were determined by optically aligning Box 10, the center of rotation of the scattering chamber and a pair of current reading jaws placed near the center of the scattering chamber. The jaws were spaced approximately 0.250 inches apart, so they normally intercepted no beam. Current in the small steering magnet behind Box 10 was adjusted to intercept half of the beam on one side of the jaws in the scattering chamber then the other, and the average of these current values was used as the central position.

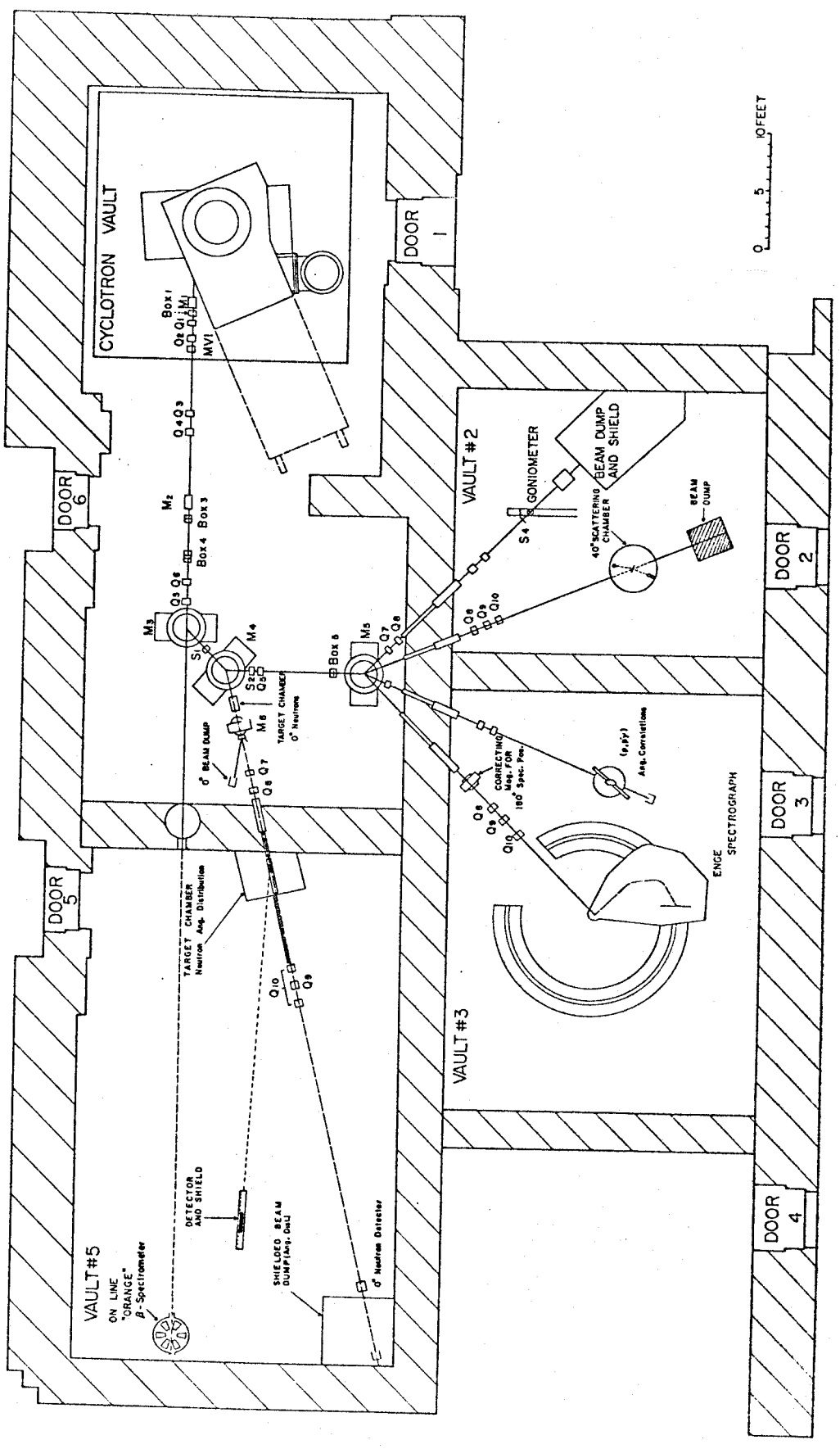

Fig. II. 1. a Layout of the Michigan State University cyclotron experimental area.

Alignment was further checked by viewing a small vertical wire placed over the quartz scintillator in the target holder.

Angular readout of the moveable arm was done remotely by an electrical system. The calibration of this system was checked against a scribed aluminum protractor. Agreement between the electrical system and the protractor was within 0.15^{o} over the range 0^{o} to 160^{o}.

Two $\Delta E,E$ counter telescopes mounted 10^{o} apart were used to take most of the data. The angular position of these telescopes on the mount was determined optically by establishing the zero degree line then rotating the arm until the detector collimators were aligned with the telescope. On three different runs, particles were then detected at a forward angle on both sides of zero degrees to establish that the optical zero degree line agrees with the beam axis. When the beam was carefully aligned as previously described, the beam zero degree line was within 0.3^{o} of the optical zero degree line.

III.3. Faraday Cup and Charge Collection

A long (3 to 6 foot) piece of aluminum beam pipe, electrically insulated from the scattering chamber by a three inch piece of Delrin* beam pipe, was used as a Faraday cup. A 3 kilogauss permanent magnet was attached to the Faraday cup to act as a trap for secondary electrons. For most of the runs, the Faraday cup was placed inside, and insulated from, a 50 gallon drum filled with water to reduce neutron flux at the detectors.

The beam current was monitored and the charge collected with an Elcor model A310 B current integrator. The calibration of the current

*Cadillac Plastic and Chemical Co., Detroit, Michigan.

integrator was frequently checked against the internal calibration source. It was found to be within approximately 1% on the current ranges used (10 na - 1 μa full scale). In addition to monitoring the current in the Faraday cup at the console, the output of the current integrator was used with a voltage-to-frequency converter as a dead time monitor when this was required.

III.4. Targets

All of the data taken with ^{16}O as the target used gas cells filled with natural oxygen gas (99.76% abundance of ^{16}O). The $^{19}F(p, ^{3}He_{t})$ data were taken with foil targets (CaF_2 evaporated on 50 μg/cm^2 carbon foils), then normalized to the ground states of data taken with a gas cell filled with CF_4 (freon 14 obtained from Matheson Gas Products). The normalization is described in section III.8.b.

The gas cells used were made of brass with 0.5 mil Kapton* windows epoxied to the metal (Pi 70). At forward angles three inch diameter cells were necessary to exclude the beam entrance and exit points from the region of space that the detector collimator accepts. When data was taken at back angles, cells of one or two inch diameter were used to reduce energy straggling in the gas.

The gas pressure was reduced to 3 - 5 inches of mercury at forward angles to compensate for the increase in target thickness due to the longer effective target viewed by the collimator. The pressure was monitored by either a mercury manometer or a Wallace and Tiernan type FA-145 pressure gauge viewed by a television monitor. The Wallace and Tiernan gauge has a guaranteed accuracy of ±0.03 inches

* E. I. DuPont de Nemours, Wilmington, Delaware.

of mercury (absolute). In the pressure range used (three to twenty inches of mercury), this gauge agreed with the mercury manometer to the accuracy with which the manometer could be read (approximately ±0.1 inches of mercury). The gas in the cell was assumed to remain at room temperature (Pi 70).

The Kapton cell windows deteriorated rapidly at the beam entrance and exit points when filled with oxygen gas and bombarded with either alphas or helions, both of which had a differential energy loss of approximately 140 kev cm^2/mg. The cells usually began leaking after 1 to 2 hours of exposure to 75 - 100 n amps of beam. When the deuteron beam was used (dE/dx = 40 kev cm^2/mg), the cells filled with oxygen gas would withstand 3 to 6 hours of bombardment at approximately the same beam current. The time of failure for the cells when bombarded with 21 Mev deuterons was extended when nitrogen was used as the target (Pi 70).

A "target twister" (Figure III.4.a) was constructed to use with the gas cells to extend the window life by moving the beam spot over a large area. It used the existing scattering chamber target angle drive and analog readout. The positive analog signal from the target angle readout is fed into an inverter. The output of the inverter is then added to a positive comparison signal. The amplitude of the comparison signal determines a zero angle about which the gas cell oscillates. The null signal obtained is fed into a variable sensitivity flip-flop which turns on a relay driver when the flip-flop is in the (+) mode. The gas cell in then rotating c.w. for a (-) mode of the flip-flop and c.c.w. for a (+) mode.

The cells were rotated at two R.P.M. through approximately $\pm 15^{o}$.

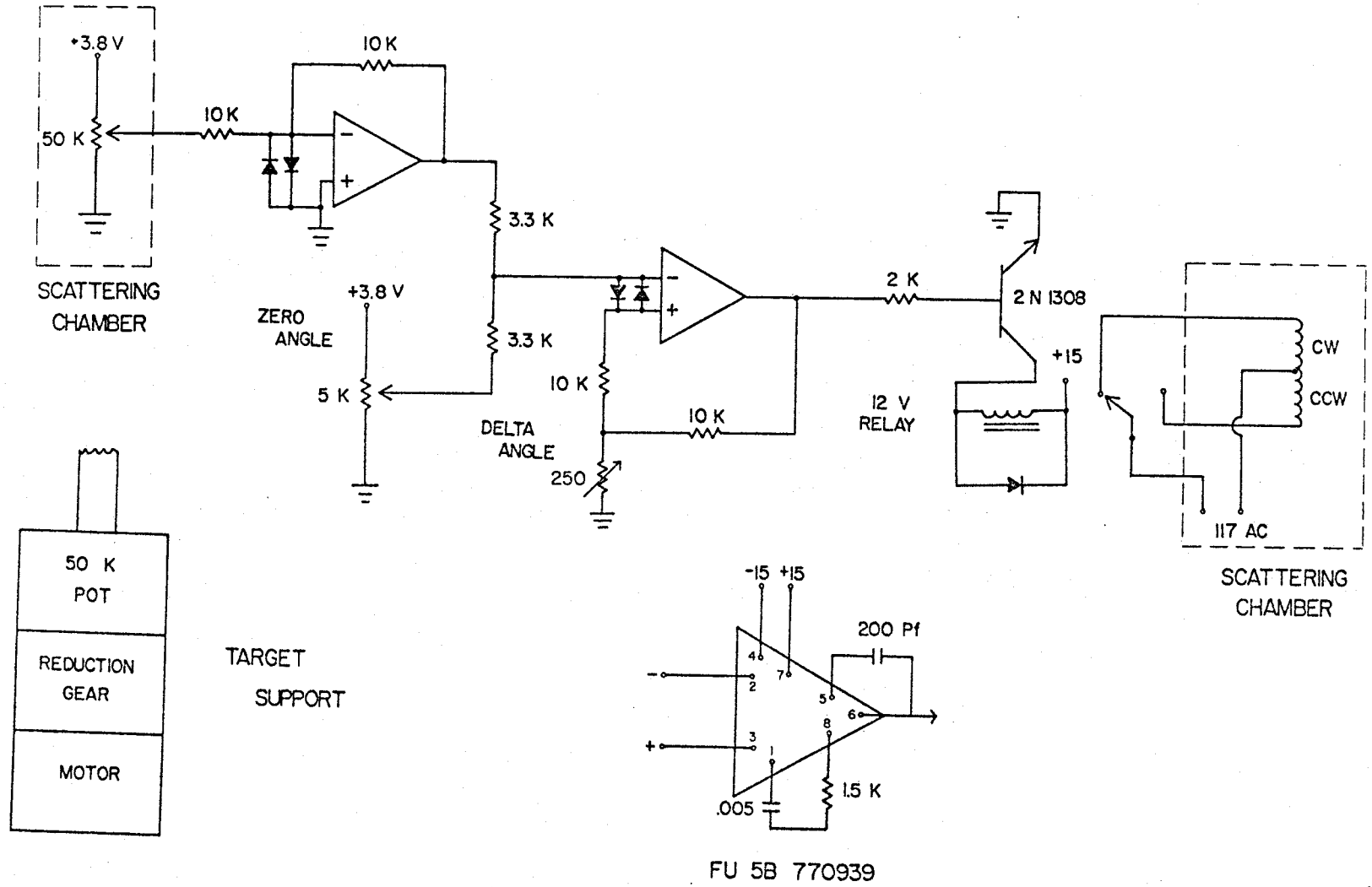

Fig. III. 4.9 Schematic diagram of the target twister used to rotate the gas cell targets.

This extended the failure time of the windows to approximately one beam day with the alpha and helion beams as compared to the 1 to 2 hour lifetime when no rotation was used.

III.5. Counter Telescopes and Electronics

III.5.a Detector Telescopes

Most of the reactions studied have small cross sections (approximately 10 mb/sr maximum) and large kinematic broadening (from 90 to 190 kev/degree at 60° lab). The angular acceptance of the detector telescope was normally chosen to give a 60 kev maximum energy spread from kinematics, 0.4° to 0.8° for most of the experiments.

To reduce the counting time, two ΔE-E telescopes mounted ten degrees apart were used for most of the experiments. For a fixed solid angle and a gas cell of fixed diameter, the smallest lab angle at which the detector does not see the beam entrance and exits points is determined mainly by the distance to the front collimator. Two front collimators and side shields were constructed that could be placed 0.75 inches from the center of the cell when separated by ten degrees. Modular detector mounts, which were physically small and permitted easy access to detectors, collimators and cooling connectors, were constructed for the dual telescope. These mounts included a built-in summing resistor.

III.5.b Detectors

All of the data for these experiments was taken with commercial surface barrier or lithium drifted silicon detectors. The detectors were cooled by pumping alcohol at dry ice temperature (-78.5°C) through the detector mount. For the ΔE-E particle identification telescope, a totally depleted ΔE detector and an E detector thick

enough to stop the particles of interest was used. The ΔE detectors were chosen thick enough to give good identification of the particle(s) of interest.

The $^{16}O(d,p)^{17}O$ experiment used an E*T time of flight particle identification system. Two 2mm totally depleted silicon surface barrier detectors were stacked for an E detector with the gold surface (minimal dead layer) facing each other to reduce energy spread due to straggling.

The $^{16}O(^{3}He,d)^{17}F$ experiment used two ΔE-E detector telescopes. The detectors in the two telescopes were 260 μ + 5 mm and 500 μ + 2 mm, respectively.

The experiments for simultaneous detection of t and ^{3}He particles required changing the ΔE detectors between forward and back angle runs. A ΔE detector that was thick enough to give good particle identification at the forward angles would not pass the lower energy ^{3}He particles at back angles. For the $^{19}F(p,x)$ experiment, two 260 μ + 2 mm telescopes were used at forward angles, and at back angles a pair with 200 μ + 2 mm and 160 μ + 2mm. For the $^{16}O(\alpha,x)$ experiment at the forward angles, a pair with 260 μ +22 mm and 170 μ + 2 mm were used. These were replaced at the back angles by a pair with 170 μ + 2 mm and 80 μ + 2 mm.

III.5.c Electronics

The block diagram of the electronics used for a single ΔE-E telescope is shown in Figure III.5.a. ORTEC 109A charge sensitive preamplifiers were used to amplify pulses from the cathodes of the ΔE and E detectors and Σ, the sum of the ΔE and E, taken from the anodes of the detectors across a 200 KΩ resistor. Pulses from the preamplifiers

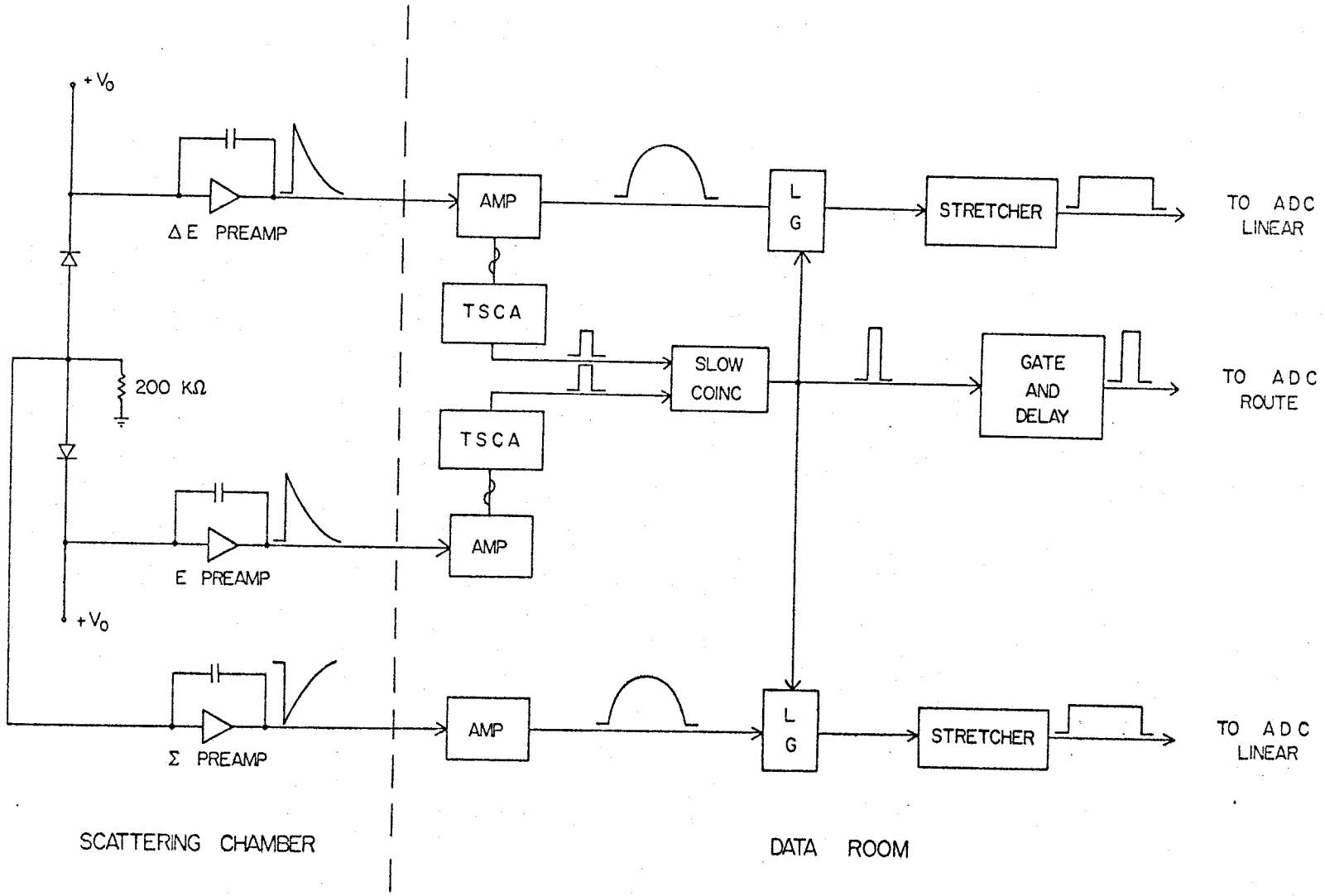

Fig. III. 5. a Schematic diagram of the electronics for a single counter telescope ΔE, E particle identifier using a summing resistor to obtain the energy signal.

were sent to the data room where they were amplified by ORTEC 440 or 451 amplifiers. The prompt bipolar output of the ΔE and E signals was sent to a timing single channel analyzer (TSCA). The TSCA outputs were fed into a slow coincidence module. The coincidence signal was used to gate the delayed unipolar pulses from the ΔE and Σ amplifiers and as a routing signal for the ADC's.

The summing resistor makes matching the gains of the ΔE and E amplifiers unnecessary. This shortens the setup time, especially when identification of particles with large differences in specific ionization is desired. The resolution of the summing resistor signal was compared to summing the ΔE and E signals at the data room, once with particles and a pulser and once with a pulser only. No difference in resolution was found.

For the $^{16}O(d,p)^{17}O$ experiment, a charged particle time of flight identification system was used. The block diagram of the electronics used is shown in Figure III.5.b. Two 2 mm thick silicon surface barrier detectors were stacked to stop the protons.

The signal from the detectors is sent through an ORTEC 260 inductive time pickoff (TPO) to an ORTEC 109A preamplifier. The linear signal is then amplified and sent to a linear gate (LG). A timing single channel analyzer (TSCA) was used as a noise descriminator to furnish the gate signal. The gated signal was sent through a delay, then to the ADC's.

Particle identification is performed by comparing the time of arrival of a particle at the detector (T) to the next time the RF voltage passes through zero (τ). The TPO signal is sent to a threshold discriminator in the TPO control which is set just above background noise. The output of this discriminator is sent to a fast discriminator in the data room which triggers the start on an ORTEC 437A time

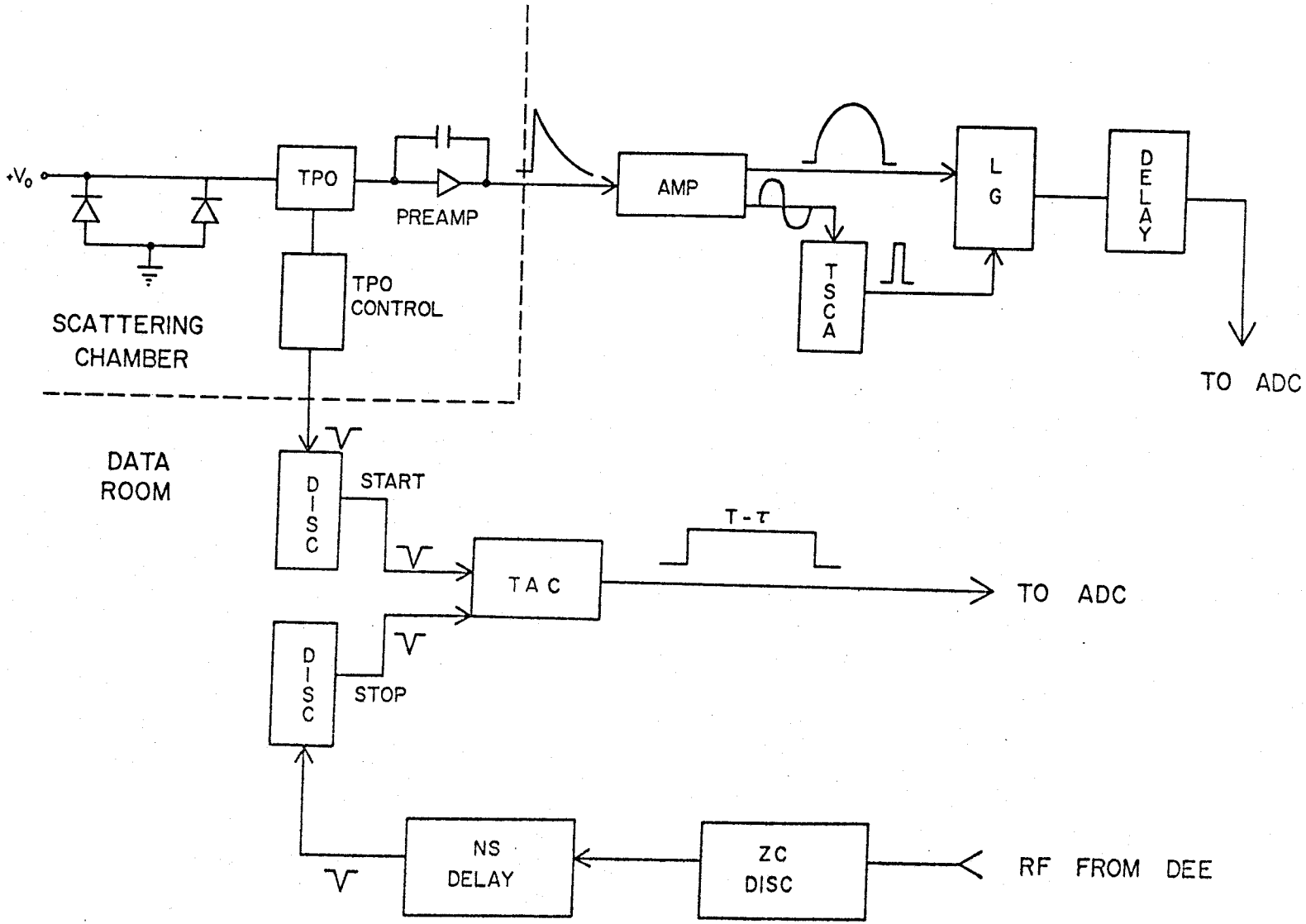

Fig III. 5.6 Schematic diagram of the electronics for time of flight particle identification.

to pulse height converter (TAC). The TAC stop pulse is obtained by feeding an attenuated signal from the cyclotron dee into an ORTEC zero crossing (ZC) discriminator. This is sent through a nanosecond delay to the fast discriminator which feeds the TPHC stop.
The charged particle time of flight identification system has the advantage of working over a large energy range for a given particle type. However it will not discriminate between tritons and helions, so it could not be used for most of these experiments.

III.6. Data Acquisition

Data for these experiments was collected on a X.D.S. Sigma-7 computer. A Northern Scientific quad 4096 channel ADC was used to convert the linear signal to digital form. The ADC's and routing pulses were read by the data acquisition code TOOTSIE (Ba 69, Ba 70).

TOOTSIE has two modes of operation, a setup mode for particle identification and a run mode in which the particles are stored as one dimensional spectra. For these experiments the setup mode stores ΔE (or $T-\tau$) pulses as the y axis, energy pulses as the x axis and number of events as the z axis of a three dimensional array. Cuts through the x-y plane are then displayed on a CRT and particle identification is performed by fitting polynomials on either side of a region of interest. In the run mode, x information from the regions selected in the x-y plane are stored as one dimensional arrays.

The dead time was monitored using channel zero of the ADC's. When a monitor counter was used, the single channel analyzer output was scaled and fed into channel zero of the ADC's. When a monitor counter was not used, the output of the current integrator was sent through a

voltage to frequency converter whose output was then scaled and fed into channel zero. The beam current and/or gas pressure was adjusted to keep the dead time less than ten percent at the forward angles.

At the end of each run the data was punched out on cards and a line printer listing was obtained. At least one data point was repeated during each experiment as a consistency check. If the collimators or detectors were changed during an experiment, a data point was repeated as a geometry and efficiency check.

III.7. Collection Efficiency for Tritons and Helions

Since the trition and helions were detected simultaneously in the $^{19}F(p, ^{3}He_{t})$ and $^{16}O(\alpha, ^{3}He_{t})$ experiments, any systematic error in the geometry or charge collection cancels out in the ratio of the cross sections. The only other uncertainties in their relative cross sections are statistical errors and detection efficiency differences for the two particles.

The detection efficiency of Si detectors is essentially unity for particles that deposit more energy in the sensitive region of the detector than the inherent noise of the detection system. However, because the detectors are of finite size and the ΔE and E crystals are mounted separately, it is possible that some particles will be lost through scattering. To reduce this effect, the height of the detector collimator was always less than 53 mm, as compared to the diameter of the detector crystal, which was 80 mm, and the ΔE detector was placed with the gold coated side facing the E detector, which reduces the crystal separation from 7 mm to 4 mm.

The detection loss for the ΔE-E system was calculated for helions and tritons assuming that particles were lost in the E detector due to

single Rutherford scattering in the ΔE detector (Ja 62). The calculated loss for particles incident at the top and center of the collimator was less than 20 events per million for both helions and tritons. The loss of particles due to reactions in the crystal should be approximately equal for tritons and helions and of the order of 2%. Thus the relative detection efficiency for tritons and helions is approximately 98%.

III.8. Data Reduction

III.8.a Extraction of Cross Sections

The one dimensional particle spectra from TOOTSIE were reduced on the Sigma-7 computer. The area, statistical error and centroid for each peak were obtained. The statistical error is calculated as $\left((N + B) + B\right)^{\frac{1}{2}} / N$, where N is the net number of counts and B is the background. A code using card input (PEAKSTRIP written by R. A. Paddock) was used to reduce part of the data. The remaining data was reduced with MOD7 (written by D. Bayer) using a flying cross on a storage scope for input.

The reduced data, the geometry of the experiment, target characteristics, and the individual run data were input to a computer program to extract the lab and CM cross sections. For the data taken on CaF_2, the program FOILTAR (Pa 69) was used. The program GASCELL (Pa 69) was used for the remaining data. These programs calculate the cross sections, the CM angle of the detected particle, the statistical and total errors per point. These errors were formed by adding in quadrature the statistical and experimental errors. When cross sections had been obtained for all of the data for a given reaction, the cross sections for repeated points were added by weighting a point

X_i as $(w_i/\Sigma w_j)X_i$, where w_k is the square of the error for the point x_k.

III.8.b Normalization of CaF_2 Foil Data

The $^{19}F(p, ^3He_t)$ data taken with CaF_2 evaporated on a carbon backing was normalized to the ground states of data taken with a gas cell filled with CF_4. This was necessary because a reliable measure of the thickness of ^{19}F as CaF_2 was impossible to obtain. The NaI monitor counter used did not resolve the elastic peaks of ^{16}O and ^{19}F and the possible presence of calcium as CaO or CaO_2 made normalization to the calcium elastic scattering unreliable. Very small pieces of the CaF_2 were observed to flake off the backing, making a single normalization for all the data unreliable also.

The ground states of the CaF_2 data were normalized to the CF_4 data, point by point, then these normalization constants were applied to the remaining data. A polynomial least squares fitting routine was used to extrapolate over any small angular difference between the two sets of data. The statistical and total errors for the ground state CF_4 data were retained for the ground state cross section errors. The normalization error was taken as the statistical errors for both sets of ground state data added in quadrature. This was then added in quadrature with the total error for each of the other states in the CaF_2 data to get the total cross section error for the remaining states.

III.9. Experimental Uncertainties

The beam energy was determined by measuring the magnetic fields of the analyzing magnets with NMR probes. A beam transport calibration was performed with protons between 23 and 41 Mev by the spectrograph

crossover technique (Tr 70). The NMR measurements agreed with the determined beam energies to less than 75 kev. No corrections were made to the beam energy as measured by the NMR probes.

The total uncertainty in the lab angle measurement is estimated as $\pm 0.3^{\circ}$ with contributions from the electrical readout and beam alignment. No corrections to the angluar distributions were included for the angular acceptance of the collimators (0.4° to 0.8°).

The geometry error, including solid angle and gas target thickness, is angular dependent. These errors were calculated by the program GASCELL (Pa 69) assuming an error in the solid angle of approximately 0.4%, a gas pressure error of 0.05 inches of mercury and a temperature error of 1.5°C.

A 1% error was assigned to the charge integration (Pi 70). This is probably somewhat optimistic for an absolute error, but is quite reasonable for a relative error between experiments.

The statistical error including background subtraction is discussed in section III.8.a. Except for the ground state transitions, this is normally the dominant source of error.

The compiled experimental cross sections include a measurement error, a statistical error and a total error. The measurement error is calculated in the data reduction programs (Pa 69) by adding in quadrature all of the errors except the statistical error. The total error is then obtained by adding the measurement and statistical errors in quadrature. All of the errors are to be interpreted as one standard deviation.

III.10. Particle Spectra and Resolution

The experimental energy resolution (Figures III.10.b-e) varied with the incident particle, the target used and the particle detected. The electronic noise, as determined by a pulser, was typically 30 to 45 kev FWHM. The energy spread of the beam was less than 25 kev for deuterons, 40 kev for protons and helions and 50 kev for alphas. The remaining contributions to the energy resolution are due to kinematic spread, the difference in target energy loss per unit length for the incoming and outgoing particles, and energy straggling.

The energy level diagrams of ^{17}O and ^{17}F are shown in Figure III. 10.a. With the exception of the state in ^{17}F at 5.215 Mev, which had not previously been observed, the energy, spin and parity assignments are taken from Ajzenberg - Selove (Aj 71). The energy assignment of 5.215±0.012 Mev for the state in ^{17}F is a weighted average obtained from $^{16}O(^{3}He,d)^{17}F$(5.204±0.013 Mev), $^{16}O(^{4}He,t)^{17}F$ (5.227±0.010Mev) and $^{19}F(p,t)^{17}F$ (5.217±0.014 Mev). The error of this weighted average is then added in quadrature with a 10 kev uncertainty due to energy extrapolation in all of the above determinations.

Representative particle spectra are shown in Figures III.10b-e. The experimental resolution shown is the FWHM of the ground state. Many of the states above approximately 5.5 Mev are unresolved (Aj 71).

Triton and helion spectra from ^{19}F + p are shown for both the CF_4 and CaF_2 targets (Figures III.10.d and III.10.e respectively). At approximately 40 degrees in the lab, the $^{13}C(p,t)^{11}C$ ground state would not be resolved from the state in ^{17}F at 5.215 Mev. However, the ^{11}C ground state was not observed in the spectra from either target at angles where it would have been resolved.

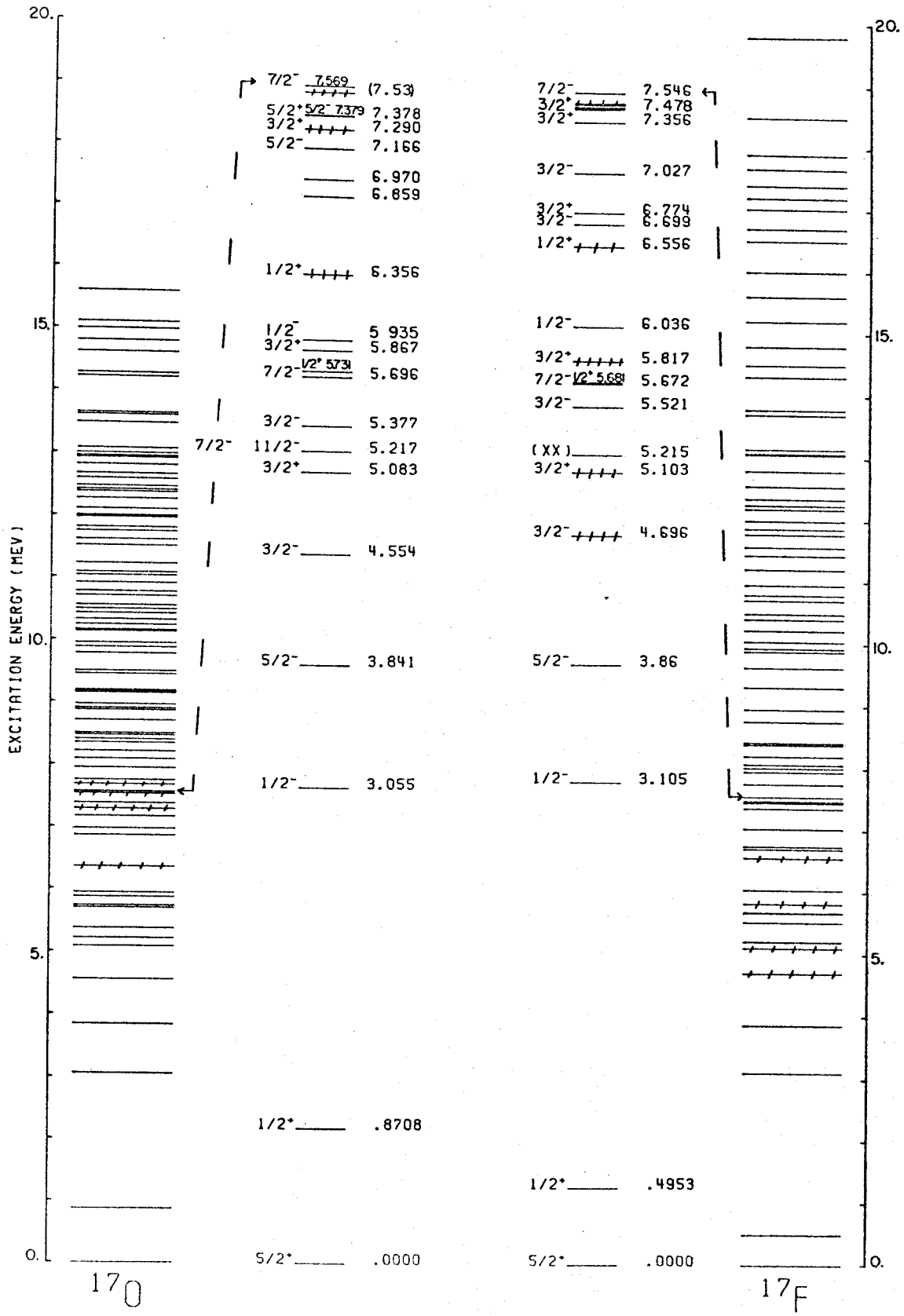

Fig. IV.10.a Level structure of the mirror pair ^{17}O - ^{17}F from Reference Aj71. The first 7.5 Mev of excitation is expanded in the center. The state at 5.215 Mev

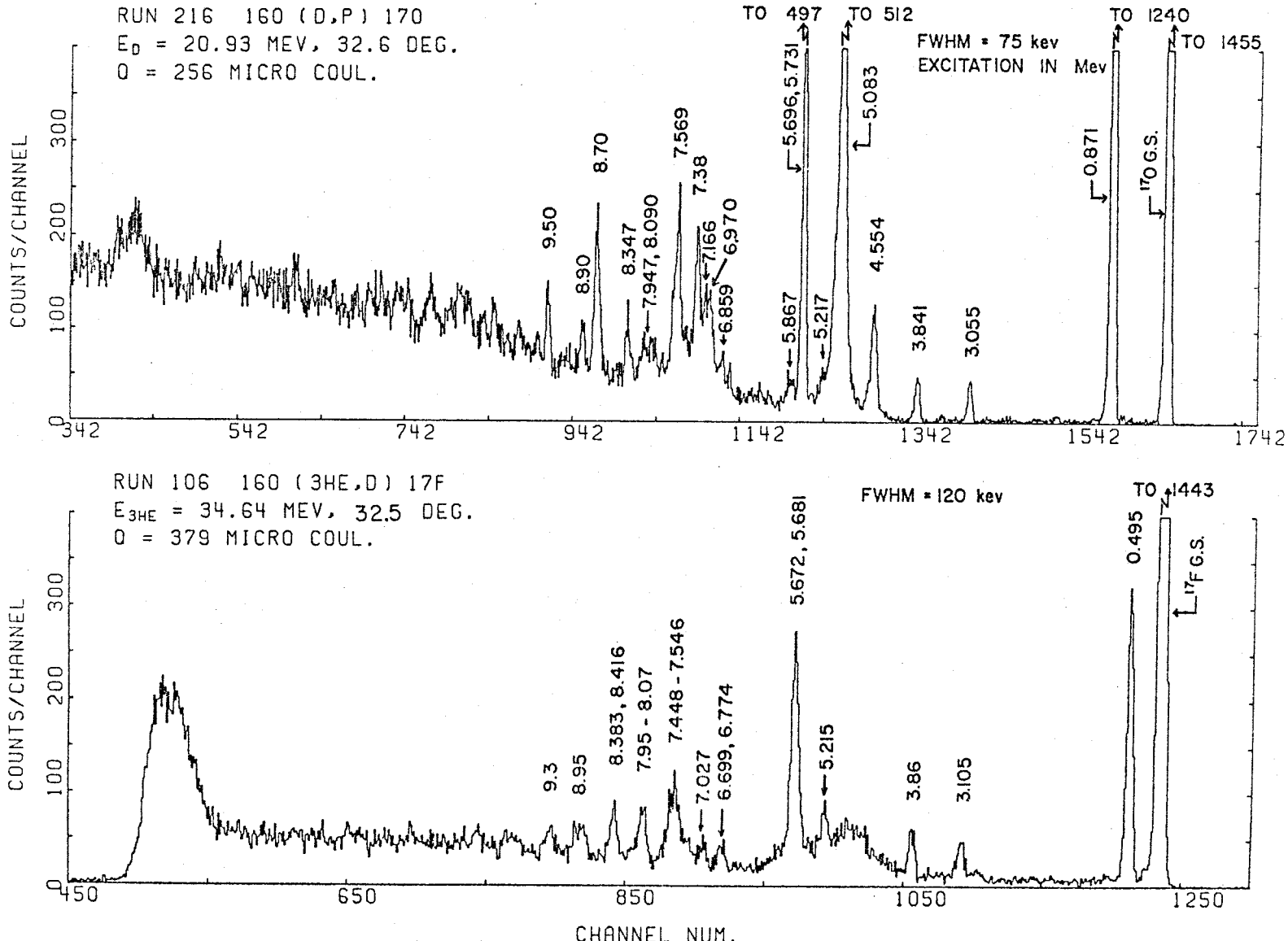

Fig III. 10. b Spectra of ^{17}O from the (d,p) reaction and ^{17}F from the (h,d) reaction. The large group at high excitation in ^{17}F are from deuterons going through the collimator.

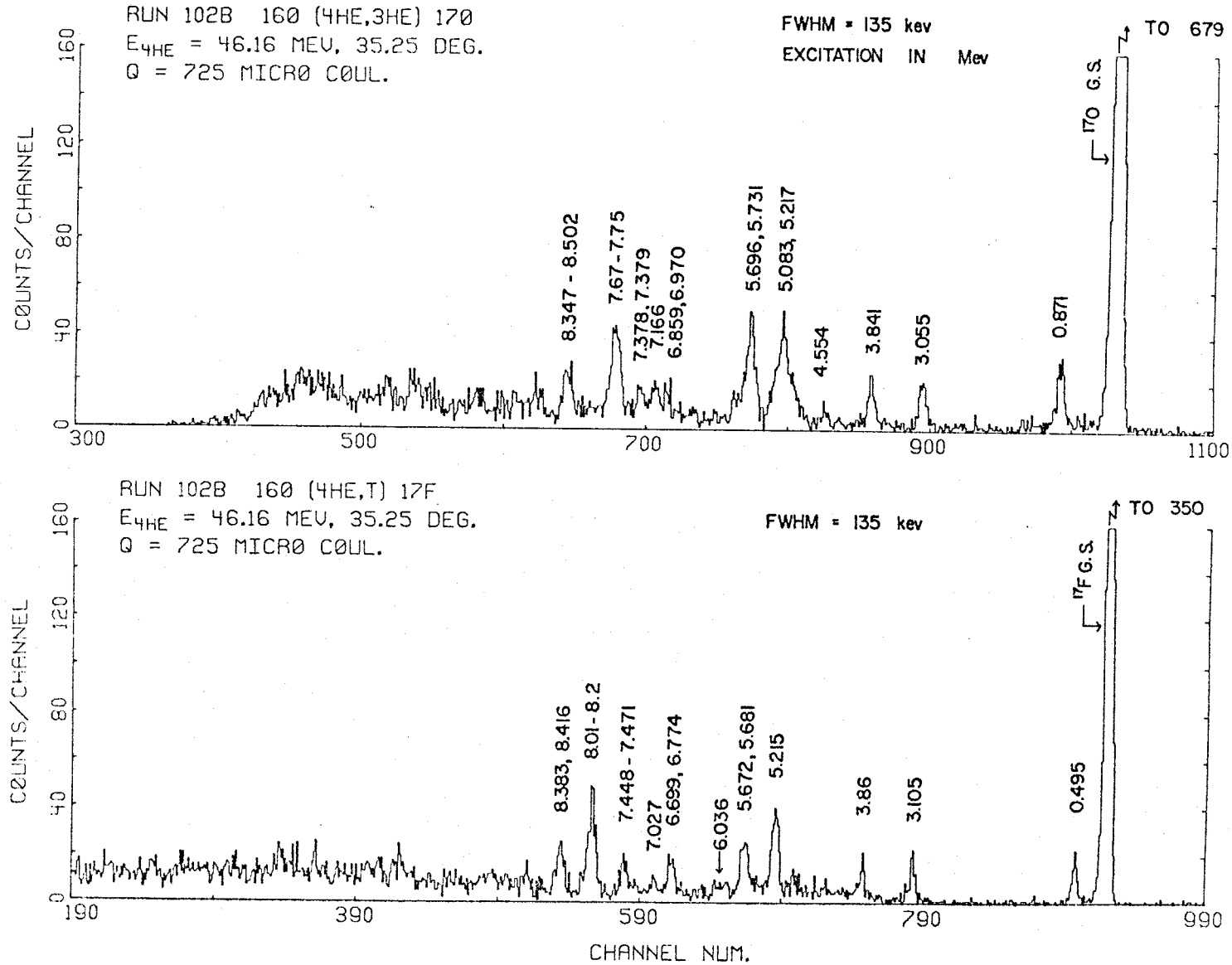

Fig III. 10. C
Spectra of ^{17}O and ^{17}F excited in the (α,h) and (α,t) reactions.

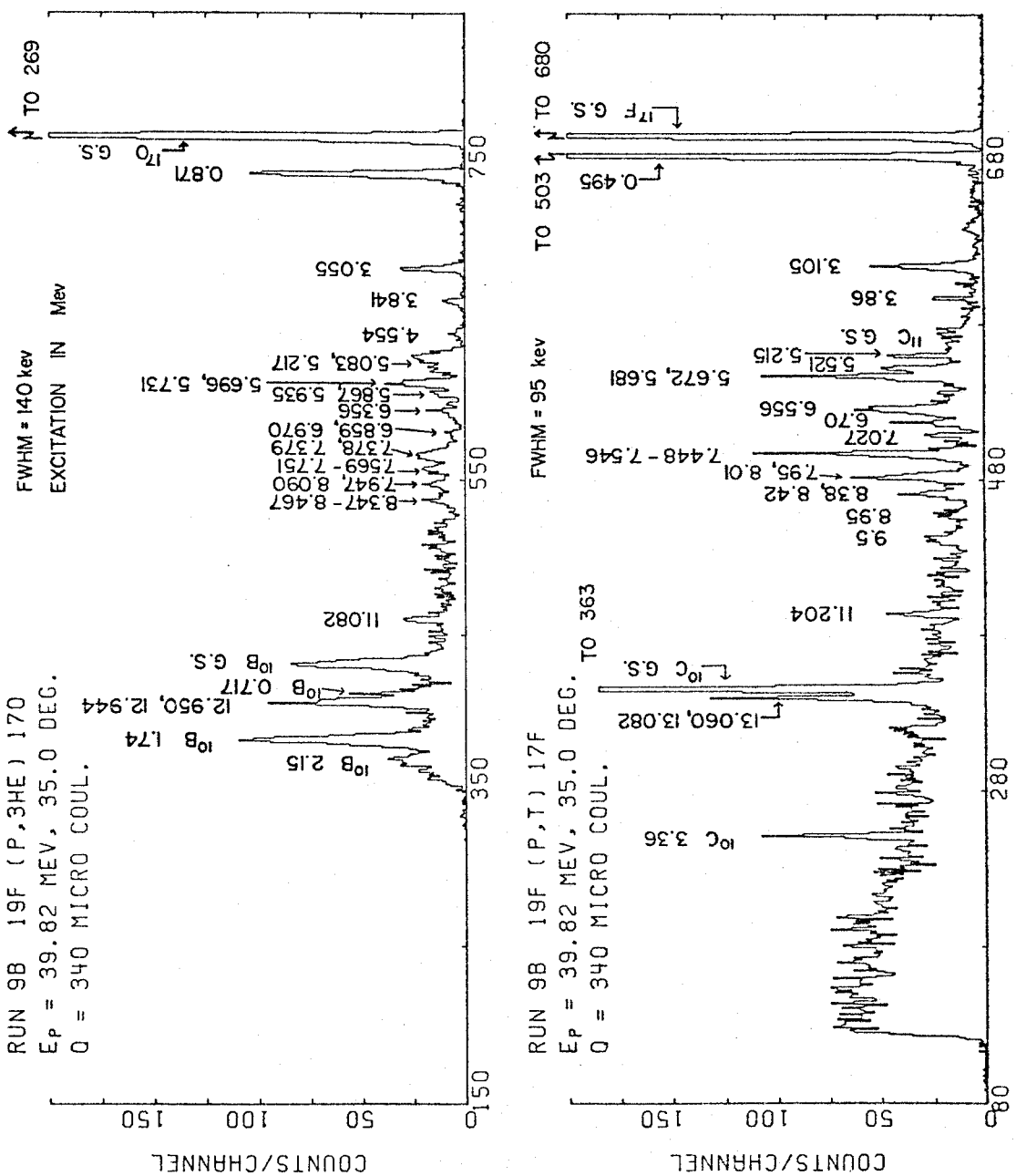

Fig III. 10. d (p, t) reactions

Spectra of 17O and 17F spotted in the (p, 3He) and

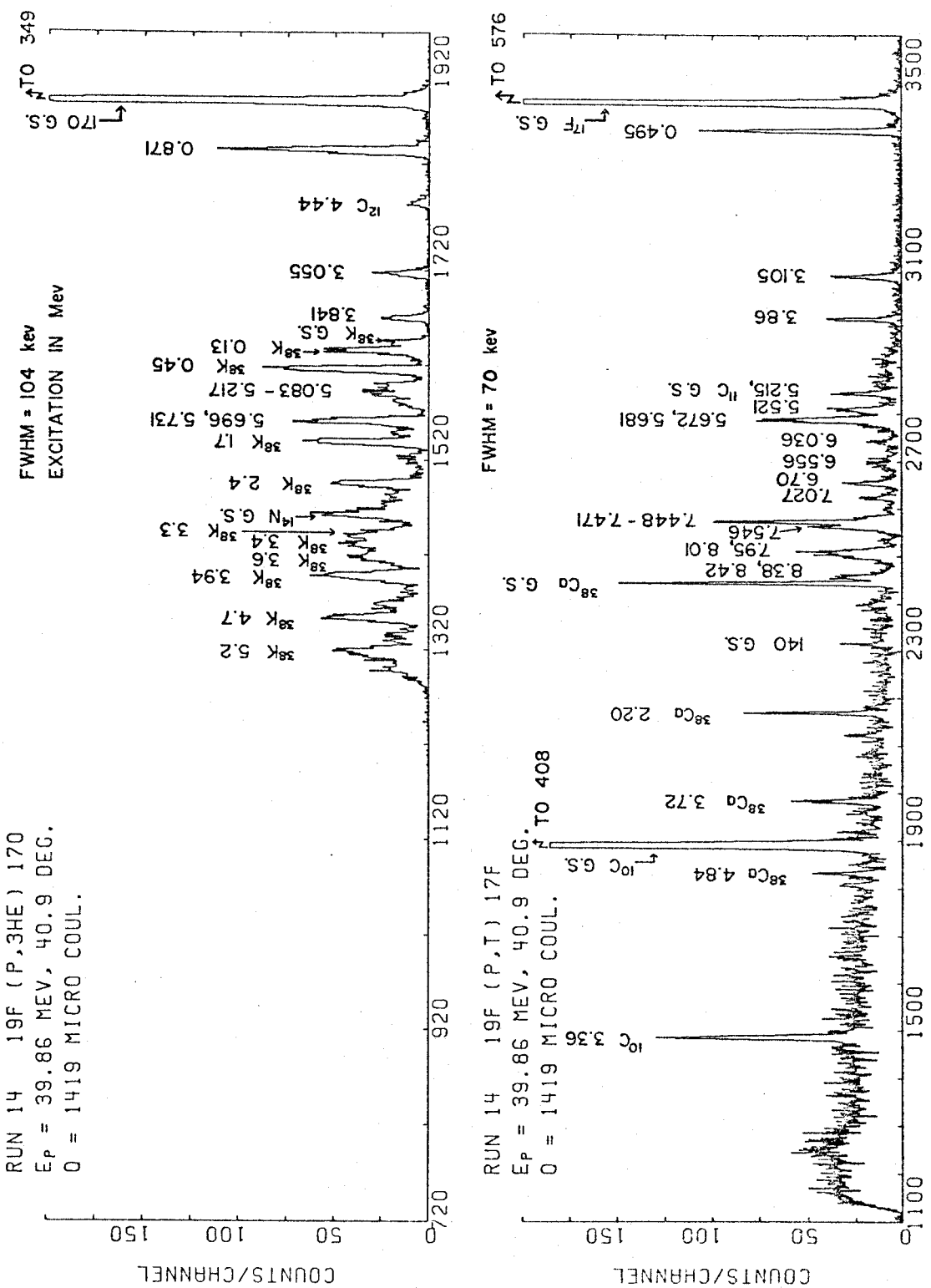

Fig. III. 10. a On F_2 Target
Spectra for the minor reactions (p, ^{3}He) and (p,t)

IV. EXPERIMENTAL RESULTS

IV.1. Introduction

The measured angular distributions and ratios of cross sections are presented in this chapter. The error bars shown on the angular distributions represent the total experimental error and indicate plus and minus one standard deviation from the measured value. The error bars shown on the cross section ratios $(\alpha,t)/(\alpha,{}^3He)$ and $(p,t)/(p,{}^3He)$, represent only the relative statistical error. The relative measurement errors for tritons and helions are discussed in Sections III.9. and III.7., respectively.

A simple shell model picture of ^{17}O and ^{17}F will help the interpretation of the experimental results. Figure IV.1. gives the shell model single particle energies (from reference Ir 70) and some of the basic shell model configurations for ^{17}O. The corresponding configurations for ^{17}F are the same, with all neutrons (ν) and protons (π) interchanged. If one considers ^{16}O as a closed core, then the addition of a single particle in the 2S1d shell gives only positive parity levels. This would give a $5/2^+$ G. S., a $1/2^+$ state at approximately 0.8 Mev, a $3/2^+$ state at approximately 5.1 Mev and no others. These states should be strongly populated in a single particle stripping reaction.

Core polarization with n particles in the 2s1d shells and (n-1) holes in the p shells account for the negative parity states. Considering only 2p-1h excitations (although higher excitations are certainly important), one can easily imagine configurations which could give all the low lying negative parity states. For example, the $1/2^-$ state at approximately 3.1 Mev could have the configuration

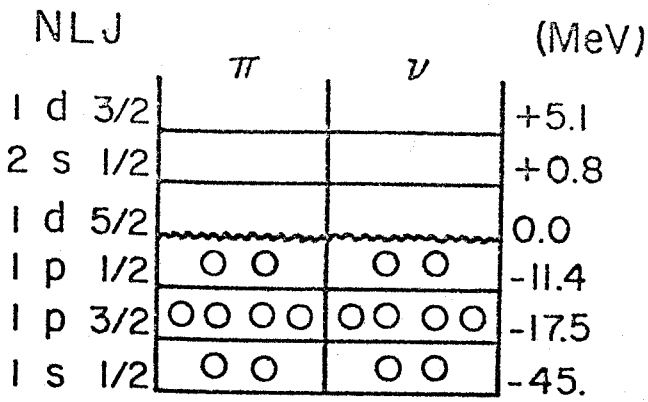

^{16}O (G.S.)
+ 2p2h + 4p4h + ···

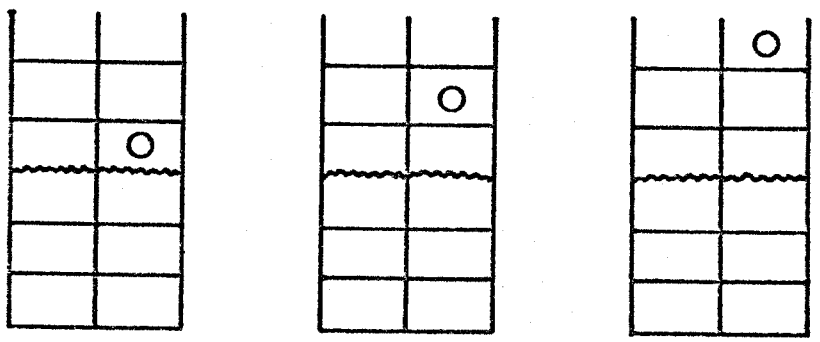

+ 3p2h + 5p4h + ···

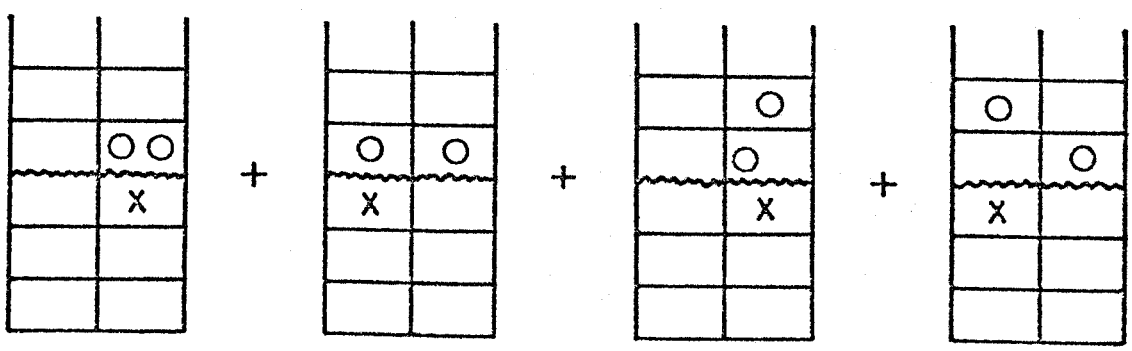

^{17}O ($1/2^- \rightarrow 11/2^-$)
+ higher 2p1h + 4p3h + ···

Fig. 1 Simple shell model description of ^{16}O and the low lying levels of ^{17}O. Core excitations are possible.

$$\left[\left(d_{5/2}^{2} \right)_{j_1=0}^{t_1} \times \left(p_{1/2}^{-1} \right)_{j_2=1/2} \right]_{J=1/2}^{T=1/2} .$$

The isospin coupling that would lead to the lowest $1/2^-$ state with this $j_1\ j_2$ configuration is not well understood (Wi 71). According to the prescription of Zamick (Za 65), the $t_1=1$ configuration would lie lower than the $t_1=0$. The pairing energy of the $d_{5/2}^2$ configuration reduces the $(d_{5/2} - p_{1/2})$ difference from 11.4 Mev to the observed 3.1 Mev.

The ^{16}O core is known to be deformed by p-h excitations without the addition of the extra nucleon (Mo 56, En 65, Br 66). The addition of 3p-2h and 5p-4h excitations are necessary to account for the four extra $3/2^+$ states in the region of 5 to 8 Mev (Bi 68). The low lying negative parity levels in ^{17}O and ^{17}F are thought to have an appreciable 4P-3h component (Go 67, El 70).

IV.2. $^{16}O(d,p)^{17}O$

This reaction has been studied extensively in the energy range 0.3 to 15.0 Mev (Aj 71). The only previously published results above 15 Mev are for the ground and first excited states. These are at 19 Mev (Fr 53) and 26.3 Mev (Ma 62, Te 64).

A spectrum for the $^{16}O(d,p)^{17}O$ reaction at 20.93 Mev is shown in Figure III.10.c. The first three strong states in the spectrum have previously been assigned as single particle states (Co 63). These are the ground state (1d5/2), 0.871 Mev (2s1/2) and 5.083 Mev (1d3/2).

On the basis of the strength and shape of the state in the (d,p) reaction, Hosono (Ho 68) assigned the known $7/2^-$ state at 5.696 Mev

as a $1f_{7/2}$ single particle level. This is somewhat questionable since the $1d_{5/2} - 1f_{7/2}$ spacing is typically 14 Mev in the heavier nuclei (Co 63). If this state were the $1f_{7/2}$ single particle state, it should be strongly excited in an $(\alpha, {}^3He)$ reaction (Section IV.4). Since this was not observed, it is concluded that the 5.696 $(7/2^-)$ level does not contain a large amount of $1f_{7/2}$ strength.

The remaining states below approximately 7 Mev are not strongly populated as expected from their np - (n-1)h interpretation. No attempt was made to extract the weak 5.217 Mev state from the tail of the strong 95 kev wide state at 5.083 Mev.

The extracted angular destributions are shown in Figure IV.2. These were compared to the results of Hosono at 14.3 Mev (Ho 68), Keller at 15. Mev (Ke 61), Freemantle et al. (Fr 53) at 19. Mev, and Mayo and Testoni (Ma 62) at 26.3 Mev. All of the results of Hosono are approximately 75% higher than the present data and the three other sets of data. For the first two negative parity levels, these data are a few per cent lower than that of Keller. The other levels of Keller are quite similar in shape and magnitude. Freemantle et al. and Mayo and Testoni only extracted cross sections for the ground and first excited states. The results of Keller and this data agree within the errors. The data of Mayo and Testoni are a few percent higher than these data at the extreme forward angles. At the other angles their data are very close to these results.

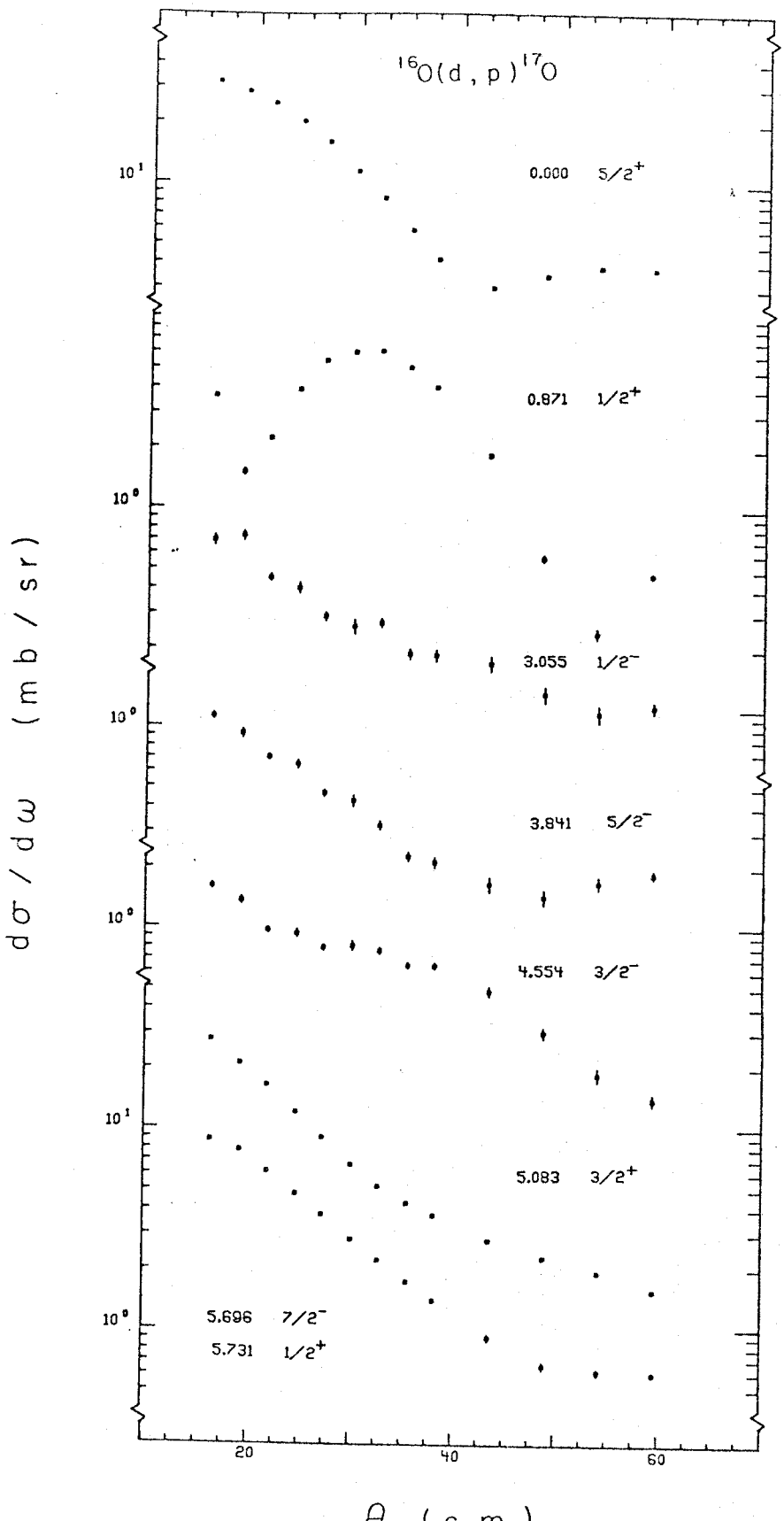

Fig. IV. 2 Experimental angular distributions obtained for the (d, p) reaction.

IV.3. $^{16}O(^{3}He,d)^{17}F$

A spectrum for the $^{16}O(^{3}He,d)^{17}F$ reaction at $E_{^{3}He}$ = 34.64 Mev is shown in Figure III.10.c. The very broad group appearing at large excitation energy is due to deuterons which passed through the rear defining aperature. The state at 5.215 ±0.012 Mev has not been reported previously (Aj 71). From the energy and angular distribution of the state, it is assigned as the analog of the 5.217 Mev $(^{7}/_{2}\ \ 11/_{2})^{-}$ state in ^{17}O. As in the $^{16}O(d,p)^{17}O$ reaction, the strong transitions are to the single particle states. The $1d^{3}/_{2}$state at 5.103 Mev is 1.5 Mev wide and was not extracted from the data.

The extracted angular distributions are shown in Figure IV.3. In general they are more forward peaked than the $^{16}O(d,p)^{17}O$ angular distributions. The second minimum in the $1/2^{+}$ distribution at approximately 30^{o} c.m. is less pronounced than in the (d,p) reaction. The distribution to the 5.215 Mev state shows very little structure indicating a possible two step formation process.

IV.4. $^{16}O(\alpha,^{3}He)^{17}O$

Because of the large Q values involved, reactions of the type $(\alpha,^{3}He)$ and (α,t) are expected to populate states involving large angular momentum transfers (St 67). For these reactions on ^{16}O at E_{α} = 46.16 Mev, the momentum matching condition $|K_{I} - K_{0}|\ R \sim L$ suggests that states of angular momentum transfer L = 2, 3, 4 would be preferentially populated over states with L = 0, 1.

A spectrum for the $^{16}O(\alpha,^{3}He)^{17}O$ reaction is shown in Figure III. 10.b. The extracted cross sections are shown in Figure IV.4. As expected from the momentum matching condition, the $2S^{1}/_{2}$ state at

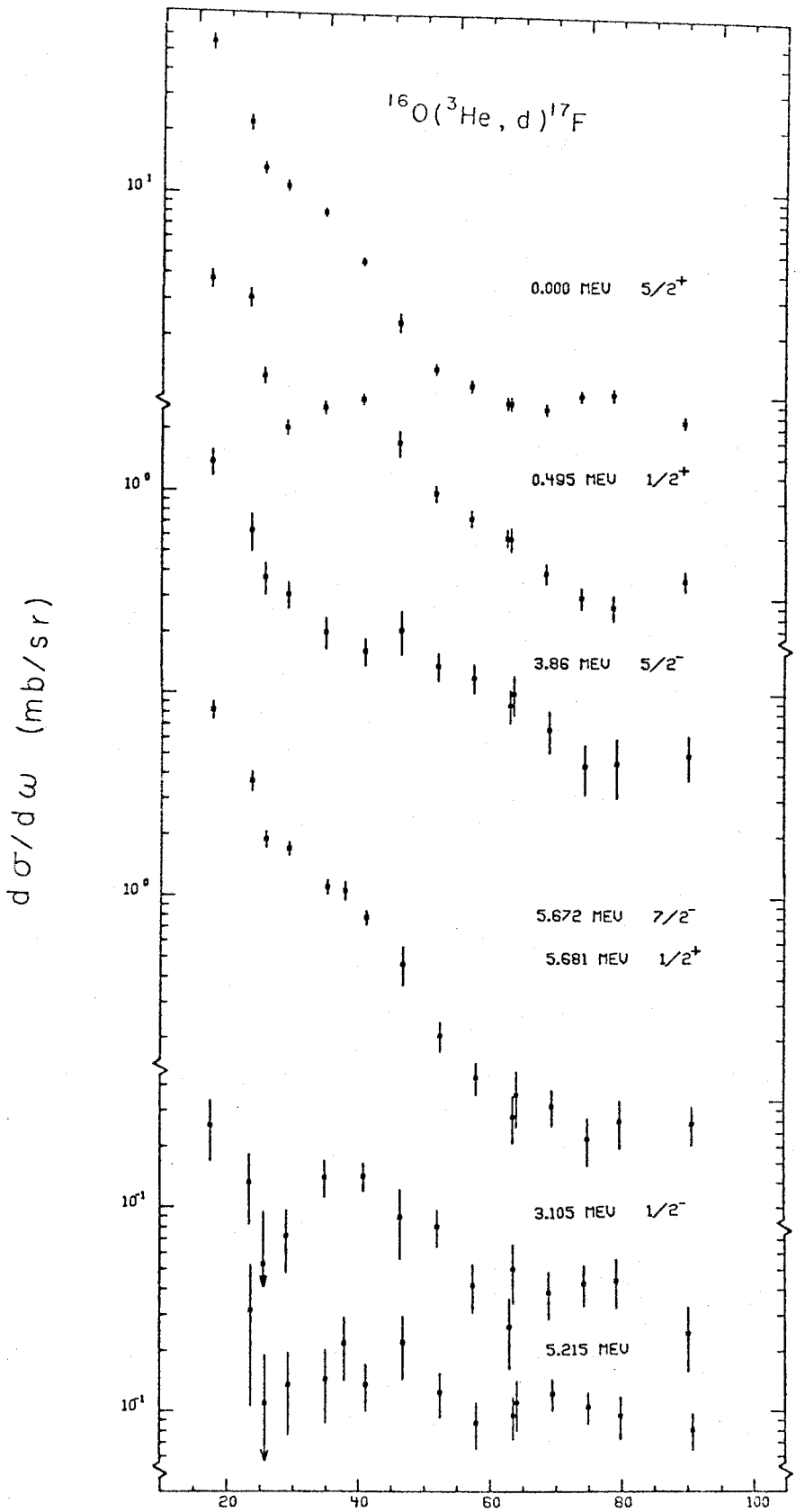

fig III. 3

Experimental angular distributions obtained for the (3He, d) reaction.

0.871 Mev is weakly populated. The 3.814 Mev $5/2^-$ state is also weakly populated. Thus this state is interpreted as having a (n+1)p - nh configuration that corresponds to a small component of the np - nh ^{16}O ground state wavefunction (Br 66). From a comparison with the (α,t) reaction (Section IV.5) and from the angular distribution (Figure IV.4), the 5.1 Mev doublet is primarily the 5.217 Mev state. The angular distribution of the 5.7 Mev doublet indicate that it is largely the 5.696 Mev $7/2^-$ level. From the strength of the transition and the slow fall off with angle, it is concluded that this state is not the $1f_{7/2}$ single particle level as assigned by Hosono (Ho 68).

The ground and first two excited states exhibit the characteristic $(\alpha,{}^3He)$ angular distributions for reactions that are considered as direct (St 67). The large momentum mismatch results in a forward peaking for all L values, a rapid fall off and not very much structure. This makes the complex stripping reaction a rather poor tool for spin-parity assignments.

IV.5. $^{16}O(\alpha,t)^{17}F$

A spectrum for the $^{16}O(\alpha,t)^{17}F$ reaction is shown in Figure III.10.b. This spectrum was obtained at the same time as the $(\alpha,{}^3He)$ spectrum shown in the same figure. The extracted angular distributions are shown in Figure IV.5. The general features of the (α,t) reaction are interpreted in the same manner as the preceding $(\alpha,{}^3He)$ reaction. The previously unobserved state at 5.215 Mev is strongly populated in this reaction.

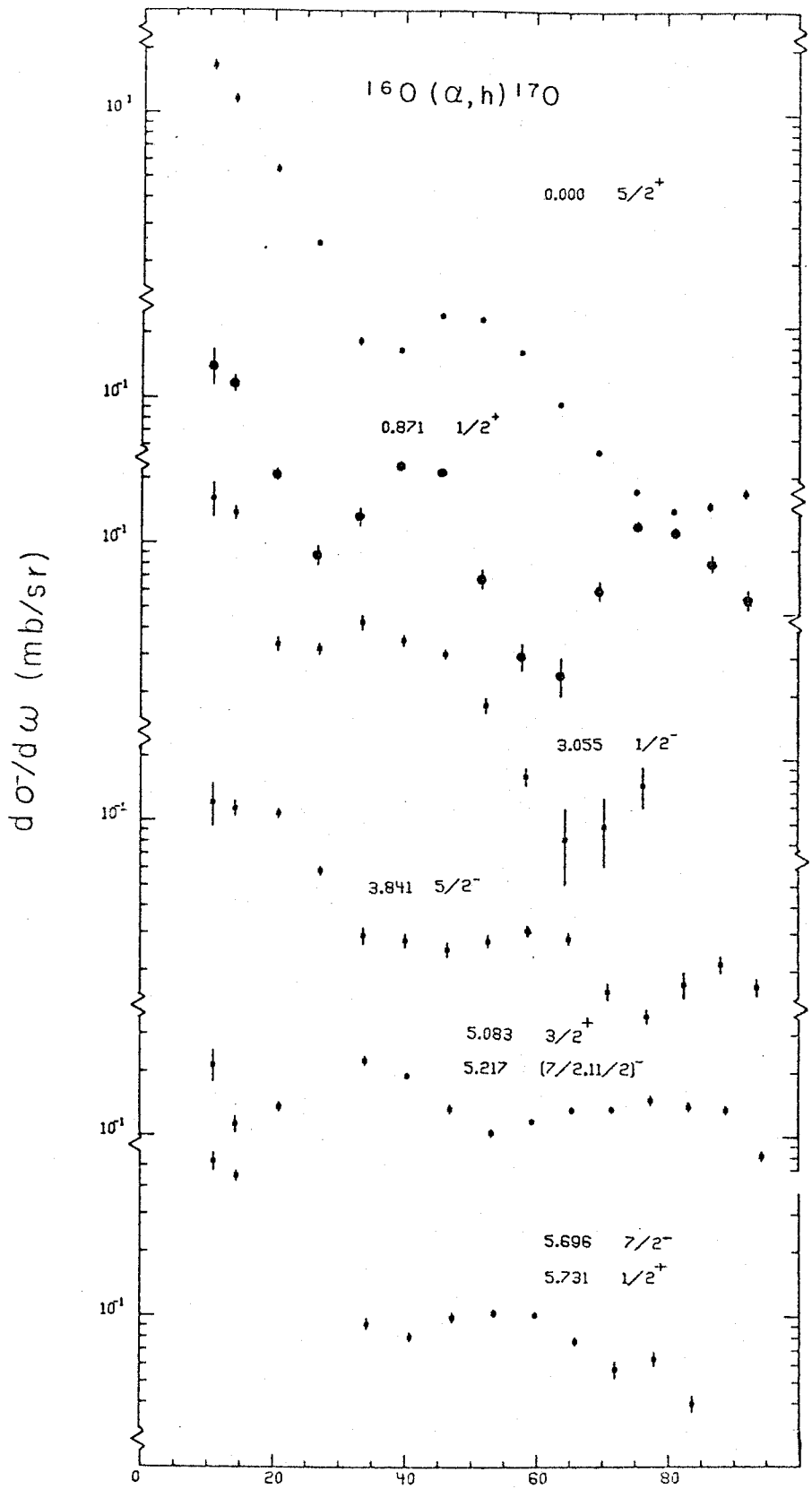

Fig. III. 4

Experimental angular distributions obtained for the (α,h) reaction.

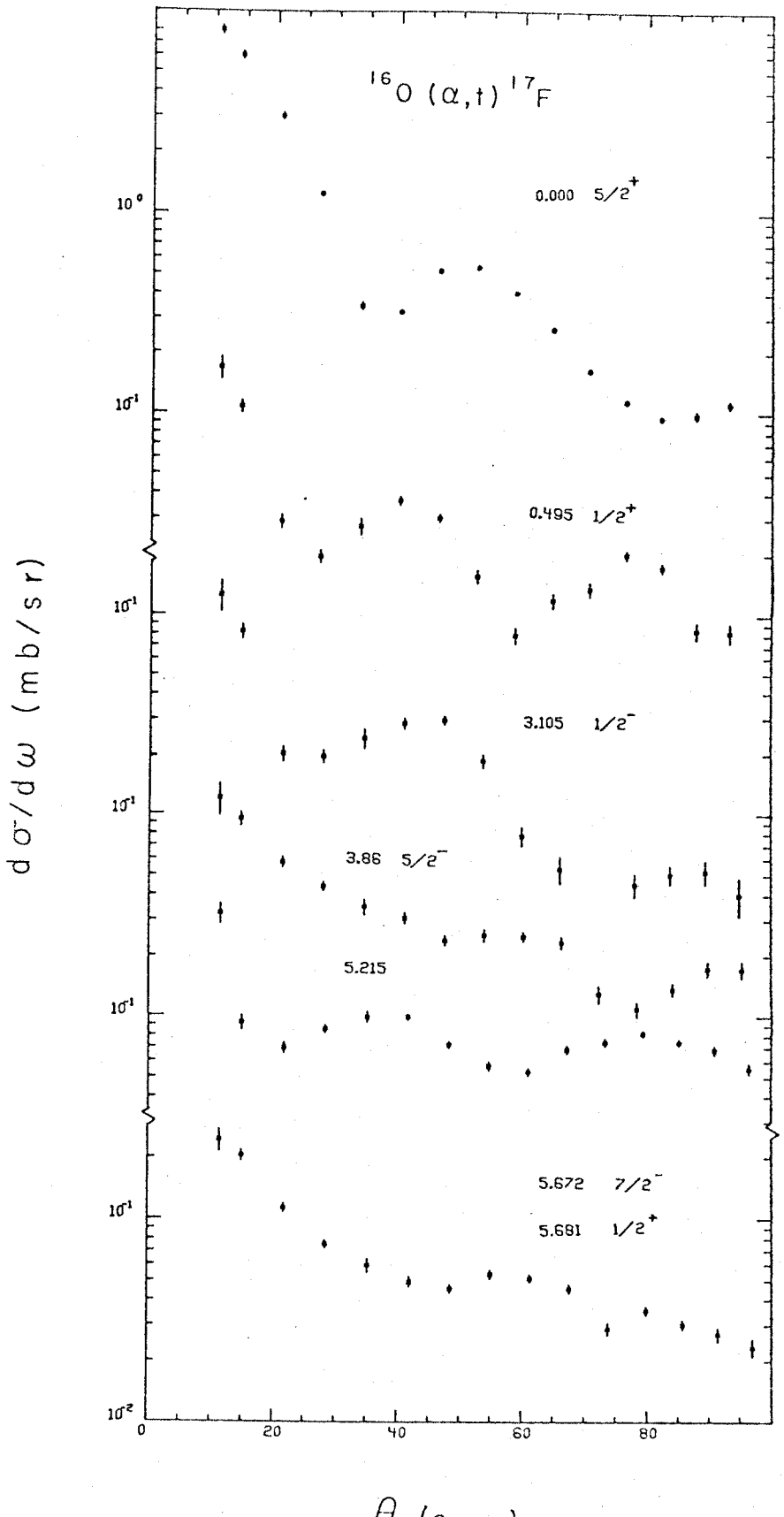

Fig. IV. 5
Experimental angular distributions obtained for the (α,t) reaction.

IV.6. The Ratio $(\alpha,t)/(\alpha,{}^3He)$

The experimentally observed angular distribution ratios for (α,t) to $(\alpha,{}^3He)$ on an oxygen 16 target are shown in Figure IV.6. The error bars shown represent the total statistical error. A weighted average for each angular distribution is shown, where each data point is given a weight in inverse proportion to the square of its error. The structure of the ratios and their deviation from unity are interpreted as Q value effects and differences in the bound state for the captured nucleon. The effects are discussed in Chapter V.

IV.7. $^{19}F(p,{}^3He)^{17}O$

Spectra for $^{19}F(p,{}^3He)^{17}O$ reaction are shown in Figures III.10.d and III.10.e for the CF_4 gas and CaF_2 foil targets respectively. The resolution difference is due to target thickness. Most of the $1p1/2$ hole strength appears in the 3.055 mev state (Figure III.10.a).

The extracted angular distributions are shown in Figure IV.8. The angular distributions for the ground and first excited state were compared to the results of Cole et. al. at 30.5 Mev (Co 67). Their results are a few per cent higher than these data. The angular distribution shapes are quite similar.

IV.8. $^{19}F(p,t)^{17}F$

Spectra for the $^{19}F(p,t)^{17}F$ reaction are shown in Figures III.10.d and and III.10.e. The (p,t) data was taken at the same time as the $(p,{}^3He)$ data shown. The previously unobserved 5.215 Mev level is also seen in this reaction. Most of the $1p1/2$ and $1p3/2$ strengths appear to be in the 3.105 Mev and 5.521 Mev levels respectively (Figure III.10.a).

The extracted angular distributions are shown in Figure IV.8. The

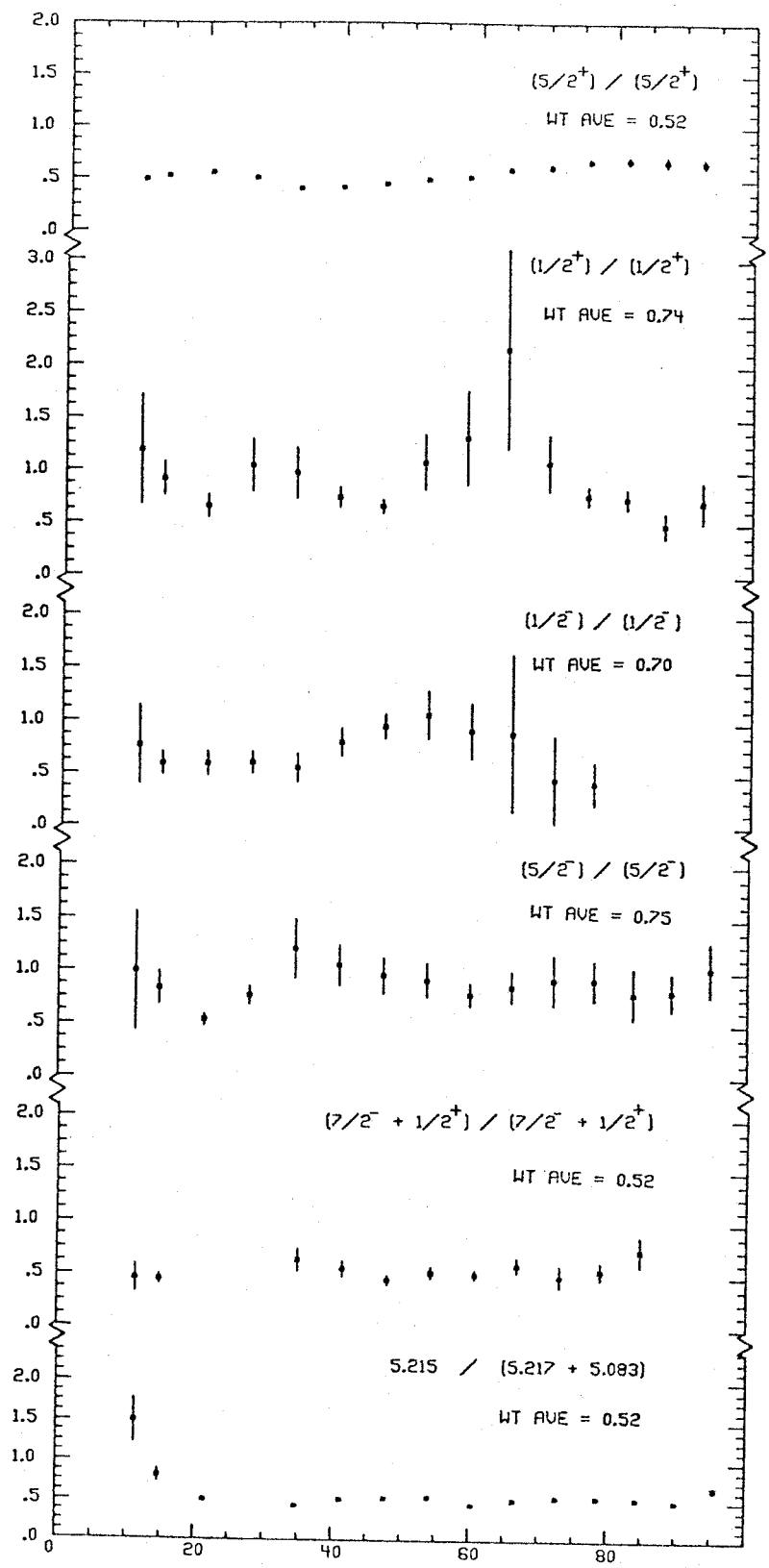

Fig. III.6

Experimental ratios for the (α, t) and $(\alpha, {}^3He)$ reactions. The weighted average is taken over all angles with no $\sin\theta$.

angular distributions for the ground and first excited state were compared to the results of Cole et al. at 30.3 Mev (Co 68). Their data are approximately 50 to 75 percent higher at the first observed maximum than these results. Their ground state angular distribution also has a sharper first minimum.

IV.9. The Ratio (p,t)/(p,^{3}He)

The experimentally observed angular distribution ratios for (p,t) to (p,^{3}He) on a Fluorine 19 target are shown in Figure IV.9. The error bars and weighted averages are interpreted in the same manner as in Section IV.6.

The two-nucleon transfer comparison reaction is more complicated than the one-nucleon transfer case because of the two possible T, S combinations for the neutron - proton pair transferred as compared to only one configuration for two neutrons. This effect as well as the Q value difference for the two reactions are probably responsible for the magnitude and structure of the ratios shown in Figure IV.9. These effects are discussed in Chapter V.

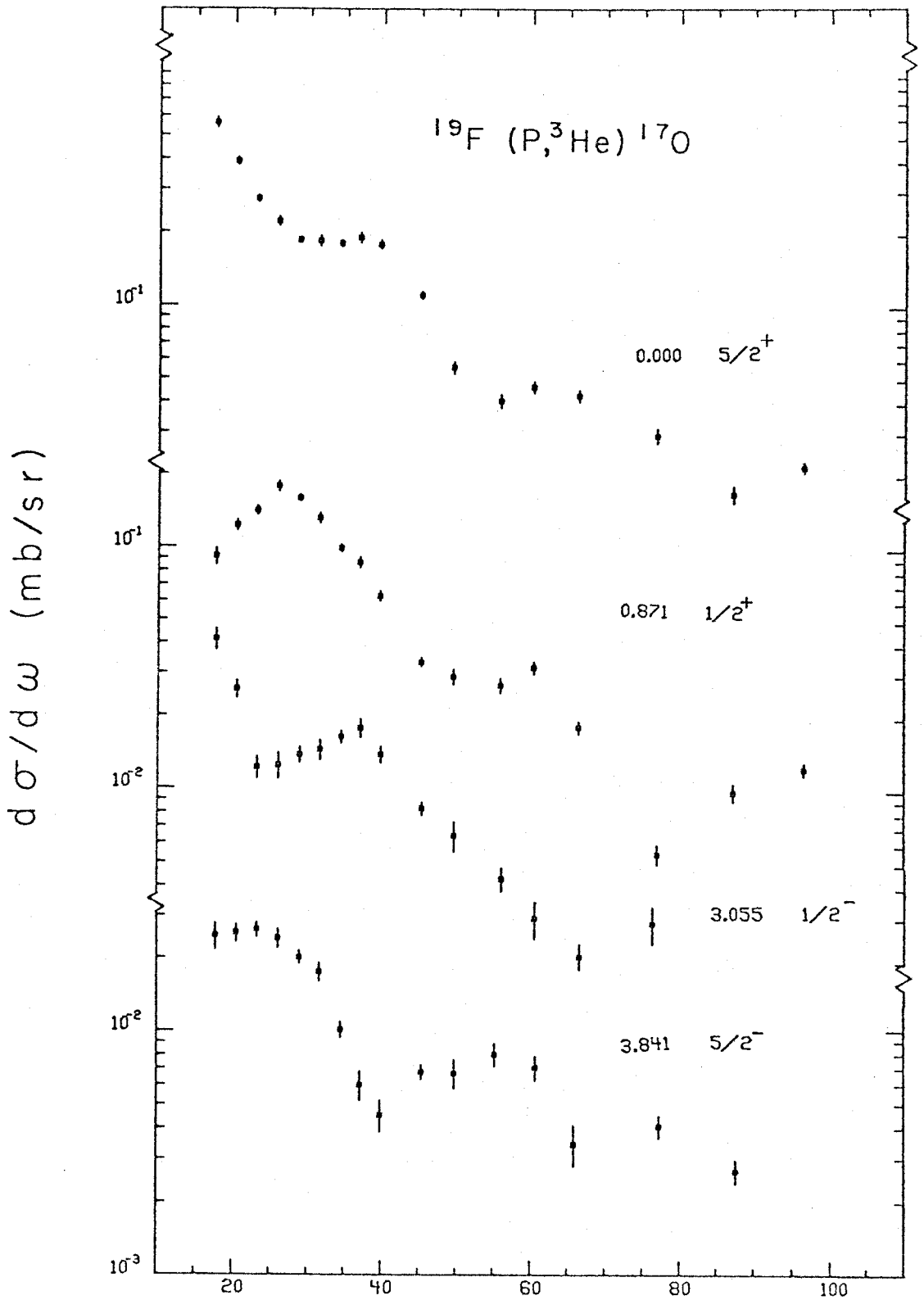

Fig IC. 7

Experimental angular distributions for the (p, ^{3}He) reaction.

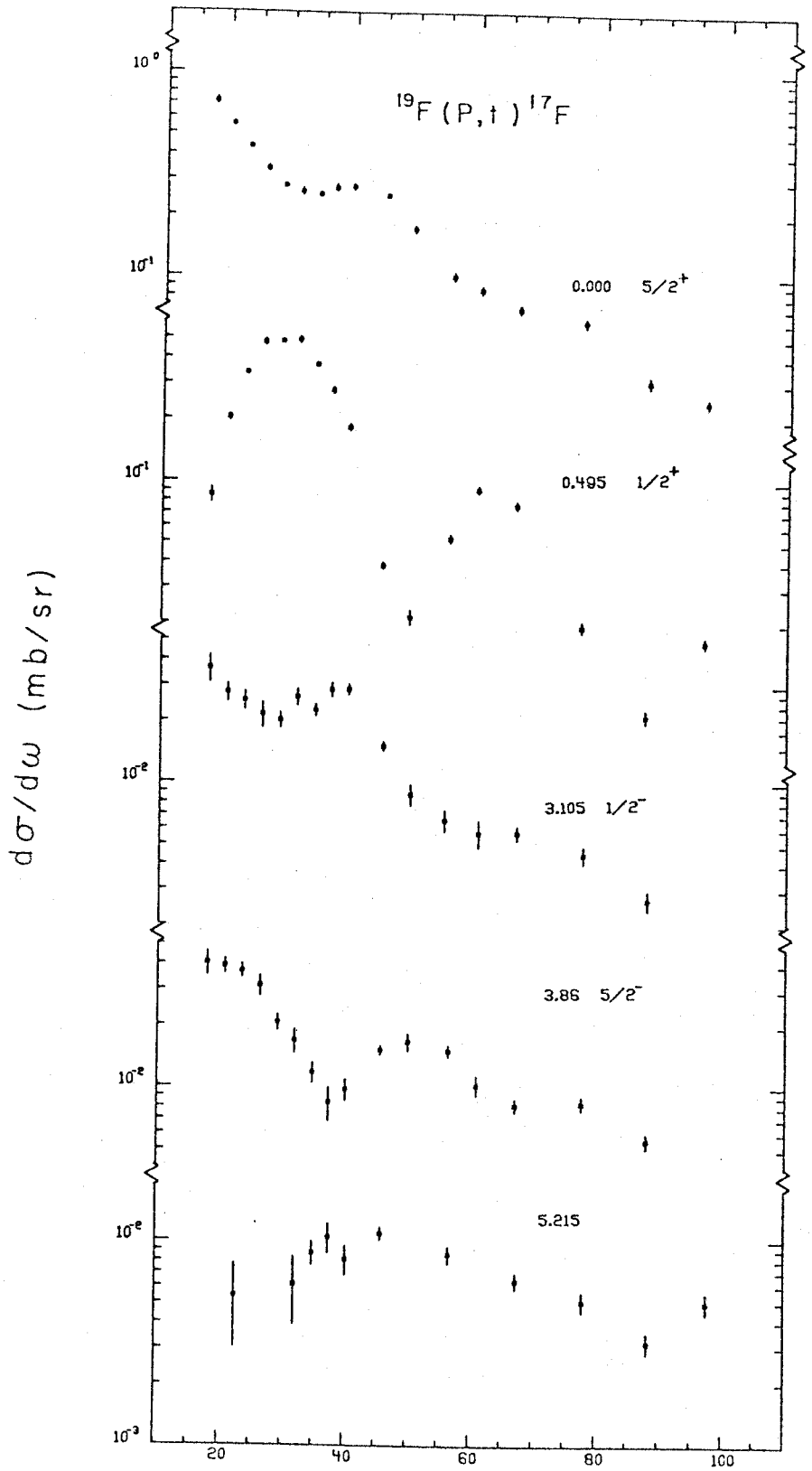

Fig. IV. 8

Experimental angular distributions for the (p, t) reaction.

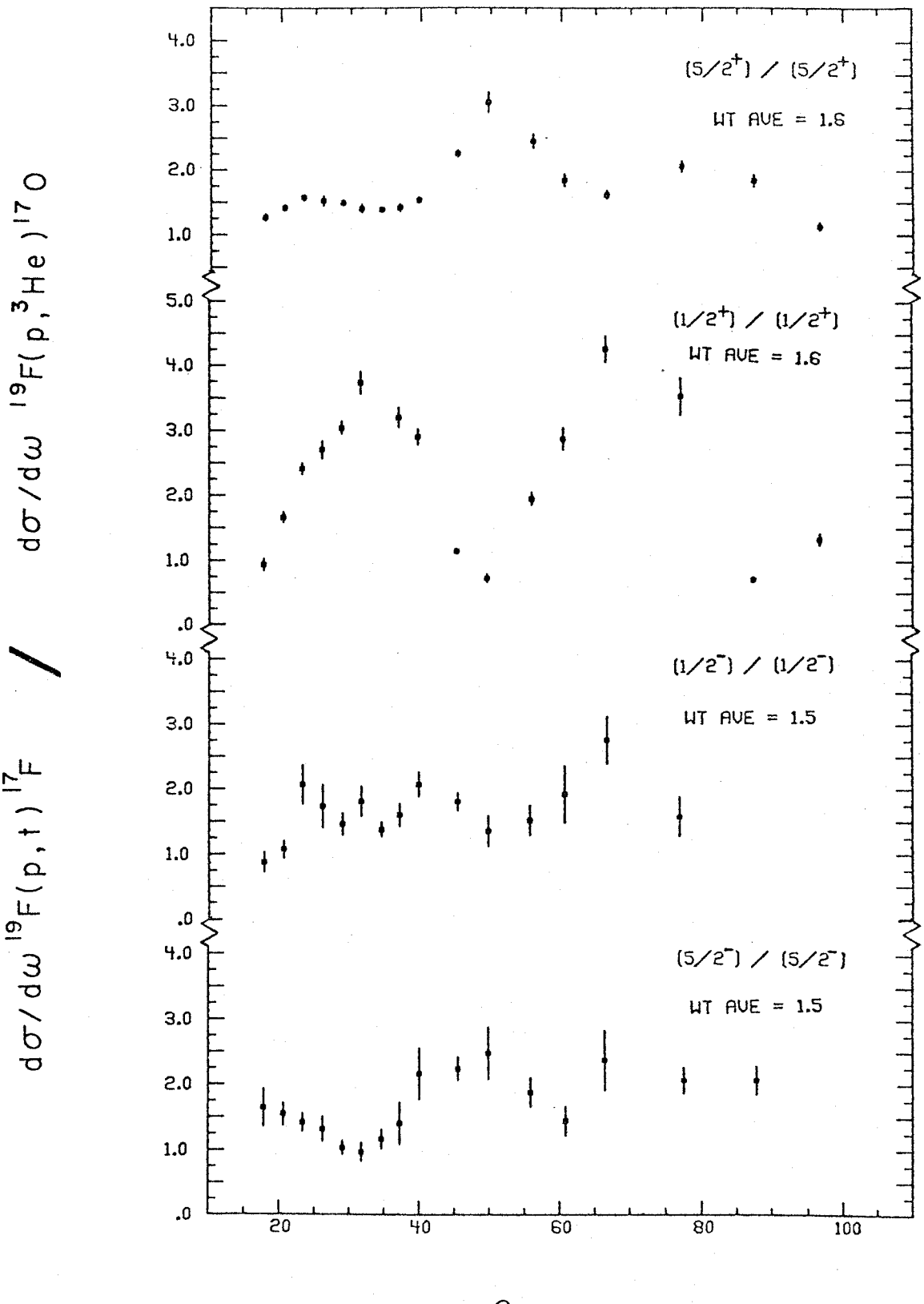

Fig IV.9
Experimental ratios extracted from the (p,t) and (p,h) data.
The solid curves are theoretical predictions [illegible]

V. THEORETICAL ANALYSIS

V.1. Introduction

The results of a DWA analysis of the six transfer reactions studied are presented in this chapter. The analysis of the $^{16}O(d,p)^{17}O$ and $^{16}O(h,d)^{17}F$ reactions consists of a more or less straightforward determination of spectroscopic information. The $^{16}O(\alpha,h)^{17}O$ and $^{16}O(\alpha,t)^{17}F$ reactions are investigated as spectroscopic tools and the DWA predictions are related to an experimental comparison of these reactions. The DWA analysis of the $^{19}F(p,h)^{17}O$ and $^{19}F(p,t)^{17}F$ reactions is based on a shell model description of the two nucleon transfer process.

The first three positive parity levels in ^{17}O and ^{17}F may be adequately described as a single particle coupled to a correlated (np-nh where n is even) ^{16}O core (Section IV.1.). Thus these states behave like a closed core to single nucleon stripping and the DWA should adequately describe this process. Stripping into the negative parity levels is much less clear in a DWA description. Zucker, Buck and McGrory (Zu 68, Zu 69) suggest that the first four negative parity levels in ^{17}O $(1/2, 5/2, 3/2, 7/2)^-$ may be adequately described by five particles in the $1p1/2$, $1d5/2$ and $2s1/2$ orbitals coupled to an inert ^{12}C core. In this limited basis set the direct DWA only allows population of the $1/2^-$ level. The remaining levels require $1p3/2$ correlated holes or $2p3/2$, $1f5/2$ and $1f7/2$ particle orbitals for their description in the direct DWA. These configurations seem unlikely, if only from the usual single particle level spacings in this region (Figure IV.1.).

The simple shell model basis of $1p1/2$, $1d5/2$ and $2s1/2$ particles to describe the first four negative parity levels may be retained if two step processes are included in the description of the reaction

mechanism. The conceptually simple two step process involved in the formation of these levels requires an excitation of the correlated ^{16}O core followed by stripping or the inverse. Penny and Satchler (Pe 64) developed the DWA formalism of this two step stripping process for the (d,p) reaction by including the generalized distorted waves for the inelastic, as well as elastic, channels in the (d,p) stripping amplitude. Unfortunately the resulting set of coupled equations are very difficult to evaluate numerically, even in the zero range approximation (deT 72, As 69). Iano and Austern (Ia 66) considered an approximate treatment of the method of Penny and Satchler in which inelastic channels describable by a collective rotation are present to compete with the allowed direct reaction. In their treatment of the (d,p) reaction, they find that, compared to the one step DWA, the direct plus two step cross sections are: 1) not affected seriously at forward angles, 2) smoothed and increased at back angles, and 3) for a given L-transfer, the two possible J-transfers, $J = L \pm 1/2$, may be selectively enhanced or retarded. Ascuitto and Glendenning (As 69) treat the two step transfer process in a coupled channels formalism which describes inelastic scattering. The transfer process is added as a source term in the residual system. With their treatment applied to the (p,t) reaction in which strong inelastic rotational states are present (AS 71), they find that the two step process can contribute significantly to the shape of the angular distribution at forward angles. In fact the two step process in one case is as strong as the allowed direct transfer.

V.2. Bound State and Optical Model

The DWA analysis of a transfer reaction is characterized by the wavefunction for the transferred particle (particles) and by the description of the incoming and outgoing elastic scattering. The wavefunction of the transferred particle is obtained from a Woods-Saxon well. The elastic scattering is represented by an optical model (OM) potential.

The bound state for the transferred particle is taken as a Woods-Saxon potential with the depth adjusted to give the correct separation energy (SE). The single nucleon SE for the (p,t) and (p,h) calculations is taken as one half the SE of the deuteron or di-neutron pair. Unless specified otherwise, all orbitals used were assumed to have zero binding energy relative to the SE of the $d_{5/2}$ ground state, and all unbound levels were assumed to be bound by 0.1 Mev. For the stripping reactions on ^{16}O, the normal orbital for the bound state of the captured particle is given by j^{π} of the final state. The bound state geometry was taken as $r_o = r_{oc} = 1.25f$, $a_o = 0.65f$. The non-locality (NL) correction suggested by Kunz (Ku 69) was applied to the bound particle as well as the scattering channels in the NL DWA calculations.

The form of the optical model potential used for the analysis is

$$U_{OM}(r) = V_c(r) + V_0 f(X_R) + W_0 f(X_I) + 4W_D \frac{d}{dX_I} f(X_I) + V_{SO} \frac{1}{r} \frac{d}{dr} \frac{d}{dX_{SO}} f(X_{SO}) \vec{L}\cdot\vec{S} \quad , \tag{V.2.a}$$

where $f(X_i) = 1/(1+\exp(X_i))$, $X_i = (r - r_{0i}A^{1/3})/a_i$. The term $V_C(r)$ is the Coulomb potential of a uniformly charged sphere of radius $r_{OC}A^{1/3}$.

The OM potentials given in Table V.2.a., with the exception of the sets YF and Re, are taken from a literature search. The sets YF and Re

Table V.2.a. Optical Model Parameters

Set	Type	Energy (MeV)	$-V_o$ (MeV)	r_R (F)	a_R (F)	r_C (F)	$-W_O$ (MeV)	r_I (F)	a_I (F)	$4W_D$* (MeV)	$-V_{SO}$ (MeV F^2)	r_{SO} (F)	a_{SO} (F)	Ref.
Cam	p	39.7	46.58	1.142	0.726	1.25	2.25	1.268	0.676	30.6 *	29.3	1.114	0.585	Va 69
Fr	p	40.	42.55	1.16	0.75	1.25	3.06	1.37	0.630	14.2	24.2	1.064	0.738	Fr 67
Sn	p	38.4	44.4	1.120	0.690	1.15	2.00	1.40	0.430	19.56*	28.0	1.120	0.690	Sn 68
Va	p	23.4	47.25	1.142	0.726	1.25	—	1.268	0.676	28.24*	16.4	1.114	0.585	Va 69
Ka	p	22.1	53.08	1.10	0.645	1.10	—	1.265	0.543	23.5	22.7	1.207	1.031	Ka 69
Pi-F	d	20.9	94.0	1.03	0.77	1.02	—	1.57	0.83	19.6	17.2	0.78	0.47	Pi 70
Pi-A	d	20.9	72.39	1.23	0.72	1.21	3.62	1.63	0.84	9.44	14.0	0.95	0.48	Pi 70
Ro	d	20.	96.5	1.25	0.69	1.3	—	1.25	0.74	50.0	22.0	1.25	0.69	Pr 72a
Mps	d	20.	114.0	1.15	0.62	1.3	—	1.15	0.615	48.0	20.0	1.15	0.62	Pr 72a
Hi-Z	^{3}He,t	29.	190.	1.14	0.675	1.4	11.2	2.17	0.426	—	—	—	—	Hi 67
Me	^{3}He,t	20.0	135.	1.27	0.65	1.3	23.8	1.60	1.16	—	—	—	—	Me 70
Hu	^{3}He,t	36.	127.1	1.03	0.87	1.4	2.34	1.38	0.85	46.0	6.80	1.14	0.69	Hu 68
B-C	^{3}He,t	40.	160.	1.29	0.574	1.3	12.82	1.78	0.822	—	—	—	—	Ba 69a
Du	α	49.	196.6	1.34	0.58	1.4	53.5	1.34	0.58	—	—	—	—	Du 68
De7	α	42.	206.8	1.349	0.592	1.3	21.1	1.57	0.595	—	—	—	—	De 67**
YF	α	40.	187.	1.28	0.69	1.4	17.0	1.50	0.69	—	—	—	—	YF 59**
Re	α	50.	190.2	1.30	0.663	1.4	16.0	1.65	0.632	—	—	—	—	Re 68**

* $a_D = 0.69\ a_I$

** Fits obtained for the data of these references.

were determined from an analysis of the α elastic scattering data of Yavin and Farwell (YF 59) and Reed (Re 68) using the OM search code GIBELUMP. The energy listed with each set of parameters is the beam energy used to obtain that set. The incoming or outgoing energy dependence of the OM potential was approximated by the prescription $V_0(E) = V(E_0) + 0.33\ (E_0-E)$, where V_0 is the real volume potential, E_0 is the laboratory energy used to obtain that potential and E is the actual laboratory energy of the particle (Be 71, Pr 72a). In all cases the energy extrapolation necessary to match the beam energy used in these experiments was small. The OM parameters listed were selected, by visual inspection, to be the ones which give reasonable fits to the ground and first excited state of the reaction considered. Proton parameters were selected for trial if they gave satisfactory fits to elastic scattering from several light nuclei. The parameters for the other particles were selected from the limited number available on light target nuclei. Since triton parameters of the energy required were not available for light nuclei, they were normally taken to be the same as the available helion sets. The effect of the small symmetry term difference for tritons and helions was investigated in the comparison reactions.

The proton parameters of Cameron and van Oers (Ca 69) have a Gaussian shape for the surface imaginary potential instead of the derivative Woods-Saxon shape used in DWUCK. The Gaussian potentials were converted to the Woods-Saxon form by keeping the strength and width at half maximum the same (Au 71) which gives $W_{WS} = W_G$, $a_{WS} = 0.69a_G$. Also, the spin-orbit potential in DWUCK is given in MeV-F^2 and in terms of $\vec{L}\cdot\vec{S}$, as opposed to JULIE, which used MeV and $\vec{L}\cdot\vec{\sigma}$. For

spin 1/2 particles the conversion is $V_{SO}(DWUCK) = 4 * V_{SO}(JULIE)$.

V.3. $^{16}O(d,p)^{17}O$ Analysis

The $^{16}O(d,p)^{17}O$ reaction has been studied previously (Aj 71). Data to the ground and first excited states for this reaction and the (d,n) reaction has been analyzed by Davison et.al. (Da 70) at E_d = 4 to 6 MeV and by Oliver et.al. at E_d = 8 to 12 MeV (Ol 69, Na 68). DWA analysis of (d,p) data to some of the higher lying states has been reported by Davison et.al. (Da 70) and a PWA by Hosono (Ho 68) to negative parity levels below 7 MeV. The present DWA analysis of the $^{16}O(d,p)^{17}O$ reaction at 20.93 MeV is the highest beam energy reported.

The results of the DWA calculations for the first three positive parity levels are shown in Figure V.3.1. Calculations in the LZR approximation for the ground state are shown with four sets of OM parameters from Table V.2.a. The set of parameters (Ro, Va) give the best fit to both the L = 2 and L = 0 data. In general the adiabatic deuteron parameters Ro and Mps (Jo 70) gave better fits than the standard parameters P_i-A and P_i-F. The FRNL correction slightly improves the L = 0 fit but reduces the forward angles too much for the L = 2 data. The $1d_{3/2}$ calculation to the unbound state at 5.083 MeV is shown with the binding energy taken as 0.1 MeV and with an unbound wave function calculated by the method of Youngblood (Yo 70b) as described in Section II.2.b. The FRNL calculation with an unbound wave function changes the shape and amplitude of the predicted cross section drastically. Even when the neutron is taken to be bound by 0.1 MeV, the effect of the FRNL correction for the $d_{3/2}$ state is significant.

The extracted spectroscopic factors (S) for the positive parity levels are given in Table V.3.a. $S(1d_{5/2})$ and $S(2s_{1/2})$ are in general

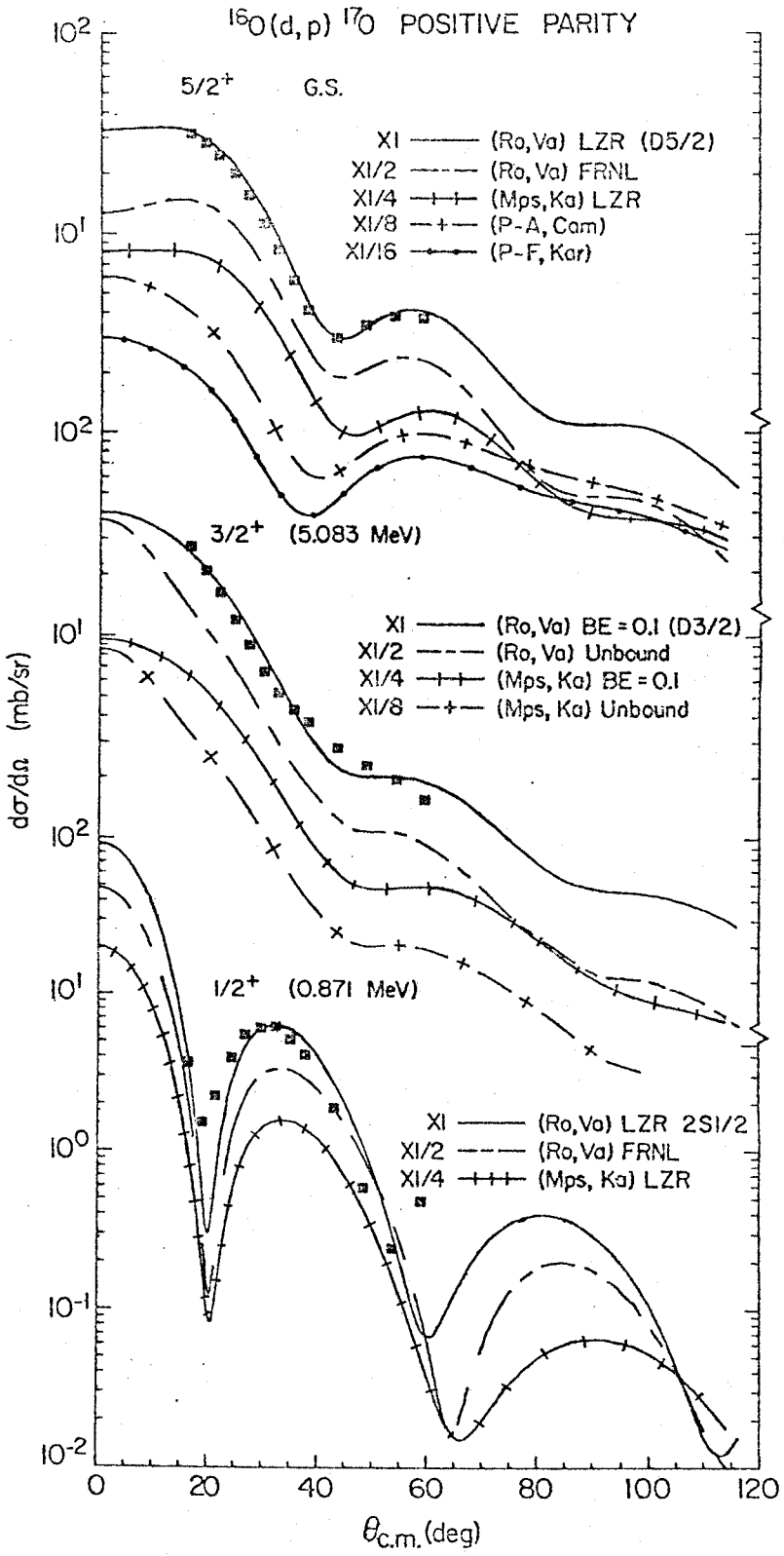

Fig V. 3.1

Calculations for the ground, first excited $1/2^+$ and $1d_{5/2}$ single particle levels observed in

agreement with measurements at lower deuteron energies (Da 70, Na 68, Ol 69). Oliver (Ol 69) and others have pointed out the sensitivity of S to the OM parameters and to the geometry of the bound state well. $S(2s_{1/2})$ is extracted at the first observed maximum (II.2.a) which occurs near 30^{o} where the cross section may not be entirely from a direct reaction mechanism. There is also an uncertainty in $S(1d_{3/2})$ due to the wave function of the captured neutron because it is unbound. Binding the neutron by 0.1 MeV no doubt overestimates $S(1d_{3/2})$. Using a quasibound wave function with the prescription of Youngblood et.al. (Yo 70a) should give a more realistic measure of $S(1d_{3/2})$, but then FRNL effects can not be investigated.

Table V.3.a. Spectroscopic factors for the positive parity levels in ^{17}O from the (d,p) reaction.

OM Potential	$S(1d_{5/2})$	$S(2s_{1/2})$	$S(1d_{3/2})$	
			a)	b)
(Ro, Va) FRNL	0.91	0.90	0.56	—
(Ro, Va) LZR	1.33	1.15	0.93	0.66
(Mps, Ka) LZR	0.89	0.72	0.71	0.52
(P-F, Ka) LZR	1.26	0.59	—	—
(P-A, Ka) LZR	1.08	0.37	—	—

a) neutron bound by 0.1 MeV
b) neutron unbound (treated by method of Section II.2.b)

The results of direct DWA calculations for the negative parity levels are shown in Figure V.3.2. The unresolved doublet at 5.7 MeV is assumed to be primarily the $7/2^{-}$ (5.696 MeV) state. The binding energy

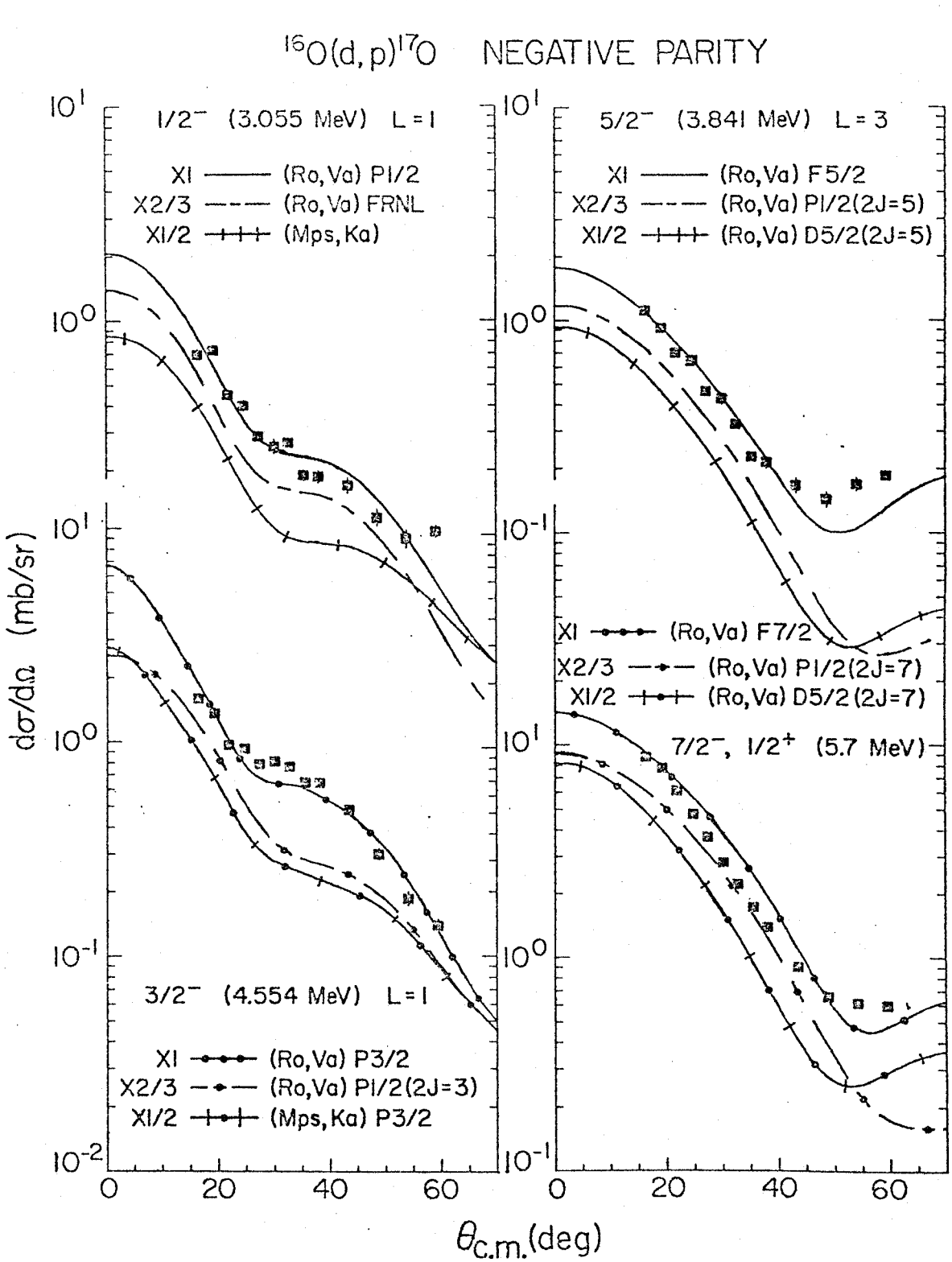

Fig. V.3.2
Calculations for the negative parity levels observed in the (d,p) reaction

of the transferred neutron is taken as described in Section V.2. The values for the binding energy of the p1/2 and p3/2 orbitals taken from experiment (Figure IV.1) gave less satisfactory fits to the $1/2^-$ and $3/2^-$ angular distributions at forward angles.

As discussed in Section V.1., a two step process going through an excited state in ^{16}O may be important in the population of these states. However, the shape of the calculated one step process should more or less characterize the transferred L, independent of any two step process (de T 72, As 71). The weak $1/2^-$, and $5/2^-$ states are fit somewhat better by the expected L = 1 or 3 shapes respectively than the stronger $3/2^-$ and $7/2^-$ levels. In fact the forward angle falloff of the $7/2^-$ state looks more like L = 2 than L = 3, although the L = 2 minima occurs at an angle different from that shown by the data. Changes in the radial shape of the captured neutron orbital did not significantly improve the fit of the L = 3 calculation for the $7/2^-$ angular distribution.

The extracted spectroscopic factors (S) for the negative parity levels as calculated in the direct DWA are given in Table V.3.b. S is calculated for the usual orbital assumed in the direct process and for the p1/2 and d5/2 orbitals in some cases where they would not be allowed by the direct process, but are allowed in the two step process. The usual orbital assumed for the captured neutron is given by the known j of the state and the required odd L transfer. The two step selection rules in the case of a 0^+ target only limit the J transfer to be j of the final state. The normal zero range direct selection rules still apply to each step. The extracted S shown for the higher three states with the p1/2 and d5/2 orbitals use the radial shape of these orbitals and the correct L,J transfer for the state populated.

Table V.3.b. Spectroscopic factors for the negative parity levels in ^{17}O from the (d,p) reaction.

OM Potential		$S(1/2^-)$	$S(3/2^-)$	$S(5/2^-)$	$S(7/2^-)$
(Ro, Va)	LZR	0.07	0.3	0.04	0.3
(Ro, Va)	FRNL	0.06	0.2	0.03	0.3
(Mps, Ka)	LZR	0.05	0.2	0.03	0.2
(Ro, Va)	LZR	0.5 [a]	1.9[a]	0.01[b]	0.1[b]
(Ro, Va)	LZR	—	0.1[c]	0.008[c]	0.07[c]

a) p shell binding energy taken from Figure IV.1
b) stripping into d5/2 orbital with L = 3, normal J
c) stripping into p1/2 orbital with normal L,J

How one interprets these calculations for the negative parity levels is only made clear by examining the possible two step contributions. Unfortunately that calculation cannot be performed with existing DWA codes. Even an estimate of the magnitude of the pure two step contribution is rather difficult (Pe 64, As 71). It seems rather unlikely that the extracted amplitudes would be correctly interpreted in either a pure single particle or a two step limit, but instead one must perform the complete coherent calculation (Au 69, As 71).

V.4. $^{16}O(h,d)^{17}F$ Analysis

The $^{16}O(h,d)^{17}F$ reaction, including angular distributions and a DWA analysis, has been reported by Eccles, Lutz, and Bohn at 17.8 Mev (Ec 66) and by Mertens et al. (Me 70) at 20.0 MeV. Eccles et al. conclude that the angular destributions are "washed out" with the DWA predicting more structure than the data shows. Eccles et al. do not report extraction of spectroscopic factors. The study by Mertens et al. included targets from ^{16}O to ^{32}S at helion energies from 16 to 20 MeV. Mertens et al. conclude

that the reaction mechanism is direct, even at these low energies, and that the extremely strong forward peaking of the angular distributions is correctly predicted by the DWA if the deuteron optical potentials are correctly chosen (Me 70). Mertens et al. do not report extraction of spectroscopic factors.

The results of the DWA calculations for the $^{16}O(h,d)^{17}F$ reaction at 34.64 MeV to the ground (1d5/2) and first excited (2s1/2) positive parity levels are shown in Figure V.4.1. The four lower curves for both angular distributions are DWA LZR approximation for four sets of OM parameters from Table V.2.a. The OM set (HiZ,Ro) is somewhat better than the other sets for both L = 0 and L = 2. The FRNL calculation shown with OM set (HiZ,Ro) improves the L = 0 fit significantly without an excess reduction in the predicted forward angle L = 2 distribution as was noted for the FRNL L = 2 (d,p) calculation. At best the L = 0 fits are far from spectacular, however.

The extracted spectroscopic factors (S) for the 1d5/2 and 2s1/2 positive parity levels are given in Table V.4.a. The lack of small angle data and the poor quality of the L = 0 DWA fits are assumed to account for the unrealistically small values of S(2s1/2). With the FRNL correction, (1d5/2) is in good agreement with similar calculations for the (d,p) reaction to ^{17}O. As was the case for the (d,p) reaction, the extracted spectroscopic factors for the (h,d) reaction are sensitive to the OM parameters.

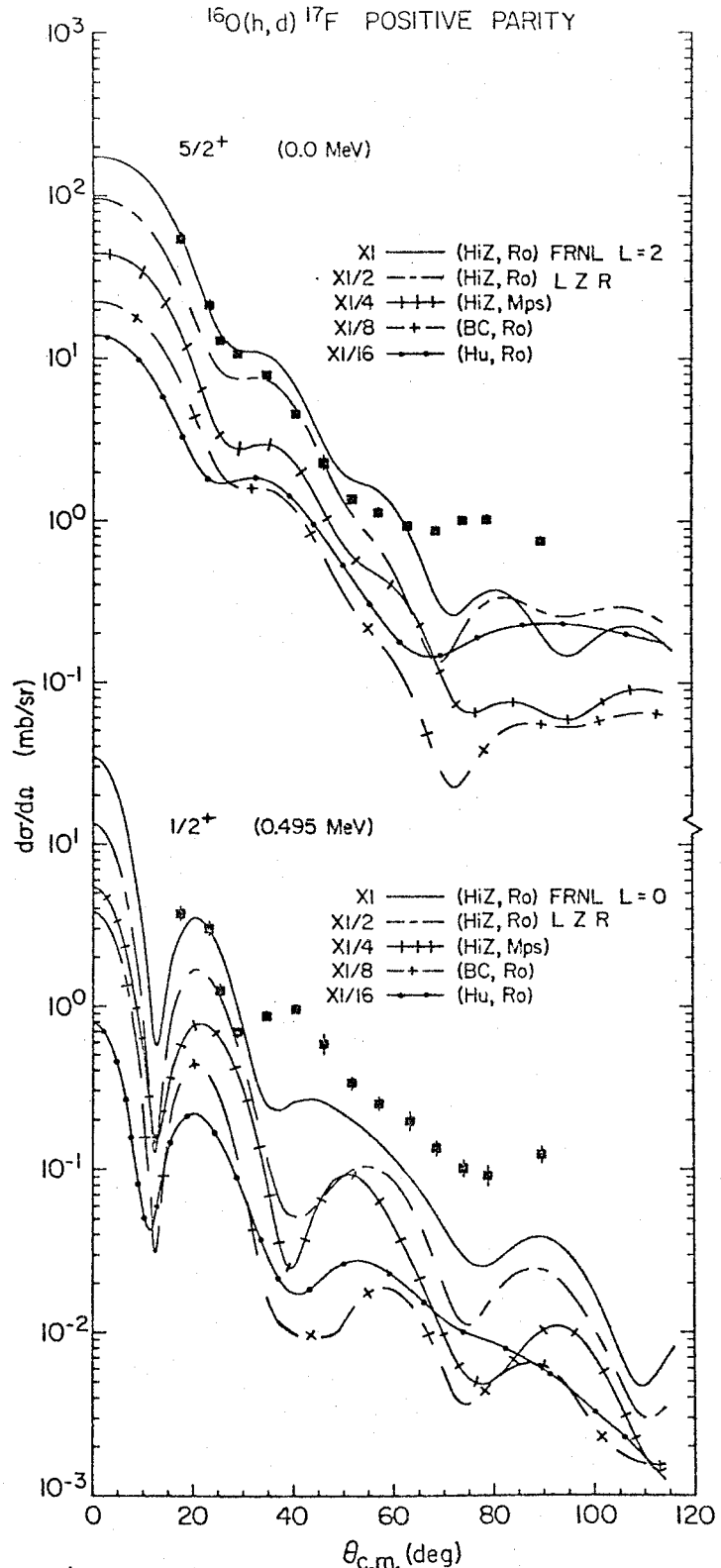

Fig. II.4.4

Calculated angular distributions for the ground and first excited state positive parity parity levels.

Table V.4.a. Spectroscopic factors from the (h,d) reaction for the positive parity levels.

OM potential	S(1d5/2)	S(2s1/2)
(HiZ,Ro) FRNL	0.86)	0.27
(HiZ,Ro) LZR	1.2	0.27
(HiZ,Mps) LZR	0.93	0.23
(BC,Ro) LZR	1.1	0.30
(Hu,Ro) LZR	1.4	0.21

The results of DWA calculations to the negative parity levels and the 5.215 MeV state (Pr 72, Th 72) in ^{17}F are shown in Figure V.4.2. Om sets (HiZ,Ro) and (BC,Mps) were used with the bound state of the captured neutron taken as described in Section V.2. The resulting changes in the shape of the calculated angular distribution due to variations in the shape of the bound state orbital were similar to those for the (d,p) stripping discussed in Section V.3.

The $1/2^-$(3.10 MeV) and 5.215 MeV angular distributions are similar in shape to each other, being nearly flat. The L=1 transfer calculation for the $1/2^-$ level is also out of phase with the small structure of the data. It is assumed that both of these levels are formed with a large two step contribution. Since the $1/2^-$ level should have a direct component (Au 69) there may be a destructive interference between the direct and two step processes going through the even parity states in ^{16}O (Pe 64). The lack of structure prohibits even a tentative spin assignment for the 5.215 MeV level. The $5/2^-$(3.86 MeV) and assumed $7/2^-$(5.672 MeV) levels have shapes consistent with the expected L=3 stripping pattern. A FRNL calculation with OM set (HiZ,Ro) gives S(5/2)=0.40 and S(7/2)=0.15. As in the (d,p) calculations in V.3, the interpretation of these amplitudes is unclear.

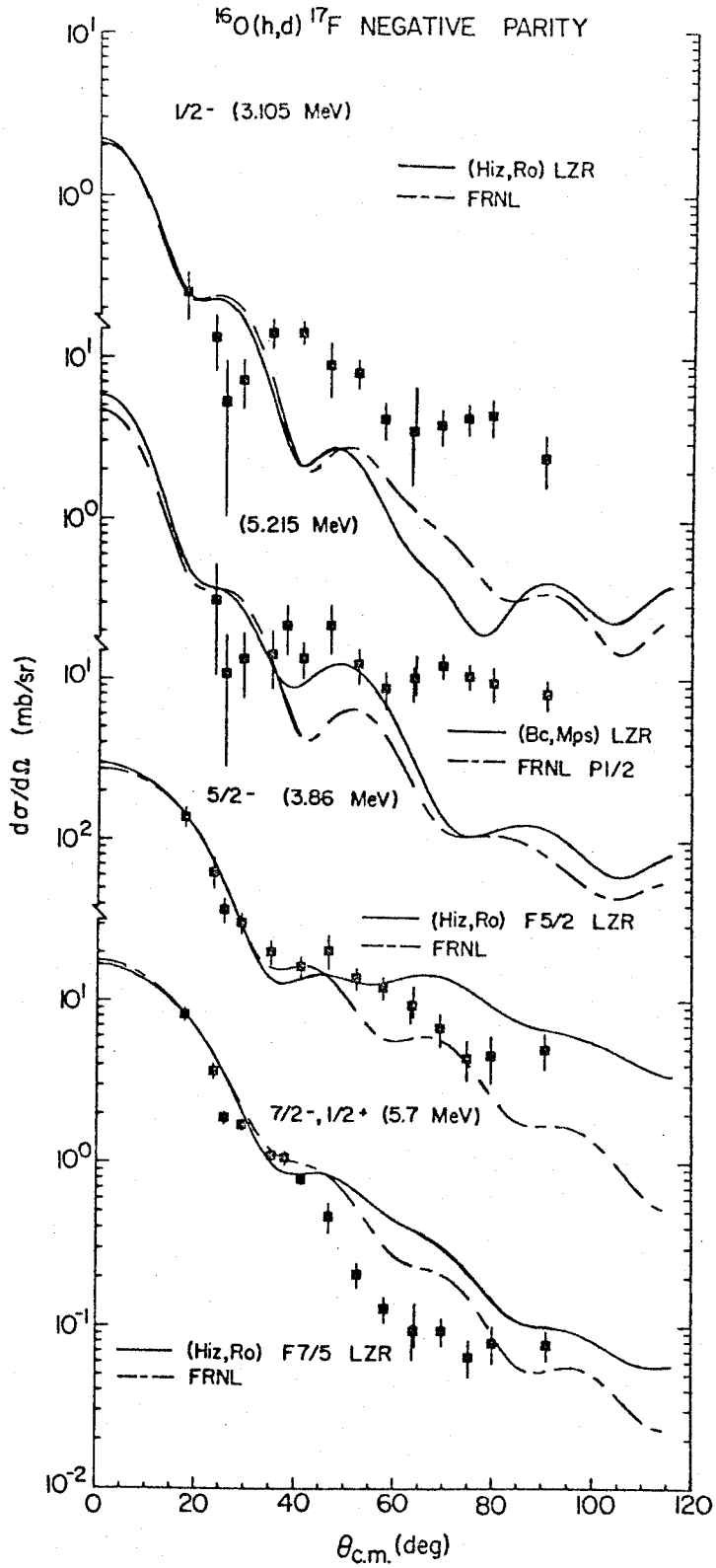

Fig. V.4.2

Calculated angular distributions for the negative parity levels observed in the (h,d) reaction.

V.5. $^{16}O(\alpha,h)^{17}O$ and $^{16}O(\alpha,t)^{17}F$ Analysis

V.5.a Introduction

A simultaneous study of the (α,h) and (α,t) reactions on a N = Z target allows one to investigate in detail the kinematic and Coulomb aspects of the reaction mechanism. The kinematic and Coulomb aspects of the reaction mechanism may then be related to the spectroscopic information extracted from experiment. Previous comparisons of the (α,h) and (α,t) reactions on some N = Z nuclei ranging from ^{12}C to ^{40}Ca have been reported by Gaillard, et al. (Ga 69) at 56 MeV, and by Hauser, et al. (Ha 72) at 104 MeV. Their results show that the helion yield is always enhanced relative to the yield of tritons and that the enhancement is considerably greater than would be expected from purely kinematic considerations as given by equation II.5.b. Both of these studies conclude that the DWA zero range normalization factor D_o^2 given in equation II.4.b must be different for the (α,h) and (α,t) reactions. The value of D_o^2 is not yet well established (Ha 72).

Much of the difficulty encountered in performing a DWA analysis of the (α,h) or (α,t) reactions appears to be directly attributable to the large binding energy of the α-particle (St 67, Au 70). Removing a particle from the tightly bound α system results in a large negative Q-value and a consequent momentum mismatch between the incident and exit channels. This loss of momentum localization complicates the DWA description of the stripping process.

The DWA description of a stripping reaction assumes that the initial and final channels are described by an optical potential obtained by fitting elastic scattering data. Only a few partial waves contribute strongly to the elastic scattering, which is pictured as occuring near

the nuclear surface (Sa 66). In the (d,p) and (d,n) stripping processes the reaction appears to be confined to the nuclear surface and the same partial waves contribute to the stripping and elastic scattering (Sa 66). In the α-stripping reactions, where the large negative Q-values give a momentum mismatch, there is an appreciable contribution to the DWA cross section from the lower partial waves which are strongly absorbed in the elastic channels (St 67). Thus it appears that much of the reaction comes from within the nuclear surface and the measured optical potentials, describing primarily surface scattering, must be carefully chosen to reproduce the stripping process. As discussed by Stock et al. (St 67), the momentum mismatch condition removes some ambiguity in the choice of α-particle optical potentials suggesting that the α potential be roughly the sum of a helion plus neutron potential. In practice this has been difficult to achieve, apparently because of the basic difference in the interaction of the helion and α-particle with the nucleus (St 67, Ch 71).

V.5.b Optical Model Survey for α Induced Stripping

The limited optical model studies with h,t and α's above 25 MeV on the lighter nuclei, together with the loss of surface localization in the (α,t) reactions, combine to make the optical model parametrization a weak point in the DWA analysis of the α induced stripping reaction. The usual (Pr 71) α-particle parameters appear to be especially poorly defined, in the sense that a set which more or less gives an adequate description of the elastic scattering does a poor job in fitting the transfer reaction cross section (St 67). Hauser, et al. (Ha 69) studied elastic α scattering at 104 MeV on nuclei from ^{6}Li to ^{209}Bi. They found that scattering from the lighter nuclei ($A \leq 16$) was fit better by a "wine bottle"

potential, where the nuclear interior is purely absorptive, than by the usual volume parameters, where the interior remains attractive. In a later paper using their "wine bottle" α potential, Hauser, et al. (Ha 72) were also able to get satisfactory agreement between experiment and the shape of the calculated DWA cross section for (α,h) and (α,t) reactions on ^{12}C. The α potentials of Hauser, et al. are not in the potential family of $^{3}He + n$ suggested by Stock (St 67) and others (Au 70). However, the form of their potential appears desirable, for it reduces the calculated contribution from the nuclear interior in agreement with experiment (St 67).

The criteria for selecting optical parameters from the literature for the (α,h), (α,t) analysis was to fit satisfactorily the ground and first excited state angular distributions. No parameter sets were found in a literature search which met this criteria, even with small changes allowed in the real and imaginary strengths and radii. Agreement between the DWA shape and experiment was especially poor for stripping to the $1/2^{+}$ first excited state. The predicted shape of the angular distribution was quite sensitive to small changes in either of the optical potentials or the radial wave functions describing the stripped particle. With the hope of improving the shape of the predicted angular distribution and reducing this sensitivity of the L = 0 angular distributions, the $^{16}O + \alpha$ elastic scattering data of Yavin (YF 59) and Reed (Re 68) was used to generate several sets of α optical model parameters. The sets YF and Re given in Table V.2.a are a minimum χ^2 solution in the 200 MeV six parameter family with the normal real and imaginary volume Woods-Saxon parameterization. Other six parameter volume sets were obtained with the real radius fixed to more closely match a particular set of

helion parameters. No general improvement in the DWA α stripping calculations was found using this alpha-helion or triton geometry matching condition, so the minimum χ^2 set was retained. The agreement between prediction and experiment for stripping to the $1/2^+$ angular distribution was not improved by any of the parameter sets found.

Following the results of Hauser, et al. (Ha 69, Ha 72), a search was conducted for a surface peaked real α potential, as opposed to the usual real volume Woods-Saxon potential. The code GIBELUMP was modified to permit searching on a real derivative Woods-Saxon potential. The search was limited to the 200 MeV real volume family which was approximated by the 400 MeV surface family with a reduced diffusivity. The resulting fits to the elastic scattering data were no better than the volume parameter set. The derivative real Woods-Saxon potential did not significantly improve the agreement between prediction and experiment for the L = 0 stripping angular distributions and markedly deteriorated the L = 2 agreement. Also, no appreciable reduction in parameter sensitivity was noted for the L = 0 angular distributions. The investigation of a parameter set with a damped interior and the same exterior shape as a volume Woods-Saxon potential as used by Hauser (Ha 69) was not undertaken.

The success of the adiabatic deuteron potential (Jo 70) used in (d,p) and (d,p) DWA calculations, and other recent studies (Sc 72, Ch 71) using a folded potential to describe three body and alpha scattering, motivated a cursory investigation of the folded potential for these alpha induced stripping calculations. The folded potential was generated with a code called THET obtained from P. D. Kunz (Ku 72). This code folds the nucleon optical potential into a wave function

for the incident particle, which was taken as a three or four body Gaussian function, whose parameters are adjusted to give the correct RMS charge radii (Ku 72). The resulting potential is not of the Woods-Saxon form. For the stripping calculations, the folded potential was approximated by a Woods-Saxon form with a volume real term and volume plus derivative imaginary terms. The parameters of the Woods-Saxon potential were determined by adjusting them to apporxomate the folded potential at radii of $R = r_o A^{1/3}$, $R + a_o$, and $R - a_o$. Folded potentials were obtained from the optical potentials of van Oers (Va 69) and Becchetti-Greenlees (Be 69). Stripping calculations were then performed for several combinations of folded and normal potentials. The predicted angular distributions were generally worse for the folded potential sets than for the normal α and h parameters. The prescription of Scherk and Falk (Sc 72) was also tried for the absorptive part of the folded potential. In this prescription the absorptive potential is given the same radial shape as the real potential and the strength of the absorptive potential adjusted as a free parameter. This prescription also failed to give satisfactory predicted angular distributions.

The DWA calculations presented in this section were performed with the conventional optical parameters from Table V.2.a. The energy dependent modification for the real volume potential given in Section V.2. generally adversely affected the shape of the predicted angular destributions, so this modification was not applied to any of the optical potentials used in the calculations of this section. The shape of the predicted angular destributions for the h potential set BC was improved by reducing the real strength by 8 MeV. This set of potentials is denoted as BC-8 in the calculations.

V.5.c Analysis and Comparison for the 1d5/2 Ground States

Because of the difficulty in predicting correctly the shape of both the ground and first excited state angular distributions, the discussion of a comparison of the (α,h) and (α,t) reactions will be limited to population of the ground state in the residual nucleus. Unfortunately even this comparison is made somewhat questionable due to the inadequaces of the usual optical model description of scattering in the entrance and exit channels. The predicted L = 2 angular distributions at forward angles are relatively insensitive to the vagaries of the optical model, however, so the calculated ratios will be evaluated in this region of the angular distribution.

Figure V.5.1 shows the results of some of the DWA calculations performed for the ground state angular distributions. The sensitivity of the calculated angular distributions to the shape of the radial wave function is shown for the set of parameters (Re, BC-8). The non-locality and finite range correction factors significantly alter the shape of the calculated angular distributions. The agreement in shape between calculation and experiment for the L = 2 angular distribution is generally poorer when the finite range and non-locality corrections are included. As previously discussed, this sensitivity is attributed to the momentum mismatch condition between the entrance and exit channels.

The normalization factor N defined by the relation $d\sigma/d\Omega|_{exp} = N\ S\ d\sigma/d\Omega|_{DWA}$ was determined for each set of optical model parameters by setting the ground state spectroscopic factor to unity. The values of N obtained are given in Table V.5.a. The sensitivity of the calculated angular distributions to the optical model parameters is

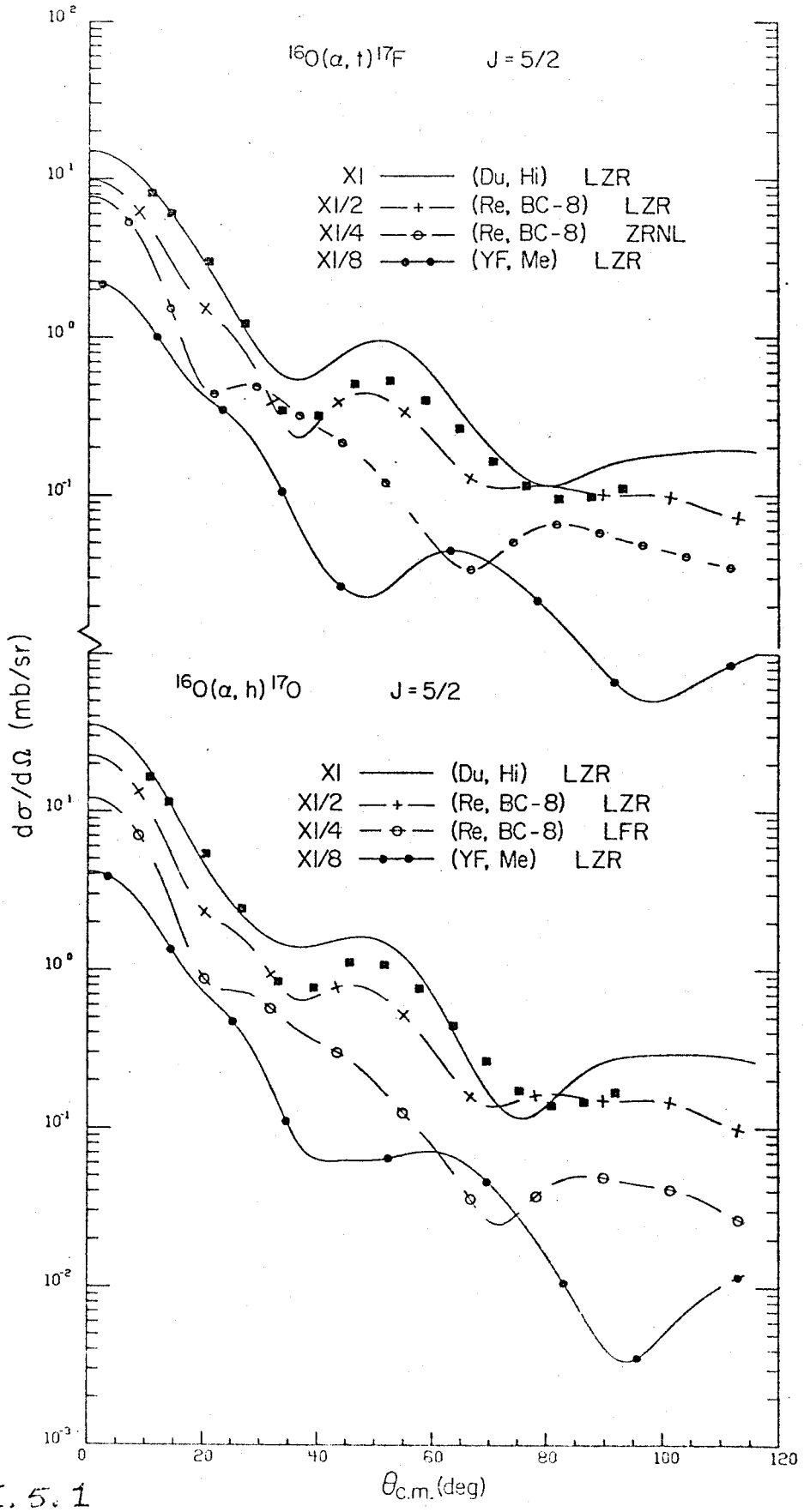

Fig I. 5. 1

Calculated angular distributions for the $5/2^+$ ground states

reflected in the large variation of N values extracted from the LZR calculations. The relative normalization for the (α,t) and (α,h) reactions are quite insensitive to the choice of optical potentials, however. Also shown in Table V.5.a. are the normalization factors obtained experimentally by Youngblood et al. (Yo 70a), and the value of N obtained experimentally by Hering et al. (He 70) for the (α,t) reaction with their calculated normalization for the (α,h) reaction. These results and those of Youngblood et al. (Yo 70a) suggest that the normalization ratio $N(\alpha,t)/N(\alpha,h)$, which is simply related to the zero range normalization ratio $D_o^2(\alpha,t)/D_o^2(\alpha,h)$ by equations II.4.a. and II.4.b., is somewhat smaller than the ratio calculated by Hering et al. (He 70).

Table V.5.a. Extracted normalization N and comparison with previous results.

Set	N(α,h)	N(α,t)	$\frac{N(\alpha,t)}{N(\alpha,h)}$
(Du, HiZ) LZR	47	37	0.79
(Re, BC-8) LZR	75	63	0.84
(Re, BC) LZR	59	48	0.81
(Du, HiZ) ZRNL	40	32	0.80
(Du, HiZ) LFR	26	18	0.69
(Du, HiZ) FRNL	23	17	0.74
Ref. Yo 70a LZR	32	23	0.72
Ref. He 70 LZR	38.6[a]	35.1	0.95

a) calculated in reference (He 70)

As is evident from equations II.5.a. and II.4.b., the DWA comparison of these reactions may be divided into three parts: 1) the

spectroscopic factor for the residual state, which is assumed to be unity in both reactions, 2) D_o^2, the normalization factor for the DWA cross section, which should be the same for both (α,t) and (α,h), and 3) the kinematic part of the reaction amplitude, which includes a multiplicative momentum dependence and the calculated DWA cross section. The details of the DWA cross section may be investigated by comparing the calculated to the experimental cross section ratio, X, where $X = \sigma(\alpha,t)/\sigma(\alpha,h)$. In particular the Q value and Coulomb effects can be investigated.

Figure V.5.2 compares the various calculated X's and summarizes the largest effects on the calculated ratio. The calculated ratios are done with $D_o^2(\alpha,t) = D_o^2(\alpha,h)$. As previously pointed out by Gaillard et al. (Ga 69) and Hauser et al. (Ha 72), the predominant factors affecting the calculated ratio are the bound state wavefunction differences, the Q-value differences and the different final state Coulomb interaction. These effects will be discussed separately, but they may be summarized by noting that the smaller binding energy of the proton favors the triton yield as does the reduced Coulomb interaction of the triton. This is offset by the lower Q value for the (α,h) reaction, which favors the helion yield.

The LZR calculated comparisons are made at 12^o in the center of mass where small changes in the optical potentials are not reflected strongly in the calculated cross sections. The optical parameter set (Re, BC-8) was used for the calculated comparison. Using this set of optical parameters at 12^o c.m., the LZR calculated ratio X = 0.60, where the LZR normalization constant D_o^2 is taken to be the same for the (α,t) and the (α,h) reactions.

The effect of the bound state wavefunction will be considered first. The geometry used for the Woods-Saxon bound state potential, r_o = 1.25 f, a = 0.65 f, and r_{oc} = 1.25 f, gives a binding energy of 51.97 MeV for the neutron and 51.98 MeV for the proton, suggesting that the difference in binding energy for ^{17}O and ^{17}F is almost entirely due to Coulomb effects. An increase in the real and Coulomb geometries to 1.3 f reduced the calculated ratio X by 1% and introduced a 180 kev difference in the Woods Saxon neutron and proton binding energies. The addition of a non-locality correction factor of 0.85 to the bound state wavefunction reduced X by 3%. The addition of a finite range correction of 0.69 increased X by 5%. Both of these modifications made major changes in the back angle cross sections as shown in Figure V.5.1., emphasizing the contribution from the nuclear interior as noted by Hauser (Ha 72).

The Coulomb interaction pushes the radial amplitude of the proton outward relative to a neutron, hence increasing the cross section. The contribution to the (α,t) reaction due to this effect may be calculated by giving the bound neutron a positive charge +1 in the calculated (α,h) reaction. This prescription increased the cross section by a factor of 1.06. Thus the increase in the radial amplitude at the larger radii where the most of the reaction takes place does not make a large contribution to the (α,t) reaction cross section.

The Q value dependence is much stronger than the multiplicative factor k_t/k_h. The effect of the Q value dependence was calculated by giving the (α,h) reaction a Q value corresponding to the correct one for the (α,t) reaction (a reduction of 2.8 MeV), then taking the ratio of this cross section to the normal calculated (α,h) cross section. At an α particle energy of 46 MeV, the factor k_t/k_h is 0.93 compared

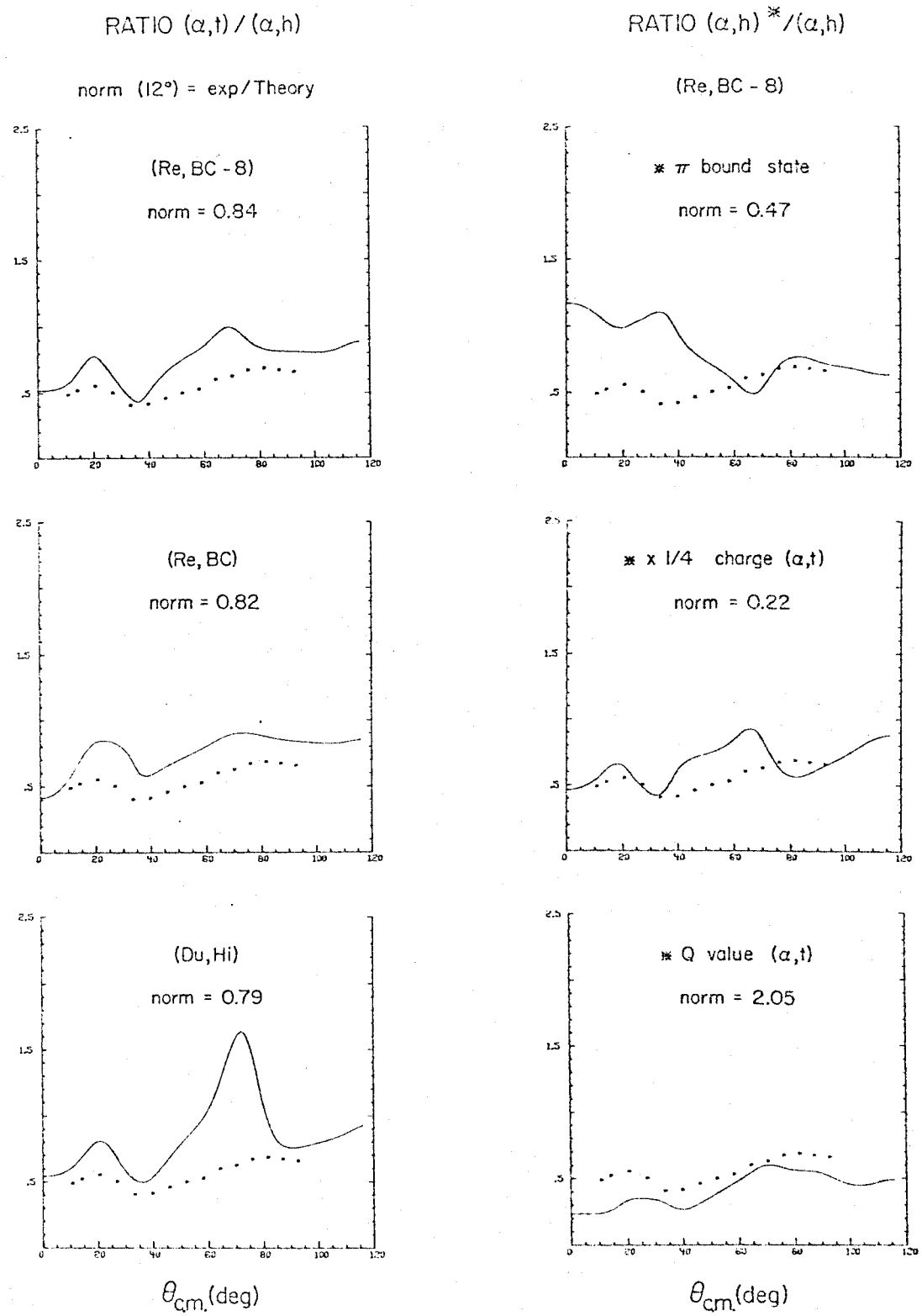

Fig. V. 5.2 On the left are shown the ratios calculated for three sets of O. M. parameters. On the right from top to bottom the effect of the proton bound state, the triton charge and the triton Q value on the calculated ratio is shown.

to a ratio of 0.24 calculated by the above prescription. This large effect is caused by a shift in localization of the partial waves contributing to the reaction amplitude. The large Q value compared to the beam energy results in a dramatic decrease in the forward angle calculated cross section as is shown in Figure V.5.2 (labelled Q value (α,t)).

The effect of the Coulomb interaction in the exit channel is also large as shown in Figure V.5.2 (labelled charge (α,t)). For this calculation the charge of the helion (+2) in the outgoing channel was changed to that of a triton (+1). The cross section was increased by a factor of 2.3 by this change. Thus the reduction of the Coulomb interaction of the triton compared to the helion has a big effect on the cross section.

Table V.5.b gives the extracted experimental ratios for these data on ^{16}O at E_α = 46 MeV and, for comparison, those of Gaillard et al. (Ga 69) at E_α = 56 MeV and Hauser et al. at E_α = 104 MeV. The ratio, X, is extracted taking a weighted average of all the angles. The experimental results show a simple dependence on Z and beam energy. The ratio X increases with increasing Z and decreases with increasing beam energy.

Table V.5.b. Measured ratio of the yields X from the targets indicated.

^{10}B	^{12}C	^{14}N	^{16}O	^{32}S	^{40}Ca
1.2±0.1 b)	1.40±0.15 b)	1.50±0.15 b)	1.88±0.11 a)	1.85±0.15 b)	2.0 ±0.2 b)
	1.23±0.15 c)				1.36±0.17 c)

a) This experiment, E_α = 46 MeV
b) Reference (Ga 69), E_α = 56 MeV
c) Reference (Ha 72), E_α = 104 MeV

V.5.d. Calculations for the Remaining States

Figure V.5.3 shows the calculated angular distributions for the two $1/2^+$ first excited states using the optical potential sets (Du, HiZ) and (Re, BC-8). Agreement between the shape of the calculated and experimental angular distributions at forward angles is poor, expecially when one considers that these two parameter combinations, of the 16 possible from Table V.2.a, represent the best agreement between calculated and experimental results. The sensitivity of the L = 0 calculated angular distributions to the parameterization used to describe them is most vividly illustrated by comparing the LZR and ZRNL calculations with the optical parameters (Re, BC-8). Damping the interior bound state wavefunction with the NL correction hardly affects the forward angle shape of the (α,t) angular distribution, but drastically alters the (α,h) shape. On the other hand, the same NL correction scarcely changes the shape of the calculated angular distribution using the optical model set (Du, HiZ). As previously discussed, this sensitivity is attributed to the momemtum mismatch condition between the entrance and exit channels.

Taking the extracted normalization factors for each set of optical parameters as given in Table V.5.a spectroscopic factors were extracted for both $1/2^+$ first excited states by matching the magnitude of the calculated maximum near 40^o c.m. to the experimental cross section at 40^o c.m. This prescription may give unreliable results due to the vagaries in the calculations and for the reasons given in Section II.2.a, but should indicate the approximate spectroscopic strength of these levels. Using the above prescription, spectroscopic factors for both $1/2^+$ states of 0.14 were extracted for the LZR and 0.17 for the ZRNL

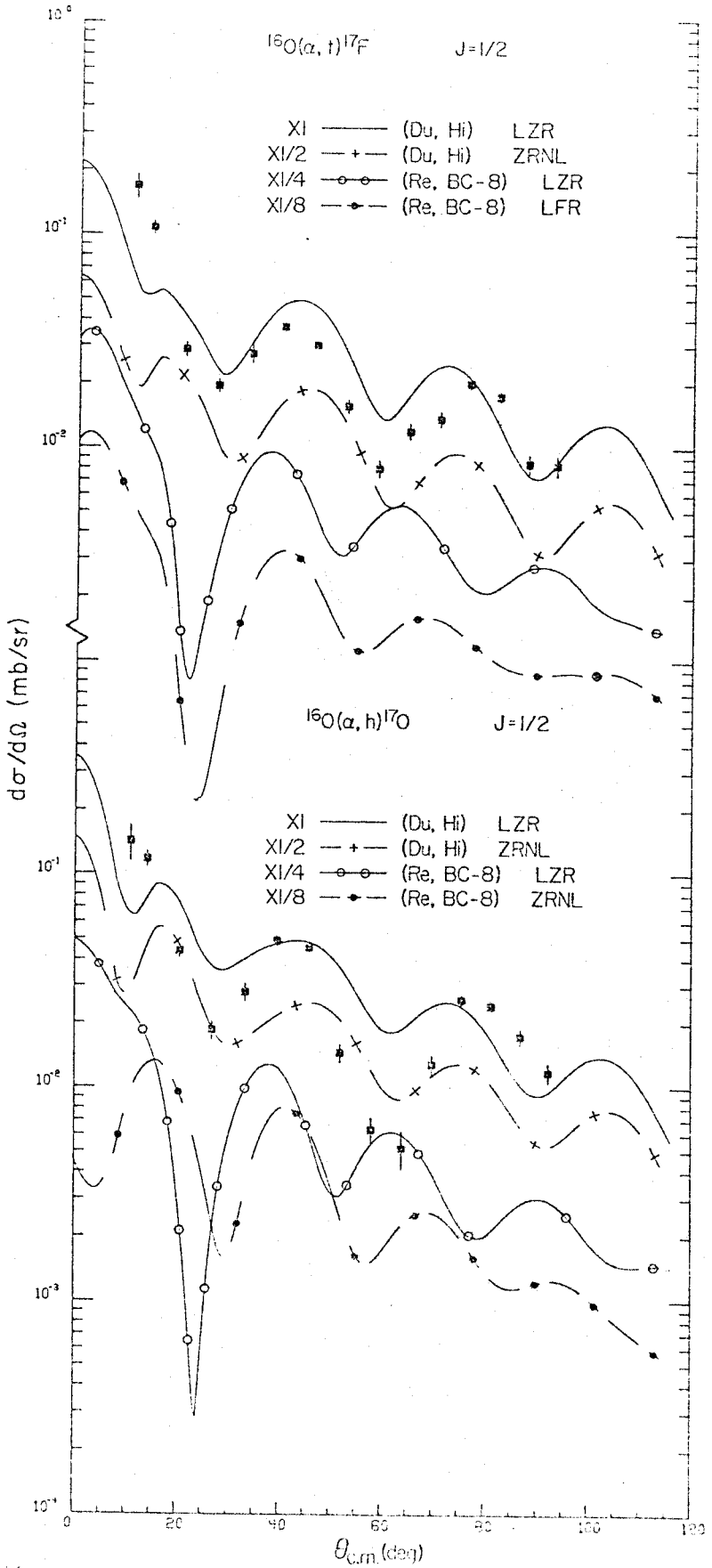

Fig. 5

L=0 Calculations to the $1/2^+$ first excited states

calculations. This small value is quite surprising. One expects the L = 0 levels to be weakly populated in α induced stripping reactions due to the momentum mismatch condition, but one also expects the DWA to account for the expected small strength. This is interpreted as a further indication that the DWA (L=0) α stripping reaction mechanism requires more study.

Figures V.5.4 and V.5.5 show the calculated angular distributions for four higher lying states populated in the (α,h) and (α,t) reactions respectively. These four states are either cleanly resolved, or from their shapes and a comparison with the angular distribution to the mirror state, represent primarily population of a single level. The bound state orbitals for the calculations shown are taken as described in Section V.2. The calculated angular distribuions are matched to the experimental data at 11° c.m. Spectroscopic factors are then extracted using the DWA normalization of Table V.5.a. These spectroscopic factors are given in Table V.5.c.

Table V.5.c. Extracted Spectroscopic Factors in the LZR Approximation for the Negative Parity Levels

OM	Nucleus	$S(1/2^-)$	$S(5/2^-)$	S(5.2 MeV)	$S(7/2^-)$
(Du,HiZ)	^{17}O	0.5	.01	.005	.08
(Du,HiZ)	^{17}F	1.0	.05	.02	.1
(Re,BC-8)	^{17}O	0.9	.007	.003	.05
(Re,BC-8)	^{17}F	1.2	.02	.01	.05

As discussed in Sections V.1. and V.3., interpretation of the extracted spectroscopic amplitudes for these negative parity levels may require the inclusion of contributions from two step processes. The puzzling thing about the amplitudes extracted from these α induced stripping reactions is the very large value obtained for the $1/2^-$ level, especially when compared to the small values found for (d,p) and (h,d) stripping in Sections V.3. and V.4. respectively. This is in complete disagreement with the usual assumptions made in the direct DWA. One is then forced to conclude that the direct reaction mechanism assumption is false.

The state at 5.217 MeV in ^{17}O has been assigned a spin-parity of $(7/2 \rightarrow 11/2)^-$ (Aj 71). The calculations shown for the (α,h) reaction to this state and the mirror state in the (α,t) reaction assume the normal odd L transfer to a state of $j = 11/2^-$. The lack of structure in the angular distributions and unreliability of the DWA calculated shapes preclude a definite spin-parity assignment for these states, but do suggest that an $L = 3$ $(7/2^-)$ transfer is extremely unlikely.

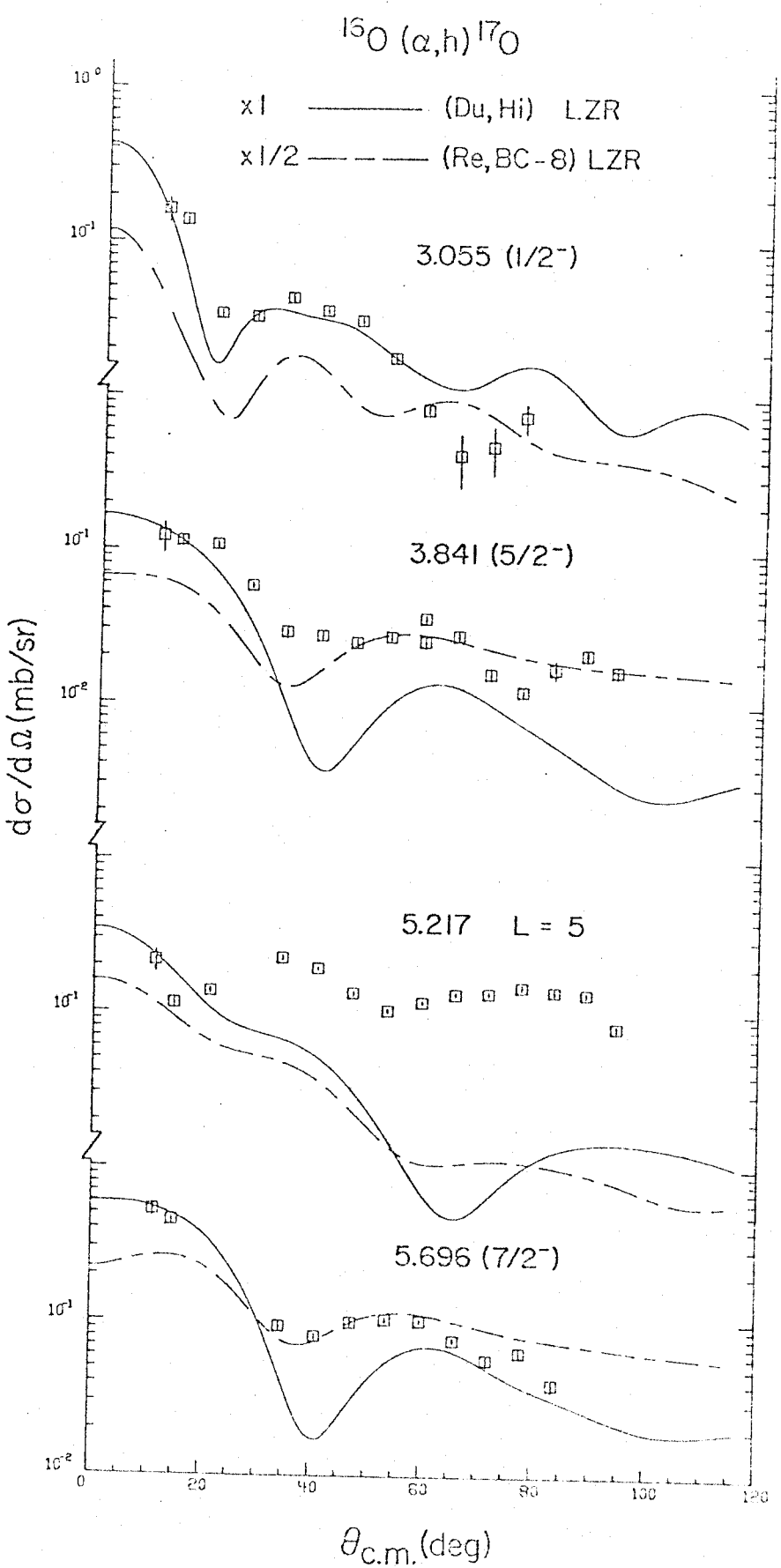

+ 3 E. 1

L2R calculations for the negative parity levels observed in the (α, h) experiment

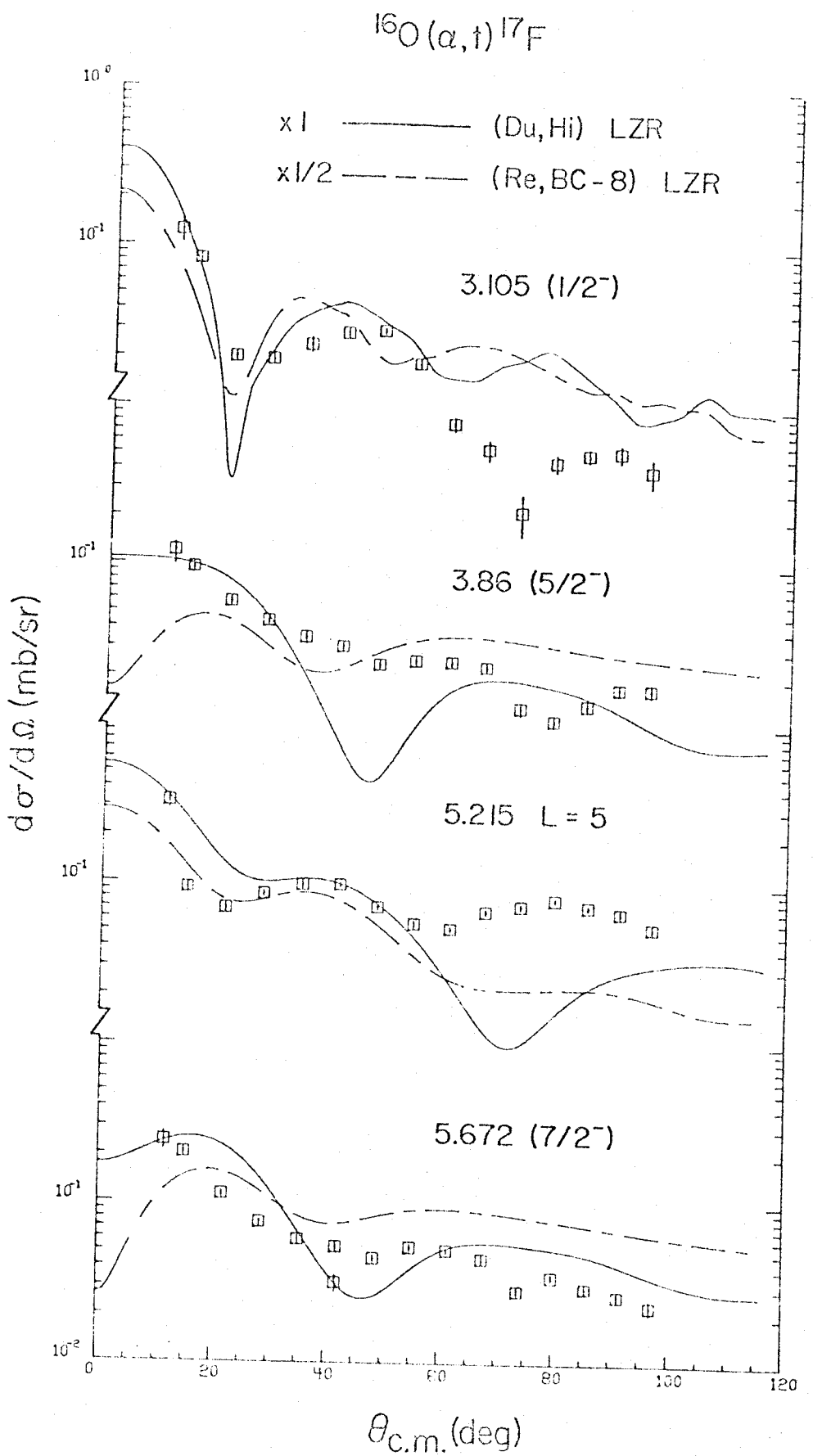

LZR calculations for the negative parity levels observed in the (α,t) reaction.

V.6. $^{19}F(p,t)^{17}F$ and $^{19}F(p,h)^{17}O$ Analysis

V.6.a. Introduction

As pointed out by Fleming, et al. (Fl 71) and Vignon, et al. (Vi 71), a simultaneous analysis of (p,t) and (p,h) reactions to mirror levels offers a stringent test of the two nucleon transfer mechanism and of the shell model description of the levels involved. No previous comparison of the (p,t) and (p,h) reactions on ^{19}F have been reported. Cole, et al. (Co 67, Co 68) have reported a DWA analysis of 30 MeV $^{19}F(p,h)^{17}O$ data. Using a cluster transfer DWA formalism and only considering a single LSJ transfer, they find that the DWA is sensitive to the sign of the ^{19}F wavefunction conponents but relatively insensitive to the amplitudes.

This microscopic analysis of the two nucleon transfer process follows the formalism of Towner and Hardy (To 69) using the DWA code DWUCK (Ku 69). For spin 1/2 particles in the incident and exit channel, the reduced matrix element β_{LSJM} calculated by DWUCK differs from the one used by Towner and Hardy by $\sqrt{2S+1}$ (Ku 72), where S is the spin transfer. Following the notation used in equation II.6.a, but in terms of the reduced matrix element β_{LSJM} calculated by DWUCK, the DWA microscopic two nucleon cross section is proportional to

$$\sigma(\theta)^{J}_{DW} \propto \left| [1][2] \sqrt{2S+1} \; C_{ST} \; G_{MLSJT} \; \beta_{LSJM} \right|^2 , \qquad (V.6.1)$$

where summation is implied over the single particle configurations [1], [2] and over the allowed values of M,L,S and T. This expression as written is coherent in M, L, S and T, but incoherent in J. DWUCK evaluates the quantity β_{LSJM} for a given two particle configuration [1], [2] whose amplitude is $\sqrt{2S+1} \; C_{ST} \; G_{MLSJT}$. The amplitude D(S,T)

appearing in the term C_{ST}, as defined in equation II.6.c, has been measured experimentally. Experimental determinations of $R \equiv |D(1,0)/D(0,1)|^2$ range from 0.2 to 0.4 (Ha 67, Fl 71). The remaining term in equation V.6.1 , the spectroscopic amplitude G_{MLSJT}, may be evaluated for a shell model wavefunction. If no spin-orbit force is included in the optical potentials, equation V.6.1 may be evaluated as an incoherent sum over L, S, and T as well as J.

A computer code written by Duane Larson was used to evaluate the spectroscopic amplitude G_{MLSJT} for shell model wavefunctions provided by Hobson Wildenthal. Two sets of wavefunctions for ^{19}F were used, one with three particles outside a ^{16}O core distributed among the d5/2, s1/2, and d3/2 orbitals and the other with seven particles outside a ^{12}C core with active d5/2, s1/2, and p1/2 orbitals. The wavefunctions used and the calculated spectroscopic amplitudes are tabulated in Appendix A.

The spectroscopic amplitudes G_{MLSJT} are obtained in a JT coupling representation for the two single particle configurations (n_1, l_1, j_1) and (n_2, l_2, j_2) (To 69). The selection rules for J are obtained by coupling the initial and final spins $\vec{J} = \vec{J}_i - \vec{J}_f$, where $\vec{J} = \vec{L} + \vec{S}$. The restriction on S and T is that only (S = 0, T = 1) or (S = 1, T = 0) transfers are allowed. Thus for a normal (+) parity transition, L + S + T is even and for a (-) parity transition L + S + T is odd. It should be noted that the phase convention used in Duane Larson's code for evaluating these spectroscopic amplitudes is different from that used in DWUCK. If a coupling is between two major quantum shells, 2s1/2 ⊗ 1d5/2 for example, then the sign of the spectroscopic amplitude obtained from the code has to be changed to agree with DWUCK. This

comes from the usual DWA convention that bound state orbitals approach zero from the positive side at infinity as opposed to the shell model convention that starts the radial wavefunctions positive from the origin.

Taking the case where no spin-orbit force is included, equation II.6.e relates the experimental to DWA cross sections. The normalization N appearing in this equation is evaluated up to the usual cluster transfer normalization D_0^2 in reference Ba 72. The remaining factors in the normalization come from the Gaussian range parameter and RMS raduus used to describe the triton or helion. For these calculations a range parameter of 1.6 f and a triton RMS radius of 1.7 f were used, which gives a normalization of 3.93 D_0^2 (Ba 72). The normalization D_0^2 was then fixed at 56.6 to give an enhancement factor near unity for the shell model (p,t) ground state calculation. To relate the experimental cross section in mb/sr to the DWA cross section in f^2, the normalization N appearing in equation II.6.e has the value 2220. The factor ε in this equation is then ~~adjusted to give~~ a measure of the agreement between experiment and the DWA normalized to the ground state (p,t) transition, as evaluated with shell model spectroscopic amplitudes.

The optical parameters for these calculations were taken from Table V.2.a. The proton parameters Cam and Sn were modified for (Z,A) dependence using the prescription of Becchetti and Greenlees (Be 69) given by $V(Z,A) = V_0 + 0.4\ Z/A^{1/3} + 24.\ (N-Z)/A$ and $W_{SF}(Z,A) = W_{SF} + 12.0\ (N-Z)/A$. This prescription resulted in somewhat better agreement between calculated and experimental angular distribution shapes than was obtained for the unmodified proton parameters. The helion and triton parameters used were the set (BC-8) defined in Section V.5

and the set HiZ from Table V.2.a. For the calculations including a non-locality correction labelled NL, the non-locality correction was only applied to the optical channels, and not to the bound state.

The finite range (FR) correction was found to significantly alter the shapes of the calculated angular distributions (Ro 71). A large improvement in agreement between experiment and calculation was found for a FR parameter of 0.60. The value of 0.69 suggested by Kunz (Ku 72, Ro 71) resulted in a drastically worse calculated shape. The value of the two nucleon FR parameter necessary is related to the binding energy of the single particle configuration, and for these relatively weakly bound particles ($\sim$7 MeV for (p,h)), the value of 0.60 vas adequate (Ku 72).

V.6.b. Analysis for the Positive Parity $1/2^+$ to ($5/2^+$, $1/2^+$) Transfers

The results of calculations to the $5/2^+$ ground state and $1/2^+$ first excited state are presented in this section. The normalization of the calculations is chosen such that the enhancement factor $\mathcal{E}$ is unity for the (p,t) calculation to the $5/2^+$ ground state using the shell model wavefunction for ^{16}O + three particles. No other normalization is included. Thus the "relative goodness" for a set of calculations is indicated by their deviation from this normalization. In particular the (p,t) to $1/2^+$ and (p,h) to ($5/2^+$,$1/2^+$) calculations should give the same enhancement factor $\mathcal{E}$ as the (p,t) to $5/2^+$ calculation since all four levels are assumed to be nearly pure single particle states with unit amplitude. Calculations for the ground state transitions are set equal to the data at 18° c. m. to extract $\mathcal{E}$. For the first excited state angular distributions, $\mathcal{E}$ is obtained by matching the calculated maximum near 30° c. m. to the experimental maximum value obtained near

30^{o} c. m.

Calculations are shown in Figures V.6.1 and V.6.2 for the ground state and first excited state angular distributions, where for both, the summation over L, S, T is incoherent. These calculations were performed using the shell model wavefunction for ^{16}O + three particles with three sets of optical model parameters and no spin-orbit force. The calculation using parameter set (Cam, BC) is shown in the local zero range (LZR) and finite range non-local (FRNL) approximations. Agreement between calculation and experiment is considerably better for the FRNL calculation. The extracted enhancement factors $\mathcal{E}$ for these calculations are given in Table V.6.a. Also shown in this table are the enhancement factors obtained for a pure $(d5/2)^2$ configuration. Agreement is much better for the shell model wavefunction than the pure configuration calculations. The shell model calculations did not significantly improve the shape of the calculated angular distributions however.

+ 19F(P.T) 0.0 MEV $(5/2^+)$

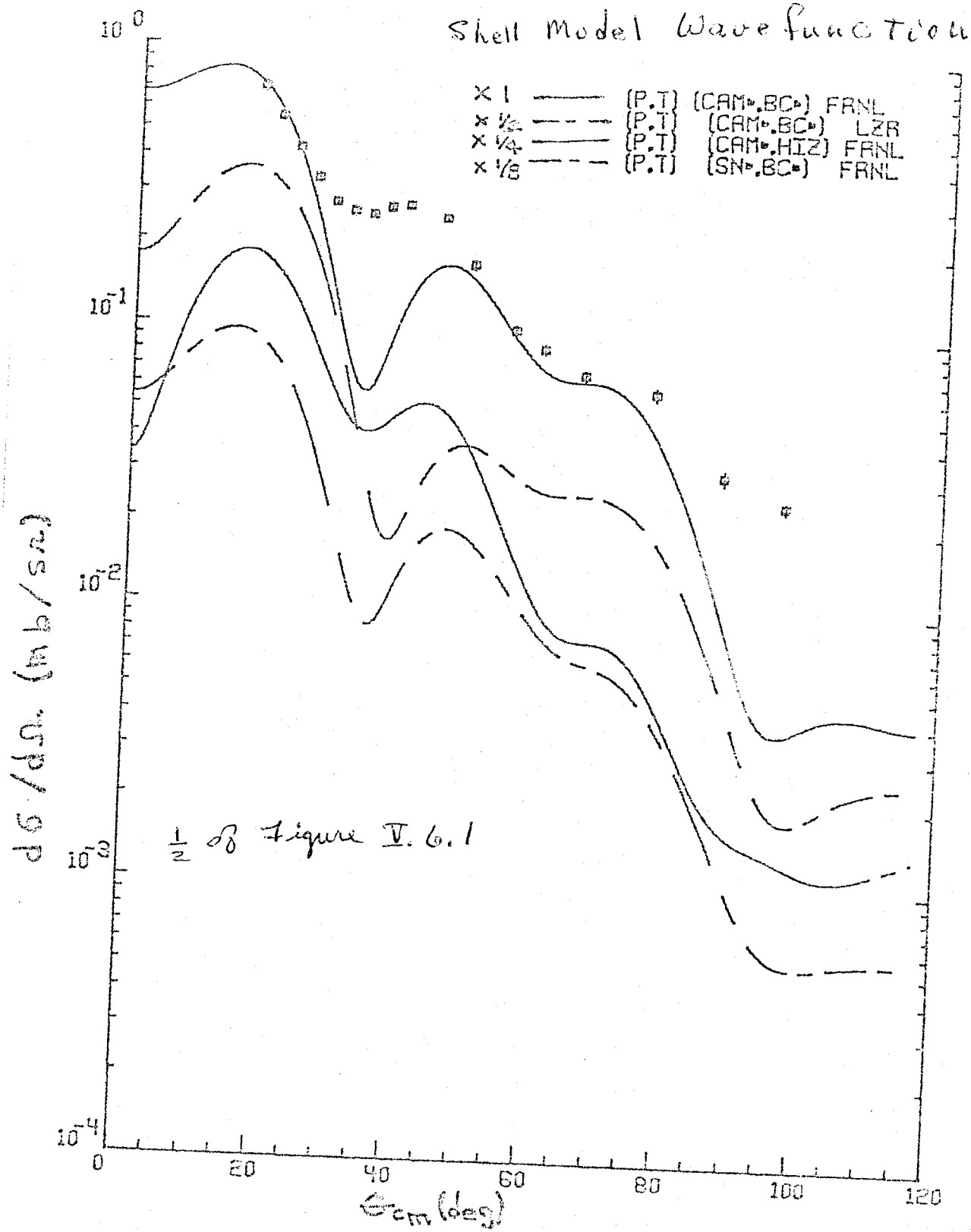

Inelastic L, S, J calculations for the $5/2^+$ levels using three optical model sets. FRNL and LZR calculations are shown for the set (Cam, BC).

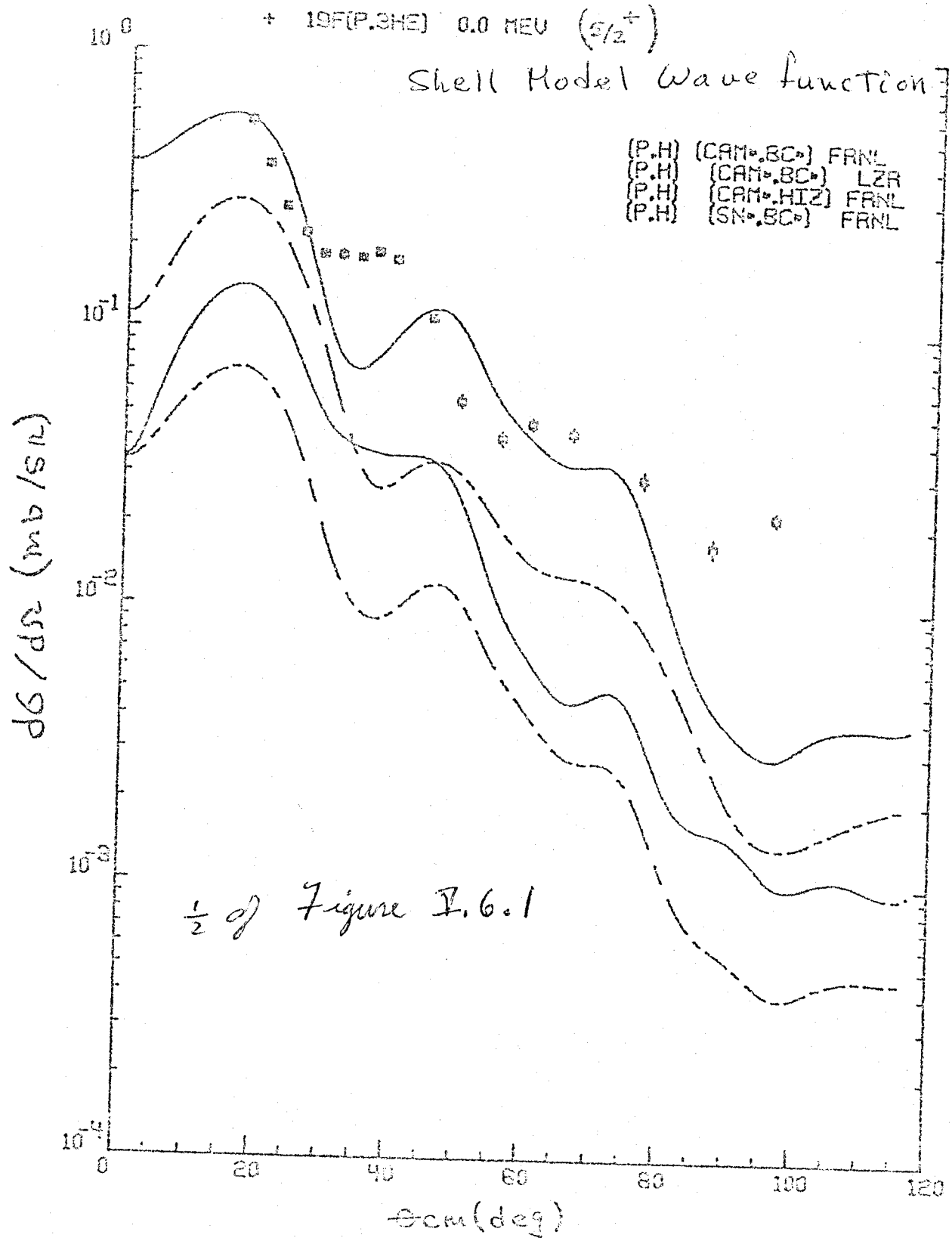

½ of Figure V.6.1

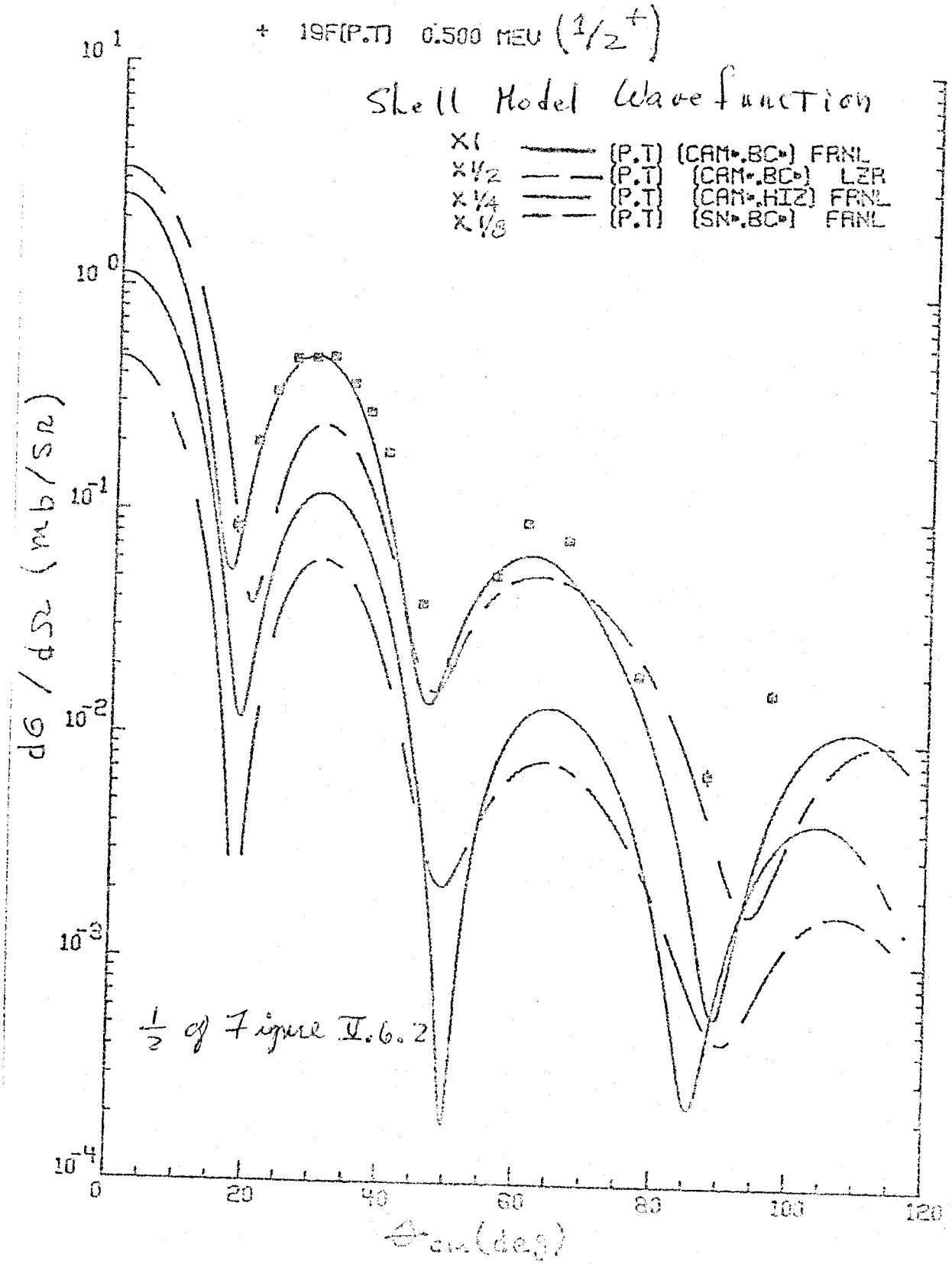

Incident L, S, J calculations for the ½+ levels.

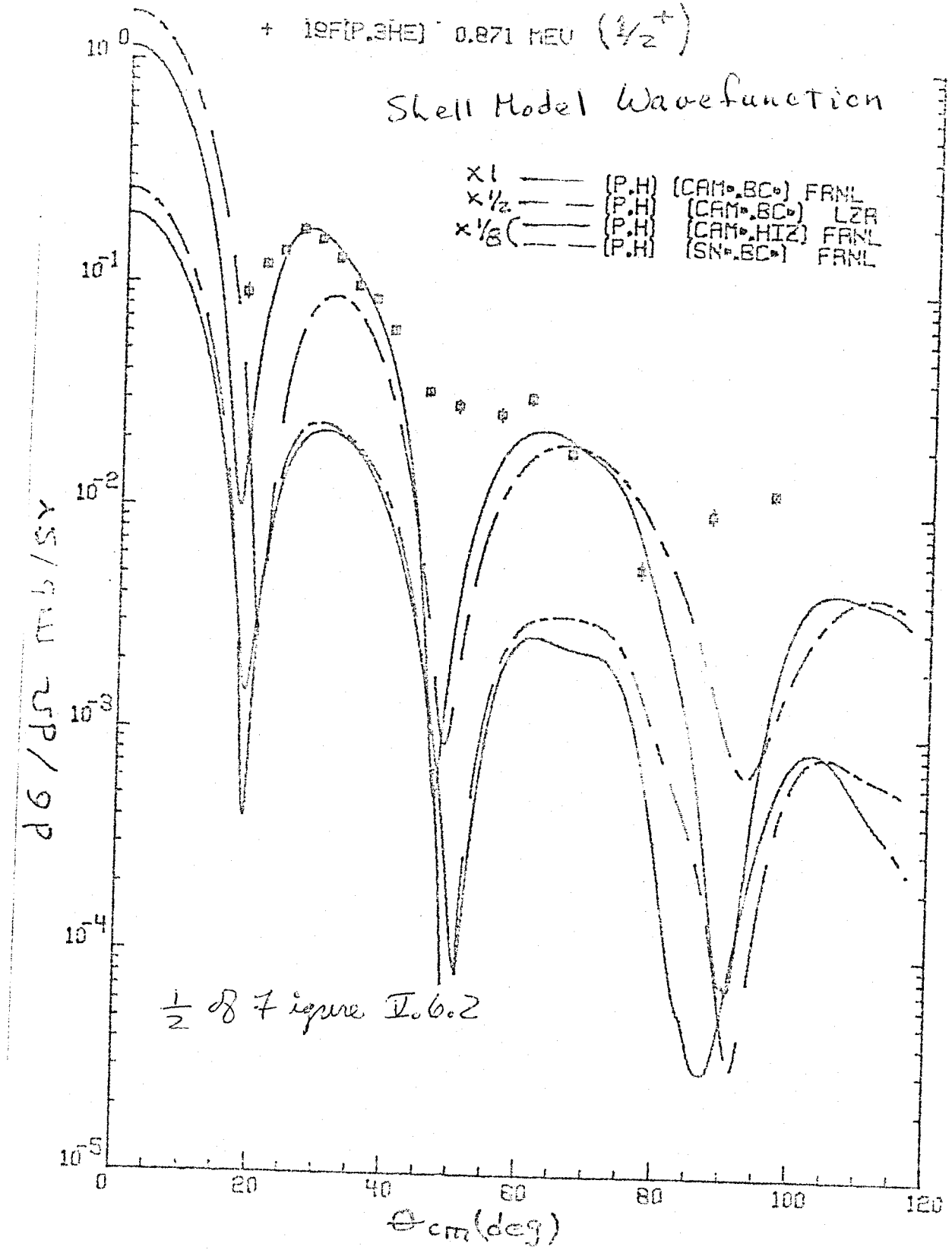

$\frac{1}{2}$ 8 7 igure V.6.2

Table V.6.a Extracted Enhancement factors $\mathcal{E}$ for the Incoherent L,S,J,T Calculations

O.M. - B.S.	$\mathcal{E}(1d_{5/2})$ t	h_1	h_2	$\mathcal{E}(2s_{1/2})$ t	h_1	h_2
A - LZR - SM	0.88	0.76	0.94	1.96	1.30	1.3
A - FRNL - SM	1.15	0.99	1.03	1.24	0.77	0.8
A - FRNL - $(d_{5/2})^2$	7.67	6.79	8.27	2.35	1.72	1.9
B - FRNL - SM	1.64	1.27	1.55	2.13	1.10	1.1
C - FRNL - SM	1.02	0.81	0.99	1.36	0.97	1.05

Optical Model: (No S.O.)
A ~ (Cam, BC)
B ~ (Cam, H.Z)
C ~ (Sn, BC)

t = triton
h_1 = ^{3}He (R = 0.3)
h_2 = " (R = 0.2)
where R = |D(1,0)/D(0,1)|

$$\mathcal{E} = \sigma_{exp} / \sigma_{DWA}$$

where $\sigma_{DWA} = 2223. \sum_{LSJT} (2S+1) C^2_{ST} \frac{\sigma(\theta)^{LSJT}}{(2J+1)}$

Table Not Complete

BIBLIOGRAPHY

BIBLIOGRAPHY

Aj 71 F. Ajzenberg-Selove, Nucl. Phys. A166, 1 (1971).

As 69 R. J. Ascuitto and N. K. Glendenning, Phys. Rev. 181, 1396 (1969).

As 71 R. J. Ascuitto, N. K. Glendenning and B. Sørenson, Phys. Lett. 34B, 17 (1971).

Au 70 N. Austern, Direct Nuclear Reaction Theories (Wiley-Interscience, 1970).

Au 71 S. M. Austin, P. J. Locard, S. N. Bunker, J. M. Cameron, J. R. Richardson, J. W. Verba, and W. T. H. van Oers, Phys. Rev. C3, 1514 (1971).

Ba 62 R. H. Bassel, R. M. Drisko, and G. R. Satchler, Oak Ridge National Laboratory Report ORNL-3240, 1962.

Ba 64 B. F. Bayman, Argonne National Laboratory Report No. ANL-6878, 1964 (unpublished).

Ba 66 B. F. Bayman and A. Kallio, Phys. Rev. 156, 1121 (1967).

Ba 69 G. C. Ball and J. Cerny, Phys. Rev. 177, 1466 (1969).

Ba 69a D. L. Bayer and W. Benenson, Bull. Am. Phys. Soc. 14, 1243 (1969).

Ba 71 J. B. Ball, R. L. Auble and P. G. Roos, Phys. Rev. C4, 196 (1971).

Ba 71a D. L. Bayer, "The Data Acquisition Task TOOTSIE", MSU Ch-34 (unpublished) 1971.

Ba 72 H. W. Baer, J. J. Kraushaar, C. E. Moss, N. S. P. King, R. E. L. Green, P. D. Kunz and E. Rost, University of Colorado (COO-535-660), to be published.

Be 64 B. Bencze and J. Zimanyi, Phys. Lett. 9, 246 (1964).

Be 66 G. Bencze and B. Zamanyi, Nucl. Phys. 81, 76 (1966).

Be 68 W. Benenson, R. De Forest, W. P. Johnson, and E. Kashy, Nucl. Instr. Meth. 64, 40 (1968).

Be 69 F. D. Becchetti and G. W. Greenlees, Phys. Rev. 182, 1190 (1969).

Be 71 F. D. Becchetti,Jr. and G. W. Greenlees, Polarization Phenomena in Nuclear Reactions, ed. by H. H. Barschall and W. Haeberli (University of Wisconsin Press, 1971).

Bi 68 J. Birkholz and F. Beck, Phys. Lett. B28, 18 (1968).

Bl 64 A. G. Blair, Argonne National Laboratory Report No. ANL-6878, 1964 (unpublished).

Bl 66 H. G. Blosser and A. I. Galonsky, IEEE Trans. on Nuclear Science NS-B, No. 4, 466 (1966).

Br 66 G. E. Brown and A. M. Green, Nucl. Phys. 85, 87 (1966).

Bu 64 P. J. A. Buttle and L. J. B. Goldfarb, Proc. Phys. Soc. 83, 701 (1964).

Ch 70 N. S. Chant and N. F. Mangelson, Nucl. Phys. A140, 81 (1970).

Ch 71 H. H. Chang and B. W. Ridley, University of Colorado, Technical Progress Report, COO-535-653, p. 57, 1971 (unpublished).

Co 63 B. L. Cohen, R. H. Fulmer, A. L. McCarthy and P. Mukherjee, Rev. Mod. Phys. 35, 332 (1963).

Co 67 R. K. Cole, R. Dittman, H. S. Sandhu, C. M. Waddell, and J. K. Dickens, Nucl. Phys. A91, 665 (1967).

Co 68 R. K. Cole, K. A. Huber, C. N. Waddell, R. R. Dittman, and J. K. Dickens, International Conference on Nuclear Structure-Tokyo, Japan, Institute for Nuclear Study, University of Tokyo, 283 (1968).

Da 70 N. E. Davison, W. K. Dawson, G. Roy and W. J. McDonald, Can. J. Phys. 48, 2235 (1971).

De 65 C. Detray, J. Cerny, and R. H. Pehl, Phys. Rev. Lett. 14, 708 (1965).

De 67 D. Dehnhard and C. Mayer-Böricke, Nucl. Phys. A97, 164 (1967).

deT 72 N. deTakacsy, private comminication.

Du 68 H. H. Duhm, B. G. Harvey, D. L. Hendrie, J. Saudinas, J. Mahoney, Nuclear Chemistry Annual Report UCRL-17989, 1968 (unpublished).

Ec 66 S. F. Eccles, H. F. Lutz and T. S. Bohn, Bull. Am. Phys. Soc. 11, 735 (1966).

El 70 P. J. Ellis and T. Engeland, Nucl. Phys. A144, 161 (1970).

En 65 T. Engeland, Nucl. Phys. 72, 68 (1965).

Fa 71 W. R. Falk, P. Kulisic, and A. McDonald, Nucl. Phys. A167, 157 (1971).

Fa 72 L. C. Farwell, J. J. Kraushaar, and H. W. Baer, Nucl. Phys. A186, 545 (1972).

Fl 68 D. G. Fleming, J. Cerny, and N. K. Glendenning, Phys. Rev. 165, 1153 (1968).

Fl 71 D. G. Fleming, J. C. Hardy, and J. Cerny, Nucl. Phys. A162, 225 (1971).

Fo 69 H. T. Fortune, T. J. Gray, W. Trost, and N. R. Fletcher, Phys. Rev. 179, 1033 (1969).

Fr 53 R. G. Freemantle, W. M. Gibson, D. J. Prowse, and J. Rotblat, Phys. Rev. 92, 1268 (1953).

Fr 67 M. P. Fircke, E. E. Gross, B. J. Morton, and A. Zucker, Phys. Rev. 156, 1207 (1967).

Ga 69 P. Gaillard, R. Bouché, L. Feuvrais, M. Gaillard, A. Guichard, M. Gusakow, J. L. Leonhardt, and J. R. Pizzi, Nucl. Phys. A131, 353 (1969).

Gl 63 N. K. Glendenning, Ann. Rev. Nucl. Sci. 13, 191 (1963).

Gl 65 N. K. Glendenning, Phys. Rev. 137, B102 (1965).

Go 67 A. Goswami and A. I. Sherwood, Nucl. Phys. A91, 64 (1967).

Ha 67 J. C. Hardy and I. S. Towner, Phys. Lett. 25, B98 (1967).

Ha 69 G. Hauser, R. Lohken, H. Rebel, G. Schatz, G. W. Schweimer and J. Specht, Nucl. Phys. A128, 81 (1969).

Ha 72 G. Hauser, R. Lohken, G. Nowicki, H. Rebel, G. Schatz, G. Schweimer, H. Specht, Nucl. Phys. A182, 1 (1972).

He 70 W. R. Hering, H. Becker, C. A. Wiedner, and W. J. Thompson, Nucl. Phys. A151, 33 (1970).

Hi 67 J. C. Hiebert, E. Newman, and R. H. Bassel, Phys. Rev. (154, 898 (1967).

Ho 63 P. E. Hodgson, The Optical Model (Oxford University Press, 1963).

Ho 68 K. Hosono, J. Phys. Soc. Japan, 25, 36 (1968).

Hu 68 R. L. Hutson, S. Hayakawa, M. Chabre, J. J. Kraushaar, B. W. Ridley, and E. T. Boschitz, Phys. Lett. B27, 153 (1968).

Ia 66 P. J. Iano and N.Austern, Phys. Rev. 151, 853 (1966).

Ir 70 J. M. Irvine and V. F. E. Pucknell, Nucl. Phys. A159. 513 (1970).

Ja 62 F. D. Jackson, Classical Electrodynamics (Wiley, 1962).

Jo 70 R. C. Johnson and P. J. R. Soper, Phys. Rev. C1, 976 (1970).

Ka 69 O. Karban, P. D. Greaves, V. Hnizdo, J. Lowe, N. Berovic, H. Wojciechowski and G. W. Greenlees, Nucl. Phys. A132, 548(1969).

Ke 61 E. L. Keller, Phys. Rev. 121, 820 (1961).

Ko 71 R. L. Kozub, private communication.

Ku 69 P. D. Kunz, "Instructions for the Use of DWUCK" and "Algebra used by DWUCK", COO-535-606 and COO-535-613, University of Colorado (unpublished version of August 1969).

Ku 72 P. D. Kunz, private communication.

Li 70 T. K. Lim, Nucl. Phys. A148, 299 (1970).

Ma 62 S. Mayo and J. E. Testoni, Nucl. Phys. 36, 615 (1962).

Ma 67 G. H. Mackenzie, E. Kashy, M. M. Gordon, and H. G. Blosser, IEEE Trans. on Nuclear Science, NS-14, No. 3, 450 (1967).

Me 70 B. Mertens, C. Mayer-Böricke and H. Kattenborn, Nucl. Phys. A158, 97 (1970).

Mo 56 H. Morinaga, Phys. Rev. 101, 254 (1956).

Na 68 I. M. Naquib and L. L. Green, Nucl. Phys. A112, 76 (1968).

Ol 69 C. J. Oliver, P. D. Forsyth, J. L. Hutton, G. Kaye, J. R. Mines and references quoted therein, Nucl. Phys. A127, 567 (1967).

Pa 69 R. A. Paddock, Ph.D. Thesis, M.S.U., 1969 (unpublished).

Pe 64 F. G. Perey and D. Saxon, Phys. Lett. 10, 107 (1964).

Pe 64a S. K. Penny and G. R. Satchler, Nucl. Phys. 53, 145 (1964).

Pi 70 W. L. Pickles, Ph.D. Thesis, M.S.U., 1970 (unpublished).

Pr 71 B. M. Preedom, "Notes Concerning the Analysis of Direct Reactions", MSUCL-27, 1971 (unpublished).

Pr 72 B. M. Preedom, Phys. Rev. C5, 587 (1972).

Pr 72a I. D. Proctor, W. Benenson, and D. L. Bayer, Bull. Am. Phys. Soc. 17, 442 (1972).

Re 68 M. Reed, Ph.D. Thesis, University of California-Berkley 1968 (unpublished).

Ro 70 P. Roussel, G. Bruge, A. Bussiere, H. Faraggi, and J. E. Testoni, Nucl. Phys. A155, 306 (1970).

Ro 71 E. Rost and P. D. Kunz, Nucl. Phys. A162, 376 (1971).

Sa 64 G. R. Satchler, Nucl. Phys. 55, 1 (1964).

Sa 64a G. R. Satchler, Argonne National Laboratory Report No. ANL-6878, 1964 (unpublished).

Sa 66 G. R. Satchler, in Lectures in Theoretical Physics, Vol. VIIIC, ed. by P. D. Kunz, D. A. Lind and W. E. Brittin (University of Colorado Press, 1966).

Sc 72 L. R. Scherk and W. R. Falk, Nucl. Phys. A183, 240 (1972).

Sn 67 J. L. Snelgrove and E. Kashy, Nucl. Instr. Meth. 153 (1967).

Sn 68 J. L. Snelgrove, Ph. D. Thesis, M. S. U., 1968 (unpublished).

St 67 T. Stock, R. Bock, P. David, H. H. Duhm, and T. Tamura, Nucl. Phys. A104, 136 (1967).

Te 64 J. Testoni and S. Mayo, Nucl. Phys. 50, 479 (1964).

Th 72 S. T. Thornton, Phys. Lett. B39, 623 (1972).

To 69 I. S. Towner and J. C. Hardy, Adv. in Phys. 18, 401 (1969).

Tr 70 G. F. Trentelman and E. Kashy, Nucl. Instr. Meth. 82, 304 (1970).

Va 69 W. T. H. van Oers and J. M. Cameron, Phys. Rev. 184, 1061 (1969).

Vi 71 B. Vignon, J. F. Bruandet, N. Longequeue and I. S. Towner, Nucl. Phys. A162, 82 (1971).

Wi 71 B. H. Wildenthal, private communication.

YF 59 A. I. Yavin and G. W. Farwell, Nucl. Phys. 12, 1 (1959).

Yo 70a D. H. Youngblood, R. L. Koyub, J. C. Hiebert, and R. A. Kenefick, Nucl. Phys. A143, 512 (1970).

Yo 70b D. H. Youngblood, R. L. Koyub, R. A. Kenefick, and J. C. Hiebert, Phys. Rev. C2, 477 (1970).

Za 65 L. Zamick, Phys. Lett. 19, 174 (1965).

Zu 68 A. P. Zuker, B. Buck, and J. B. Mc Grory, Phys. Rev. Lett. 21, 39 (1968).

Zu 69 A. P. Auker, B. Buck, and J. B. Mc Grory, International Conference on Properties of Nuclear States (University of Montreal Press, 1969).